Master's thesis

NTNU
Norwegian University of Science and Technology
Faculty of Information Technology and Electrical Engineering
Department of Electric Power Engineering

Eirik Haugen Lillefosse

Towards DC-microgrids with Stability-Preserving Plug-and-Play Features:

Passivity-Based Control Design of DC/DC Converters under Compensated Modulation

Master's thesis in Energy and Environmental Engineering
Supervisor: Gilbert Bergna-Diaz
June 2020

NTNU
Norwegian University of Science and Technology

Eirik Haugen Lillefosse

Towards DC-microgrids with Stability-Preserving Plug-and-Play Features:

Passivity-Based Control Design of DC/DC Converters under Compensated Modulation

Master's thesis in Energy and Environmental Engineering
Supervisor: Gilbert Bergna-Diaz
June 2020

Norwegian University of Science and Technology
Faculty of Information Technology and Electrical Engineering
Department of Electric Power Engineering

NTNU
Kunnskap for en bedre verden

Abstract

The aim of this thesis is to develop a passivity-based control design of DC/DC converters for stability-preserving microgrids with plug-and-play features, for the purpose of a stable DC-microgrid operation in the case of any future topology change in the microgrid.

The electric power grid is going through a major shift from being dominated by a few large-scale power plants and unidirectional power flow, towards a more local and small-scale power generation. This includes a bidirectional distribution-infrastructure using information and communication technology (ICT) to optimize the power flow, and implementing renewable energy sources (RES) and energy storage (ES) units as a part of the grid. An essential part of this smart grid transition is the implementation of microgrids, i.e. small controllable power systems which contain both loads and generation. Since the dynamics of such a small power system is very sensitive to the changes in the loads and generation, the control is very complex, especially when facilitating for plug-and-play features. This is implying a higher share of power electronics in the grid.

The nonlinear tool of passivity is typically useful when designing the controllers in a microgrid consisting of converters, since their dynamical behavior is often described by nonlinear relationships. Passivity has a very advantageous property related to interconnections, and is, therefore, a powerful tool for the development of microgrids with many interconnections. This thesis will focus on DC/DC bidirectional converters that operate exclusively under the so-called compensated modulation strategy; i.e., where the current dynamics have been linearized by means of feedback. This allows for creating a time scale separation (TSS) between the linearized current dynamics and the remaining nonlinear voltage dynamics, which will be ensured by a design criterion. Under this TSS, the analysis of the remaining nonlinear voltage dynamics through passivity and Lyapunov theory is greatly simplified. Furthermore, it allowed for designing decentralized passivity-based outer loops for each converter. Finally, by exploiting the interconnection property of passivity, i.e. plug-and-play features, a stability preserving DC microgrid can be potentially implemented, even for the case of future interconnections.

Mathematical derivations have been conducted, and simulations through computer-programs have been done to verify the derivations. It is proven that TSS can be guaranteed as long as the inner-loop proportional-term is greater than the integral term, by a factor determined by the relationship of the inductance and capacitance. The result is extended by adding a voltage-regulating outer-loop based on passivity-theory. For this converter system, a new PI control design is derived. It was found that the outer-loop integral term is the most critical parameter, and that it must be small compared to the inner-loop tuning parameters to guarantee TSS. At last, the DC/DC converter power transfer bidirectionality is investigated, such that power can be both received and transferred, while preserving the plug-and-play features. Bidirectional power transfer was achieved. Although good re-

sults were obtained for the positive power transfer direction, it was found that the negative power transfer direction did not allow a straightforward and precise regulation of current or voltage. Instead it was suggested to settle for a droop-type of behavior for the control in the case of a negative power flow. The mathematical tool of the Gershgorin circle theorem has been applied for deriving the TSS design criteria. The theorem gave an analytical insight into the convergence rate of the voltage and current variables and their dependence on the system and control parameters, which was instrumental for enforcing the desired TSS.

Sammendrag

Målet med denne masteroppgaven er å utvikle et passivitets-basert kontrolldesign for en DC/DC omformer. Det overliggende formålet er at dette kontrolldesignet skal kunne bidra til å oppnå et stabilitetsbevarende DC-mikronett med "plug-and-play" funksjoner, slik at driften er stabil om det skulle oppstå fremtidige endringer i nett-topologien.

Strømnettet gjennomgår store endringer og går fra å være dominert av få men store kraftstasjoner og effektoverføring i en retning, mot mer lokal kraftproduksjon i mindre skala. Dette inkluderer toveis effektoverføring som utnytter informasjons- og kommunikasjonsteknologi til å optimalisere kraftoverføringen, i tillegg til innfasing av fornybare energikilder og energilagring i nettet. En essensiell del av overgangen til et smartere nett er implementeringen av mikronett, dvs. små, kontrollerbare kraftsystemer som inneholder både laster og kraftproduksjon. Siden dynamikken i et så lite kraftsystem er veldig sensitivt med tanke på endringer i last og produksjon, er kontrollen veldig kompleks. Dette gjelder spesielt med tanke på "plug-and-play" funksjonene, noe som medfører store mengder med kraftelektronikk i nettet.

Et ikke-lineært verktøy som passivitet kan typisk være en god løsning for å designe kontrollerne i et mikronett bestående av omformere, siden den dynamiske oppførselen ofte beskrives av ikke-lineære sammenhenger. Passivitet innehar også en veldig fordelaktig egenskap relatert til sammenkoblinger, og kan derfor fungere som et nyttig verktøy for kontroll av mikronett. Denne avhandlingen vil fokusere på DC/DC omformere med toveis effektflyt, som utelukkende opererer under en såkalt kompensert moduleringsstrategi; altså hvor strømdynamikken har blitt linearisert gjennom en tilbakekobling. Dette gir muligheten for en tidsskala-separasjon (TSS) mellom den lineariserte strømdynamikken og den ulineære spenningsdynamikken, noe som vil bli sikret ved å lage et designkriterium. Mens TSS er tilstedeværende, vil analysen av den ulineære spenningsdynamikken bli veldig forenklet ved å benytte passivitets- og Lyapunov-teori. Videre gjorde dette at man kunne designe desentraliserte og passivitetsbaserte ytre kontrollsløyfer for hver enkelt omformer. Til slutt, ved å utnytte sammenkoblings-egenskapen til passivitet, altså "plug-and-play" egenskapen, kan potensielt et stabilitetsbevarende DC mikronett implementeres. Dette vil også gjelde for fremtidige tilkoblinger til mikronettet.

I denne masteroppgaven har matematiske utledninger blitt gjennomført, og simuleringer i dataprogrammer har blitt utført for å verifisere utledningene. Det har blitt bevist at TSS kan garanteres så lenge proporsjonal-leddet er større enn integral-leddet i den indre kontrollsløyfen, med en faktor som avhenger av induktansen og kapasitansen. Deretter har resultatet blitt utvidet ved å legge til en spenningsregulerende ytre sløyfe som er basert på passivitetsteori, hvorav ett nytt PI-kontroll-design har blitt utledet. Integral-leddet i den ytre kontrollsløyfen viser seg å være den mest kritiske parameteren, og resultatet er at denne parameteren må være liten sammenlignet med kontrollparameterne i den indre

sløyfa, for å kunne garantere TSS. Til slutt utforskes omformeren sine muligheter til å transportere effekt i begge regninger, slik at den fortsatt bevarer "plug-and-play" funksjonalitetene. Toveis effektflyt i omformeren ble oppnådd. Gode resultater ble oppnådd for positiv effektflyt, mens for negativ effektflyt var det ikke den samme muligheten for enkel og presis regulering av strøm og spenning. Som en erstatning ble det anbefalt å benytte en "droop"-type oppførsel for regulering for negativ kraftretning. Gershgorins sirkel-teorem ble benyttet for å utlede design kriteriene for å sikre TSS. Dette teoremet ledet til en analytisk innsikt i konvergenshastigheten til spenningen og strømmen, samt deres avhengighet av system- og kontrollparameterne som var essensielle for å sikre den ønskede TSS.

Preface

This master thesis is finalizing the degree Master of Science in Energy and Environmental Engineering at the Norwegian University of Science and Technology (NTNU). The thesis is delivered and conducted to the Faculty of Information Technology and Electrical Engineering, and it is a collaboration with SINTEF as a part of the CINELDI project; Center for Intelligent Electricity Distribution. The specialization project titled *Development of a Computational Tool for Assessing Uninterrupted Microgrid Operation* [1] written by the same author is functioning as a pre-project for this thesis.

The development and completion of this thesis would not be possible without the help and opinions of several contributors. First of all, I would like to thank my supervisor and companion Assoc. Prof Gilbert Bergna-Diaz for all of his help and all the time he has spent helping me with my project. I am sincerely grateful for it, and for the possibility to work with such a skillful professional. Further on, I would like to express my gratitude for the help from my co-supervisor, Dr. Raymundo Torres-Olguin, for investing time in helping me construct the project. A big thank you must additionally be given to both Assoc. Prof Gilbert Bergna-Diaz and Dr. Raymundo Torres-Olguin for proofreading this thesis.

I would like to express my gratitude to my fellow students, for interesting and thorough academic discussions and suggestions. Additionally, I would like to thank my family for constantly supporting me and believing in me throughout my five years of studying. At the very end, I would like to thank my partner for the support she has been giving me the last couple of months.

Trondheim, 2020

Eirik Haugen Lillefosse

Table of Contents

List of Tables

List of Figures

List of Abbreviations

AC	Alternating Current
DC	Direct Current
DER	Distributed Energy Resources
DES	Distributed Energy Storage
DG	Distributed Generation
DOF	Degree of Freedom
ES	Energy Storage
EV	Electric Vehicle
FC	Fuel Cell
I	Integral
ICT	Information and Communication Technology
IEC	International Electrotechnical Commission
IEEE	Institute of Electrical and Electronics Engineers
P	Proportional
PBC	Passivity Based Control
pH	port-Hamiltonian
PI	Proportional-Integral
PV	Photovoltaics
PWM	Pulse Width Modulation
RES	Renewable Energy Sources
TSS	Time-Scale Separation

Chapter 1

Introduction

In this chapter the background of this project will be presented. The main motivation and the key developments creating the need for the topic in this project will be introduced. Further on the relation to the specialization project will be explained, before the research proposal for this thesis will be presented, i.e. the objectives, limitations, outline, and methodology.

1.1 Background

During the last decade, the focus on global warming and the measures to reduce it has increased rapidly. A great majority of the countries in the world have committed to international environmental agreements, of which the Paris Agreement from 2016 [2] is the most comprehensive. This has led to both international and national goals, with the common aim of reducing the CO_2 emissions. At the same time, the global population and power demand is increasing [3]. This has led to a vast focus on electricity-based energy carriers and renewable energy generation, to reduce the amount of fossil fuel-based energy sources in the energy system.

To reach these goals, development within technology is essential. This includes development within the whole domain of the energy system, ranging from big renewable generation systems to the smallest components within the power system. A central part towards decarbonization of the power sector is to implement more renewable energy sources to the electric power grid. Solar energy, wind energy, and hydro energy are among the most important renewable energy sources (RES). These RESs are already well established for generation, and the future goal is to implement a higher share of these energy sources to the power-mix, both in big and small scale. This invokes changes in all parts of the electric power system, from generation, to transmission, to distribution [4].

The ongoing smart grid transition of the power grid is including the implementation of RES, as well as other technologies. The goal is to achieve maximal efficiency of such implementations, to optimize the operation of the electric grid. A central part for achieving

this is to implement microgrids, i.e. small-scale individual power systems. These microgrids can be either of DC-type or AC-type, depending on the dominating voltage-type. A recent trend is that DC-power becomes more and more popular. Some of the reasons are because a high share of residential loads demands DC-power, energy storage and batteries are DC-based and will be essential for the future, and since PV-systems generate DC-power [5]. As mentioned, the implementation of smaller-scale RES is essential towards achieving a low-carbon society. Rooftop solar panels, small-scale wind power, etc. have become efficient distributed energy resources (DERs), but they lead to some challenges when connecting to the grid. A solution is to apply controllable power electronics to connect the generation and loads to a microgrid. The microgrid can control the generated power, the stored energy, and the demand by the loads, in such a way that the microgrid can function by itself in an optimal way. For several reasons, this type of converter-control is very complex [6].

A possible solution, and a recent popular research objective, is to base this type of converter-control on the nonlinear concept of passivity [7]. This could simplify the control of such complex and nonlinear systems, and be simpler understood due to the direct relationship to energy. Additionally, the passivity-concept has many properties that are favorable related to microgrids, where the well-known plug-and-play feature is the crucial one. But, for the passivity property to be present, some requirements related to the system must be fulfilled [8]. The objective hence becomes to design the controller, such that these requirements are also obtained for the operating point of interest.

If such a control design can be derived and implemented, it would contribute towards the goal of a low-carbon society. In general, if one converter which for instance is connecting a PV-plant to a microgrid can be designed to be passive, the converter has stability-preserving plug-and-play features. In other words, the PV-plant can connect and disconnect to the microgrid as needed and guarantee stability, without any additional control requirements. An even greater potential of passivity-based control design is to expand from one single converter to multiple interconnected converters. A microgrid can be seen as an interconnection of many units, i.e. loads and generations, connected through individual converters. If for instance every unit connected to a microgrid has a passivity-based control, it would be possible to construct a passivity-based microgrid. This is implying a stability-preserving microgrid, which has plug-and-play features for all interconnections. In the case of any future topology changes the stability would still be ensured, as long as the new interconnection is passive.

The establishment of DC-microgrids with stability-preserving plug-and-play features could ensure that the electric power grid could safely *scale* and therefore implement more renewables, as a contribution in the fight against global warming.

1.2 Relation to Specialization Project

This thesis has a high relation to, and is partly based on, the specialization project named "*Development of a Computational Tool for Assessing Uninterrupted Microgrid Operation*"

[1], written by the same author as this thesis during the fall of 2019. The specialization project will be important for the thesis in several ways.

First of all, the created computational tool from the specialization project will be applied to some of the dynamical systems. This is necessary in order to see if the TSS is present for large-signal analysis and additionally, in general, to observe if the nonlinear systems are stable. Secondly, the system in focus is similar to one of the systems in the specialization project. One of the systems that were investigated in the specialization project was the DC/DC converter with a PI-controller for the inner loop and with a compensated modulation. This exact system is the starting point for this thesis, but further expansions will be done, including adding a passivity-based outer-loop for the voltage and investigating the possibility for bidirectional power flow. Thirdly, a very big part of this master thesis is based on the Lyapunov theory, or an expansion of it for open systems called passivity, as a tool to analyze nonlinear dynamics and design stable controllers. From the specialization project, one of the main findings while investigating the compensated modulation of the P-controlled inner loop was the TSS that occurred between the current and voltage dynamics. Because of the TSS, it was possible to create a Lyapunov function to analyze the system stability of the slower voltage dynamics. For this thesis, finding design conditions that ensure the TSS between current and voltage dynamics and designing a passivity based outer loop control for stabilizing the nonlinear and slower voltage dynamics will be the main focus. This should be contrasted with the specialization project, where the TSS occurred by chance and not by design.

Hence, some parts of this thesis are heavily based on material from the specialization project. This is both done as a time-saving measure, but additionally as a consequence of the reader not necessarily having access to the specialization project. The following sections are highly inspired by or obtained directly with smaller adjustments, from the specialization project: Chapter 2.1, Chapter 2.2 (only the introduction-part), Chapter 2.3.1, Chapter 3.1.1, Chapter 3.2.1, and Appendix B.1. As a consequence, also some parts of the limitations of this thesis are similar to the ones in the specialization project. The chosen parameter values for the simulations, validations, and examples are also based on the same papers as the values in the specialization project were. As a consequence, the parameter values are similar.

1.3 Objectives

The general objectives for this thesis are listed below.

- Examine the theory of passivity and its potential for operating a stabilizing DC-microgrid consisting of DC/DC converters.

- Derive design criteria using tools from system theory, including limitations and restrictions for both the converter and the control system parameters, in such a way that TSS is ensured by design and not by chance.

- Examine if it is possible to obtain analytical insight related to the different tuning parameters such that the design criteria for ensuring TSS described above can be further generalized.
- Design the outer loop of a single DC/DC converter with positive power transfer direction based on passivity-theory to ensure stability. First, this will be done assuming that the TSS is present, i.e. that the inner-loop current has converged to a desired reference. Next, the obtained outer loop will be tested in a more realistic system which does not include such an assumption. It will be of interest to verify if the outer-loop is able to stabilize the system while preserving the TSS.
- Investigate if it is possible to apply the design criteria detailed above to the more challenging case of a converter with a negative power transfer direction, without destroying the TSS.
- Create a time-domain simulation model to validate the control proposal.

All of the bullet-points are contributing towards the overall objective of creating plug-and-play microgrids that can guarantee stability for any future topology change.

1.4 Scope of Work and Limitations

The scope of this work is to use passivity to design decentralized outer loop controllers with a large-signal stability certificate and plug-and-play features for DC/DC converters operating under so-called compensated modulation, while providing some design criteria for the system and control parameters to ensure that the TSS is maintained. Due to among others restricted time, some limitations for the scope of work must be sat in order to achieve the objectives. Below these limitations are listed.

- The bidirectional DC/DC converter will be the converter in focus, for simplicity reasons. Since this was the relevant converter also for the specialization project, it is time-saving to exploit the obtained knowledge from that project.
- Since the area of interest is related to stability and proper operation of the converter, optimization with respect to losses and set-points will not be considered.
- As the stability and stabilization is the main area of interest, hence the component itself not so much, the averaged switching model is applied. This model is neglecting the switches in the converter.
- Compensated modulation is the focus; i.e., the case where current dynamics have been linearized via feedback. Hence other modulation methods will not be mentioned.
- Throughout this thesis, simplifications and linearizations must be done to reduce the inherent complexity of the relevant nonlinear systems. Therefore, some of the results related to the TSS conditions have been based on small-signal analysis.

- Availability of data is restricted. It is hard to obtain the values of the parameters for the converters used by the industry. Hence, the values of the parameters are mainly based on values from other papers and research.

- Finally, it must be mentioned that a big part of this master thesis should have been to validate and test the mathematical derivations and control designs in the laboratory. But due to the outbreak of the COVID-19 virus, NTNU decided to close the university and not allow anyone to do laboratory research as a measure to stop the spread of the pandemic. Hence, it has not been possible to do research and validation through experimental tests in the laboratory.

1.5 Methodology and Thesis Outline

The methodology applied in this thesis in order to achieve the previously mentioned objectives will be as follows:

First, a profound literature review will be conducted to obtain a strong theoretical foundation, in such a way that qualified theoretical justifications will be taken. Secondly, analytical research will be completed. Mathematical deductions and derivations will be carried out and justified. Further on, implementation of the analytical results in computer software such as SIMULINK and MATLAB will be done, to simulate the models. Then validation and testing through the software will be completed before the results will be evaluated. The evaluation and interpreting of the mathematical derivations, the resulting analytical expressions, the obtained converter control design criteria, and the simulation-results, are a great part of the final result.

The process to obtain the goals of this thesis consists of many steps. The approach is logical, starting with the fundamental and essential parts for the total result. Since the TSS is a demand for all of the derivations, this is the natural starting point. Further on a step-wise approach towards the final goal will be carried out, focusing only on one problem at the time. For each problem, derivations will be conducted, and simulations and tests will show if the result is consistent with the derivation. When the result is satisfactory and trustworthy, the next problem will be considered. If the obtained result for some reason is not acceptable, it might be necessary to review some of the earlier problems, hence the process is somehow iterative. Only the most important steps which actually led to some sort of essential information will be mentioned in the thesis. But there were many dead-ends in the process, which will not be discussed.

The outline of this thesis is now shortly described.

- Chapter 2 describes the system in focus.

- Chapter 3 presents the relevant mathematical theory and control theory that is applied in order to fulfill the objectives.

- Chapter 4 presents the analyses and results related to the TSS of the inner-loop dynamics. A design criterion on how to ensure the TSS is developed, before the findings will be discussed.
- Chapter 5 presents the derivation of the PI passivity-based control (PBC) for the unidirectional converter, along with analyses and discussion of the relevant design criteria on how to still ensure the TSS.
- Chapter 6 is analyzing the bidirectional converter and the PI-PBC of it, such that the TSS still is ensured.
- Chapter 7 is summing up the thesis and comes with a conclusion before suggestions for further work are presented.
- The Appendix contains information essential for obtaining the results, including some derivations and computer-scripts, which has been omitted from the main text for compactness.

Chapter 2

The DC Microgrid and the DC/DC Converter

In this chapter relevant theory about the DC microgrid and the converter system later to be analyzed will be presented. Theory about the grid will first be presented in order to put the objectives of this thesis in context, and to obtain an understanding of why this project is of great scientific interest. Then the DC/DC converter will shortly be explained, before a more specific description of the converter-model to be analyzed is given. The model and any eventual simplifications will be explained, along with the modulation technique and the relevant controlling technique.

2.1 The Smart Grid

The electric power grid is going through a major transition towards a smarter grid, shaped by the evolution of the power demand, the power generation, and the technology. *The smart grid* is a necessary evolution for the electric power transmission system. During the *2007 Energy Independence and Security Act*, some key features defining a smart grid were noted. These points can be found in [4], but in general, they define a paradigm shift in the electric power grid. The main drivers for the development of the smart grid are many [9]. First of all, there are the economic reasons. Smart grids can increase the reliability of power supply and reduce the downtime of the grid. Also by exploiting the existing infrastructure more efficiently and optimally, new investments can be avoided. Secondly, there are environmental motivations. A constant increase in renewable energy production creates new challenges for the grid. By implementing new components and new technology into the grid, these problems can be solved. A third and very important driver towards the smart grid is the society. Ever since the electricity was commercialized at the end of the 19th century it has been more and more essential in people's life. Today, the society, both citizens and industry, depend on it for the daily life to function. This trend will continue in the future [10]. For instance digitization in companies and electric vehicles (EVs) among the private residential are two trends predicting this. Therefore,

continuous and safe power delivery is getting more and more important. The structure of the power transmission and distribution has changed a lot since the infrastructure first was built. Figure 2.1.1 below is illustrating how the grid has gone from a uni-directional grid to a more complex and multi-directional system [11].

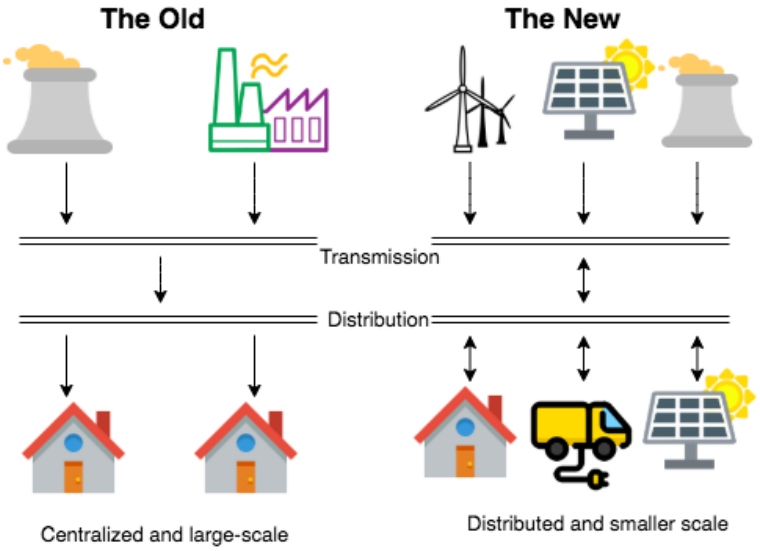

Figure 2.1.1: Evolution of the power grid, comparing the old and the new power grid system. The old system is more centralized, large-scale, and unidirectional, while the new system is more bidirectional, small-scale, and distributed.

Additionally, the expectations of society force development. For instance, when buying an EV, it is expected that it will be able to charge and extract power from the grid. For this to apply also in the future and for future technological developments, the electric grid must adapt. So, technological development in the society is also a key factor for the move towards a smarter grid.

But, many challenges appear when implementing the smart grid. First of all, it is hard to determine which technologies will give the best result, and how these technologies can cooperate to give the best solution. Research and development is the best way of solving this challenge. Also, security [12] is a challenge related to the smart grid. Cybersecurity against hacking or similar digital attacks is required to provide a safe power grid. The smarter grid will also collect and store huge amounts of data, and these need to be stored safely and treated ethically. Another issue concerning this amount of data is to determine who should have access to it. Further on, a very important challenge is related to the stability. Bidirectional power flow, a plurality of different frequencies, and nonlinear behavior introduced by some power electronics, such as the constant power loads [13], are some of the major elements which make the stability of the grid complex. In [12] a more consistent analysis of the challenges can be found.

2.2 The DC Microgrid and its Applications

One of the pillars in the process of establishing the future grid is the microgrid. As defined by L. Fusheng, L. Ruisheng, and Z. Fengquan in [14] a microgrid is: "a single, controllable, independent power system consisting of distributed generation (DG), loads, ES, and control devices, in which DG and ES are directly connected to the user side in parallel." It can be explained as a small and independent power system, which can transmit, generate, and distribute power all within an area, and therefore can function isolated from the main grid. A microgrid has the possibility to be connected to the main utility grid, and to disconnect from it, running in island mode. This implies a higher local reliability. For instance, in the case of a fault in the transmission network, the microgrid can disconnect and run in island mode, providing for itself. A basic sketch of a microgrid can be seen in Figure 2.2.1 [15].

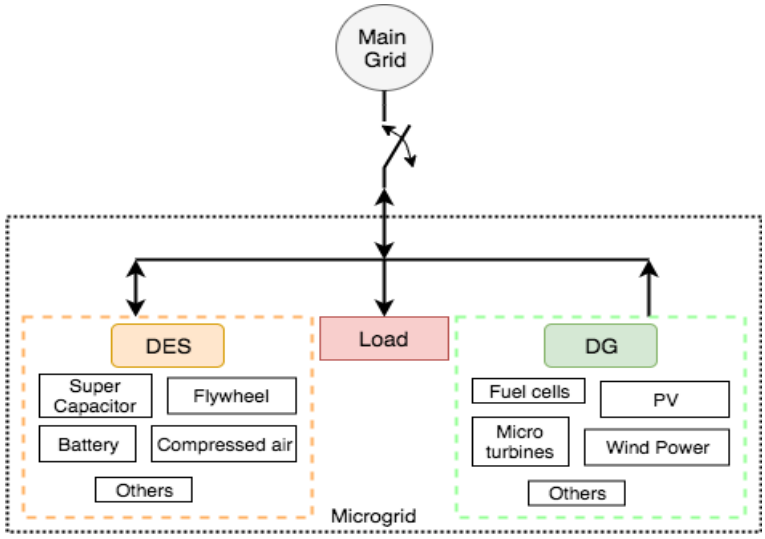

Figure 2.2.1: Sketch of a microgrid, showing some of the units that it can contain and the possible directions of the power. Distributed storage, loads, and distributed generation are typical units, and the microgrid is connected directly to the main grid through a point of common coupling.

It can be seen from Figure 2.2.1 that the power flow in the grid is bidirectional and that new technologies such as distributed energy storage (DES) and DG through renewables are implemented.

Typically, a microgrid can be classified by function demand, capacity, or by bus-voltage type [16]. The latter is used in this thesis and is further elaborated in the following lines. This kind of classification is distinguishing between AC-microgrids, DC-microgrids, and hybrid microgrids which is a combination of the two first-mentioned ones. Both the AC-microgrid and the hybrid microgrid are important for the previously mentioned development of the smart grid, but for reasons that will be mentioned later the DC-microgrid is

getting more and more important and will further on be the focus in this project.

2.2.1 The DC Microgrid

One definition of a DC microgrid is a microgrid in which the DERs, the loads, and the utility grid, are connected to a DC-bus [17]. The DC-link is connected to the utility grid through a point of common coupling such that it has the possibility to both be grid-connected and run in island mode, i.e. without connection to the main grid. The DC-link is also connected to the loads. The loads can be either DC, and can thereof be directly connected to the bus-bar though a DC/DC converter, or they can be AC and hence need an inverter to transform the power from DC to AC. The different DERs are connected to the DC-bus either through a DC/DC converter if they generate/demand DC voltage, or through inverters/rectifiers, if AC is generated/demanded. The operation of this system, i.e. the DC-link with the connections, is controlled by a DC-microgrid overall control. This control is managing the data from the DC-link and controlling the loads and DERs. In other words, depending on the state of the system, the overall controller might connect or disconnect generations depending on the need. So the difference between an AC-microgrid and a DC-microgrid is basically the voltage-type at the link that is interconnecting the loads and the DERs. A typical DC-microgrid configuration can be seen in Figure 2.2.2 below [17].

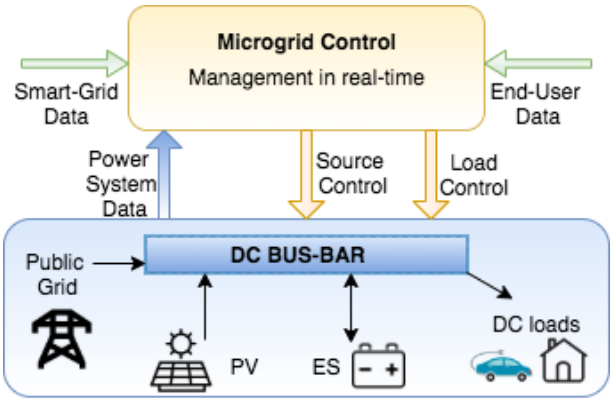

Figure 2.2.2: Overview of configurations in a DC-microgrid. The DC bus is connecting the units in the grid, and the microgrid control is managing the control of the units in the grid by receiving and processing data in real-time.

The DC-microgrid is essential for many reasons. In general, the main reasons are due to an increase in DC-loads, for simplicity reasons, because of low costs, and a higher demand for the quality of the delivered power [18]. A DC-distribution system has high efficiency for distribution and makes it easy to integrate DG and RES. In this way the energy supply can easily get more independent from fossil fuels, which is a good measure in the battle against global warming [19]. More specifically, a DC-system might be a better solution than an AC-system for a couple of reasons that will be mentioned in the next

paragraphs.

A big share of the microgrid-technologies, i.e. the DERs [20], such as batteries in energy storage systems, and photovoltaic (PV)-systems for renewable DG, and fuel cells (FC) for non-renewable DG, are based on DC. Additionally, it is a steadily increasing implementation of EVs in the car-park, which all are based on batteries. In total, approximately 50 % of residential loads are DC-based [5]. By directly connecting these loads and/or generations to a DC-microgrid, a huge amount of unnecessary voltage-transformation can be avoided. Hence, for such interconnections fewer converters are needed and fewer steps of conversion. This implies lower costs and lower losses. Hence for a low-voltage DC-microgrid the potential for energy saving is big [21]. This concept is also illustrated in Figure 2.2.3 [5].

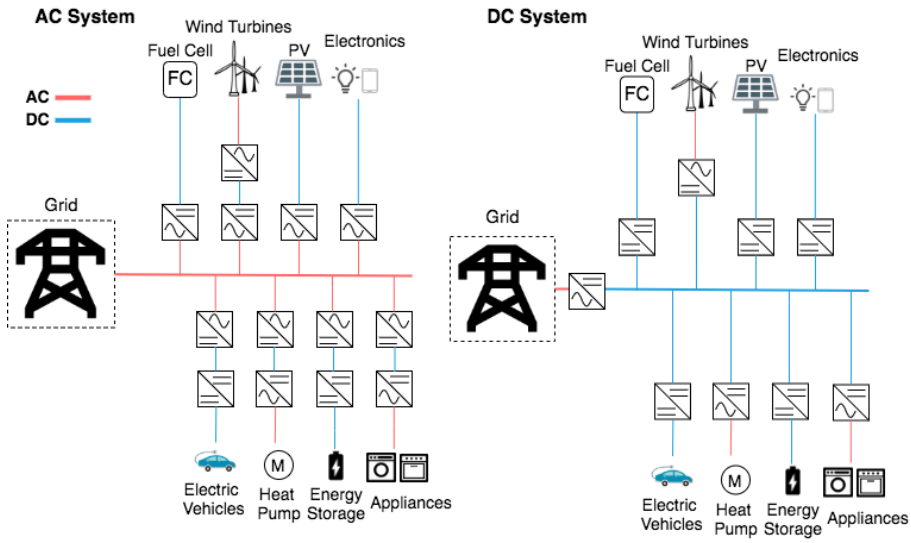

Figure 2.2.3: AC distribution system vs DC distribution system, illustrating less converters and power electronics, hence lower costs and losses, for the DC system.

The control objective for a DC-microgrid is to keep the required voltage values at the different supply points or other essential points in the microgrid [22]. Since the voltage type is DC, only the voltage level must be controlled to be at the required value. The control is hence less complex than for an AC-system, which in addition to voltage level, must control the frequency and the shape of the voltage. Compared to Figure 2.2.2, the DC-microgrid control is doing the data processing and communicates with the different nodes in the grid, while for each unit a local controller is regulating the voltage in case of dynamics changes or a required change. The main challenge with the control of a microgrid, regardless of type, is that the conditions in the system are variable and often unknown, and therefore must adapt in real-time [6]. The control-layers in a microgrid will not be explained in detail, but is further explained in [1] and [23].

Additionally, the DC-distribution is in general more efficient and less characterized by interference, leading to high power quality. This involves that phenomena such as skin-effect and reactive power losses are avoided. Additional advantages of DC over AC, in general, are also applying [24]. Of course the DC-microgrid also provides challenges and disadvantages compared to an AC-microgrid. This will be enlightened in the next section.

2.2.2 Challenges

The main challenge with DC-microgrids is related to the lack of protection technology and devices. The two main disadvantages with DC-voltage related to protection is related to the lack of natural zero-crossing of the current and challenges with the grounding [25]. Because of these challenges technologies for protection is complex, in order to provide a safe and solid grid. One example is regarding circuit breakers for DC-currents. The circuit breakers are essential in the protection scheme of an electric grid. But the fundamental theory behind the circuit breakers is related to the natural zero-crossing of the current. Since the DC currents are, generally, only positive and not are crossing the zero-axis, another approach for the circuit breakers must be taken. Many solutions have been presented in order to solve the mentioned challenges with the lack of protection devices [26, 27].

Additionally the lack of standards and regulation is a challenge for the DC-microgrid [5, 24]. The lack of standards are partial linked to the points in the previous paragraph. Since AC-grids have been so dominating for many years, the standards for them are developed. For DC-grids on the contrary, standards are lacking. Actively, several organizations such as the Institute of Electrical and Electronics Engineers (IEEE) and the International Electrotechnical Commission (IEC) are working on developing such standards. Both IEEE and IEC standards will create the foundation to develop and establish a safe and profound DC-microgrid.

It is not only the DC-microgrids that have issues with protection. Independent on the type of microgrid, some challenges with protection occurs. In general, microgrid protection includes dealing with bidirectional power flows, plenty of cooperating power electronic devices, dynamic changes of generation and loads, and changing operating conditions. These are complex phenomena, and the protection of such systems is hence troubling. One of the major issues is related to the fault currents in the case of grid-connected mode and island mode. An adaptive protection is one way of solving this type of issue [25], and additionally other solutions are being researched.

2.2.3 Plug-and-Play Features

A microgrid-system is a complex and dynamically evolving system. Scalability, or the ability to change in size, is one of the benefits with microgrids. If the total load for a microgrid-area is increasing, it is possible to connect for instance a RES to it, providing for the lack of generated power. Of course this scalability has its limitations, for instance

the control technology. Hence, the concept of *plug-and-play* features in microgrid has recently been more and more researched. From computer science the term plug-and-play is related to the ability of a component/device to connect to a system, i.e. be plugged in, and then automatically be recognized by the system and start to function with the system, i.e. starts to play. For microgrid applications, the definition is similar. It includes the possibility of the microgrid-system to integrate a component or device into the system, only by connecting it/plugging it in [28].

This involves that the connected component or device finds its natural operating conditions in the system automatically, such that it configures properly and operates efficiently. The main idea is that the units that are plugged in contribute to stabilizing the voltage (or other states) in the microgrid without any further communication [29]. From a practical point of view this means that DGs, ES-systems, and loads can be connected to the microgrid when necessary, and disconnected when that's favorable, only by "plugging" it in or out, and that the DC-voltage at the DC-link will stabilize, thus guaranteeing a safe operation. In order for this to properly work, a decentralized local controller is essential for the connected units. For instance, a local PI controller can be used [6].

A future goal, and a popular research topic, is to construct a full microgrid where every connection has the plug-and-play capability. This implies a fully autonomous microgrid-system. This objective has many challenges, and the main one is related to the control of the power electronic converters. A suggestion, and the research topic in this project, is to base the control on the property of passivity. Passivity will later be shown to have many of the wanted characteristics for such a purpose.

2.3 The DC/DC Converter

Some of the most essential components in a microgrid are the power electronic converters. Every unit and every connection needs some sort of power electronic equipment in order to provide the correct signal types. Depending on the type of connection, different types of converters are needed. For some connections, the objective is to convert the voltage-type from AC to DC or vice versa, for others it is to change the frequency of the input signal, while for others it is to change the voltage level. Based on this, there are four main types of power converters; AC/DC converter (rectifier), DC/AC converter (inverter), AC/AC converter, and DC/DC converter.

Since the focus in this project is the DC-microgrids, the DC/DC converter is the converter in focus. This is because this often is the most common converter for DC-microgrid applications. Two examples on the use of the DC/DC converter is to convert the generated PV-voltage to a suitable voltage for the DC-microgrid bus-bar, and to convert the voltage on the DC-link to a suitable format for the charging of the batteries in an EV. Since the chosen converter type and model will be explained more in detail in the next chapter, i.e. Chapter 2.4, the rest of this chapter will only give a short overview of the essentials related to the DC/DC converter.

2.3.1 Topology and Functioning

A DC/DC converter has in general only one objective, to change the voltage level from one level at the input, to another at the output. The voltage level can either be increased or decreased, i.e. the converter is either a step-up converter, or a step-down converter. Many topologies for the DC/DC converter exists, and each has advantages and disadvantages. In [30] the most important DC/DC converter topologies are explained and compared. For this thesis, as for the specialization project [1], a topology with an origin in the bidirectional Buck-Boost converter is in focus. The circuit can be seen in Figure 2.3.1, and its functioning is described below.

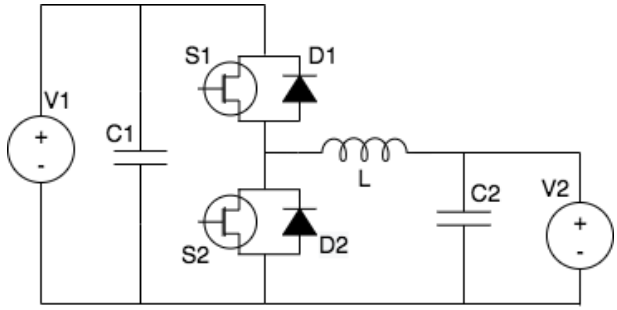

Figure 2.3.1: Topology of a non-insulated Buck-Boost converter. S1 and S2 are controlled switches, D1 and D2 are diodes, C1 and C2 are parallel capacitors, L is the inductor, and V1 and V2 are the voltage sources.

The Buck-Boost converter has the ability to both step-up (boost) and step-down (buck) the voltage level. Furthermore, as it is bidirectional, it can transfer power in both directions. This is an interesting characteristic related to the microgrid and ES-systems. The batteries must be able to both be charged, i.e. receive power, and to discharge, i.e. deliver power to the grid. Regarding Figure 2.3.1, the operational modes are described in [31], but the most important operational aspects are summarized in Table 2.3.1 below.

Table 2.3.1: Operational modes of the bidirectional Buck-Boost converter.

	Boost Mode 1	**Boost Mode 2**	**Buck Mode 1**	**Buck Mode 2**
S1	**OFF**	**OFF**	ON	OFF
S2	ON	OFF	**OFF**	**OFF**
D1	OFF	ON	**OFF**	**OFF**
D2	**OFF**	**OFF**	OFF	ON

The commands written in bold are the fixed commands for the Buck and Boost mode, while the commands written in normal letters are distinguishing between the different operational modes. The modes (mode 1 and 2) are separating between power transferred in both directions. The topology consists of a buck converter and a boost converter and is

controlled by an IGBT or MOSFET with freewheeling antiparallel diodes. The switch can be controlled with a pulse width modulation (PWM) technique. The modulation technique will not be considered in this project because the model in focus will be state-space averaged. Nonetheless, an important parameter coming from the PWM is the duty cycle, m. The duty cycle is defined as the time the PWM is giving V_{DC} over the load, divided by the switching period. V_{DC} is a reference value set by the PWM. A practical description; if the V_{DC} of the PWM is 100 V, and the input is 100 V, while the output is wanted to be 50 V, the duty cycle must be 50%. The relationship is described in Equation (2.1).

$$m = \frac{t_{on}}{T} = \frac{V_{out}}{V_{DC}} \tag{2.1}$$

A deeper analysis of the PWM technique can be found in [32].

In Chapter 2.4 the converter-model will be explained more in a mathematical way. The origin is the topology in Figure 2.3.1, but simplifications will be done in order for the mathematical analysis to be more efficient. In order to start analyzing the converter-model, an overview of some controlling techniques must be presented.

2.3.2 Control Design of the DC/DC Converter

Numerous controlling techniques for the DC/DC converter and different varieties of these techniques have been proposed and implemented. The control design is depending on the controlling objective, which is individual for different situations. The main controlling objective for every converter is to obtain a reference value for voltage, current, or a compromise between both. Some situations are characterized for instance by huge/nonlinear load variations, others connect critical components that need a fast response, while others have big voltage level differences between the input and output. So individual converter-situations needs individual controllers.

For a DC/DC converter there are mainly three types of control modes [32]. The first mode is *voltage-mode*. A converter in the voltage-mode conditions aims to regulate the voltage of the output, to achieve the desired output voltage. This is done by drawing the level of current needed to provide the given voltage. For *current-mode* the situation is identical but reversed, meaning that a desired current-level is wanted at the output, and the voltage must change to obtain this current-level. The third controlling mode is the *droop-control*, often applied for larger systems including power-sharing. The droop-control is well established and many designs related to the DC/DC converters exist. In [33] and [34] two specific cases of the implementation of droop-control can be seen.

When modeling the DC/DC converter, and describing the system dynamics as a function of its control inputs and states, the resulting model is in *open-loop*. The open-loop model is very useful in order to obtain information about the physical system itself. This set of dynamical equations *maps* a desired output with a control input. But, since it is essential and necessary to regulate the output in order to get the desired operating condition of the converter even in the presence of unmodelled system dynamics, a controller based on feedback measurement must be added. When adding a control-loop, using the states

of the converter to control the output, the system is in *closed-loop*. Depending on the objective of the converter and the requirements previously mentioned, the type of control is chosen. For this project, the PI-controller will be applied. The PI-control is well established within the discipline, and it has several advantages such as the ability to obtain zero steady-state error and a simple construction [35].

The general PI control-loop can be seen in Figure 2.3.2 below.

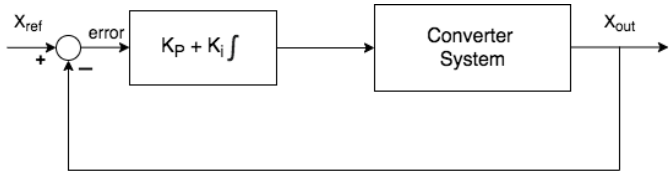

Figure 2.3.2: PI control-loop. The difference between the reference value and the output value is the input to the PI block. This is used to regulate the output-state of the converter system, to achieve the correct output value.

The converter system-block contains the equations describing the dynamics of the converter, for instance in terms of voltage and current. Depending on the control mode of the converter, the output state x, i.e. voltage or current, becomes equal to the reference value in steady-state. A requirement is that the tuning parameters K_i and K_p are tuned correctly. The function of the control is that the x_{out} state is going into a feedback loop, where it is compared to the reference value, i.e. the desired value. The error between the two is multiplied with the proportional-gain (P-gain) K_p and in parallel integrated and multiplied with an integral-gain (I-gain) K_i. These two values are the tuning variables for a PI-controller. The proportional-term is reducing the response time, and the integral-term is eliminating the steady-state error. But they also may lead to overshooting of the signal, so the tuning must be done carefully to have a satisfactory response. Additionally, a second PI-controller can be added to the outer-loop. Often the current is controlled in the inner-loop, and the voltage in the outer-loop. In this way, the full dynamics of the converter can be controlled [36].

A decision that must be taken, in addition to choosing the tuning parameters, is the choice of modulation technique. In general, there are two schools of thought within the power electronics community; compensated modulation and uncompensated modulation [37]. A compensated modulation is having a feedback-term to compensate for a non-linearity appearing in the converter current-dynamics, resulting in linear current dynamics. The consequence of such a compensated modulation is that the model might suffer from robustness issues. By contrast, the uncompensated modulation avoids any feedback linearization, and is typically used along with standard linear current control methods despite the current dynamics remaining nonlinear. This project will limit its scope exclusively to DC/DC converters under the compensated modulation technique.

There are many challenges related to the control design of converters. One of the

main challenges is associated with the changes in the electric power grid and technology related to the grid. As the power grid is in the middle of a transition where it is somehow unknown what the future will bring, the research on control techniques must continue. The main changes the future grid will bring are related to more power electronics in the grid, more renewable and decentralized distributed generation, and plug-and-play features. This enforces more autonomous control, in addition to a fast and accurate response.

2.4 System Description: The DC/DC Converter with Compensated Modulation and PI-control

In this chapter the converter-model which is the starting point for the research in this project will be presented. Throughout Chapter 5 some other elements will be added to the model, but the starting point is the same model as for the specialization-project [1].

The open-loop system consists of a state-space averaged Buck-Boost converter [31], with the possibility of bidirectional current, as seen in Figure 2.4.1.

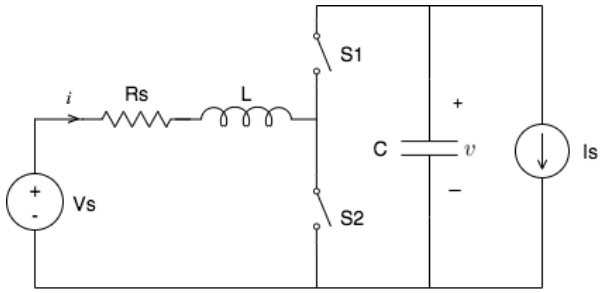

Figure 2.4.1: Converter topology of the relevant converter-system, representing a state-space averaged Buck-Boost converter.

The topology consists of a DC-voltage source and a corresponding source-side resistance, and an inductor controlling the current i though it. On the load-side a constant current-source is representing the current required at the load, and a parallel capacitor with the voltage v over it. Two switches are present, for instance PWM-controlled, which is regulated to change the output voltage v seen in Figure 2.4.1. The switches have a given duty-cycle m, described in Equation (2.1), such that the average output voltage is equal to $v \cdot m$. The equations describing the current through the inductor and the voltage over the capacitor can be seen in Equation (2.2) and (2.3) below.

$$L\frac{di}{dt} = -R_s \cdot i + V_s - v \cdot m \tag{2.2}$$

$$C\frac{dv}{dt} = -I_s + i \cdot m \tag{2.3}$$

Since this is an open-loop system, which is not of interest for any practical purposes, a control-loop is added. The controller is a PI-controller in current mode, with a compen-

sated modulation; formally referred to as partial feedback linearization [38]. First of all, the term of the internal voltage is now introduced, defined as in Equation (2.4).

$$e = V_s - K_p \cdot (i_{ref} - i) - K_i \cdot \zeta \tag{2.4}$$

The integral term also adds a new state to the system, ζ defined in Equation (2.8) below. The internal voltage contains a feed-forward signal of the voltage source V_s, and is hence eliminated from the current-equation such that the current-equation becomes as simplified as possible. In addition, the internal voltage e contains the terms coming from the PI-controller. This includes the reference current, i_{ref}, and the two tuning gains K_p and K_i. The compensated modulation/partial feedback linearization is obtained by defining m as in Equation (2.5) below.

$$m = \frac{e}{v} \tag{2.5}$$

This will eliminate the nonlinearities in the current-equation, and consequently making it independent from the voltage, such that it is easy to investigate and analyze. By inserting Equation (2.4) into Equation (2.5), and further into Equation (2.2) and (2.3), the system description of the model is obtained. The resulting system description is seen in Equation (2.6)-(2.8) below.

$$L\frac{di}{dt} = -R_s \cdot i + K_p \cdot (i_{ref} - i) + K_i \cdot \zeta \tag{2.6}$$

$$C\frac{dv}{dt} = -I_s + i \cdot \frac{V_s - K_p \cdot (i_{ref} - i) - K_i \cdot \zeta}{v} \tag{2.7}$$

$$\frac{d\zeta}{dt} = i_{ref} - i \tag{2.8}$$

Summed up, the model described in Equation (2.6)-(2.8) above is a state-space averaged DC/DC converter with a PI-control of the current, and a partial feedback linearization with respect to current-dynamics, such that the current equation becomes linear. The reason why it is called partial feedback linearization is that the system can be divided into two subsystems, one linear and one nonlinear. The consequence of this is that the capacitor-voltage equation gets even "more nonlinear" than originally.

Chapter 3

Stability and Control Theory for Dynamic Systems

As a consequence of the increasing complexity in the electric power system due to new interconnections of DERs, more nonlinear loads, and a higher share of power electronics, the importance of a proper control design providing stability increases. In this chapter, the necessary and relevant control theory and theory related to dynamic system analysis will be presented. To fulfill the control objectives of this thesis, some simplifications and approximations had to be done, and the relevant ones will be thoroughly explained. This theory will be supportive of the derivation of the TSS for the relevant DC/DC converter. The presented theory about the control and stability for electric systems will be the foundation for the derivation and analysis of the control design of the converters, especially with respect to the outer loop.

This chapter contains the preliminaries in control theory that is used in the thesis. A series of definitions in control are reviewed such as stability in the Lyapunov sense and passivity. This chapter has the objective to self-contain the necessary information, and can be overpassed for advanced readers in control theory.

3.1 Analysis of Nonlinear Dynamic Systems

The relevant DC/DC converter is a nonlinear dynamic system, where only the voltage equation is nonlinear due to the compensated modulation. Even though only one of the equations are nonlinear, this nonlinear relationship is making the stability and system analysis more complex. To extract any relevant information, simplifications must be done. There are many ways of doing this, and most methods can be applied interchangeably.

3.1.1 General System Theory

For both linear and non-linear systems, the *equilibrium point* is an important property. For a set of differential equations describing the dynamics of a system such as in Equation

(3.1), the equilibrium point can be described as in Equation (3.2). As a consequence of the neglect of the PWM mentioned in the previous chapter, the presented theory will be limited to only consider *autonomous systems*, i.e., systems where the time variable not explicitly is appearing in the differential equations.

$$\frac{d\mathbf{x}}{dt} = \mathbf{f}(\mathbf{x}) \tag{3.1}$$

$$\mathbf{0} = \mathbf{f}(\mathbf{x}_{eq}) \tag{3.2}$$

It can be noted that all the derivatives are zero for the equilibrium point, meaning that the system is not changing over time. This means that the system has stabilized, or reached its steady state, for the values $\mathbf{x}_{eq}$. For a stable converter that has experienced some sort of disturbance, the equilibrium point contains the values that current and voltage stabilizes towards after a given time of the response.

This type of representation of the equations through matrices and vectors is called the state-space representation. The vector $\mathbf{x}$ consists of the different states of the system. The state variables are the variables used to describe the state of the system. Some examples of state variables are physical quantities such as voltage, current, velocity, but also fictive variables such as the ζ for the DC/DC system description.

Another important property of a system is the *eigenvalues*. For linear systems, the eigenvalues can solely determine if the system is stable or not. A description as in Equation (3.1) can be represented in matrix form, as in Equation (3.3) [39].

$$\dot{\mathbf{x}} = \mathbf{A}\mathbf{x} \tag{3.3}$$

Here, $\mathbf{A}$ is an n·n matrix, and the equations are linear. Then the system can be written as

$$\mathbf{A}\mathbf{x} = \lambda\mathbf{A} \tag{3.4}$$

where $\mathbf{x}$ is the eigenvector and λ is the eigenvalue. By rearranging Equation (3.4), Equation (3.5) can be obtained.

$$\mathbf{0} = (\lambda\mathbf{I} - \mathbf{A})\mathbf{x} \tag{3.5}$$

Here $\mathbf{I}$ is the identity matrix. For a solution of the system to exist, the determinant needs to be zero, as described in Equation (3.6).

$$0 = |\mathbf{A} - \lambda\mathbf{I}| \tag{3.6}$$

The eigenvalues can be calculated by solving for Equation (3.6), and then the characteristic equation can be found. By solving for λ, the eigenvalues can be obtained.

The eigenvalues can either be real or complex numbers. By investigating the eigenvalues, some conclusions regarding the system stability might be taken. For real eigenvalues,

if both values are negative, the system is stable. If one or both of the real eigenvalues are positive, the system is unstable. If the eigenvalues are complex, the real part of the complex numbers needs to be negative for the system to be stable. If not, the system is unstable [40].

The *eigenvectors* are also important in system theory. An eigenvector, or a characteristic vector, is defined as the n-column vector which when multiplied with the system matrix **A**, is equal to the eigenvalue λ times the same vector [41]. This relationship is explained in Equation (3.7) below, where ϕ_i is the eigenvector corresponding to the i-th eigenvalue.

$$\mathbf{A} \cdot \phi_i = \lambda_i \cdot \phi_i \qquad \text{for i=1,2,..,n} \tag{3.7}$$

The eigenvector must be nonzero, if not, the zero-vector would be an eigenvector for all spaces. ϕ_i is on the form

$$\phi_i = \begin{bmatrix} \phi_{1i} \\ \phi_{2i} \\ \vdots \\ \phi_{ni} \end{bmatrix}$$

As a part of the modal analysis which will be explained later, the difference between the left and the right eigenvectors is important. Equation (3.7) above is the right eigenvector. The n-row vector Ψ_i, known as the left eigenvector, can be as defined as in Equation (3.8) below [39].

$$\Psi_i \cdot \mathbf{A} = \lambda_i \cdot \Psi_i \qquad \text{for i=1,2,..,n} \tag{3.8}$$

The eigenvalues and eigenvectors are linked to a linear transformation, hence they have a different meaning for a nonlinear system. But, by linearizing the system-matrix, hence making it constant, a lot of information about the system can be retrieved. This information will be valid close to the point of interest, hence it is an efficient way to analyze the small-signal stability for nonlinear systems.

One way to linearize the system is to calculate the Jacobian matrix. The formula for the Jacobian matrix can be seen in Equation (3.9), for a 3x3 system representing the DC/DC converter system with inner-loop current control evaluated in the equilibrium point $\mathbf{x}_{eq}$.

$$A = \left.\frac{\partial f(x)}{\partial x}\right|_{\mathbf{x}_{eq}} = \left.\begin{bmatrix} \frac{\partial f_1}{\partial i} & \frac{\partial f_1}{\partial \zeta} & \frac{\partial f_1}{\partial v} \\ \frac{\partial f_2}{\partial i} & \frac{\partial f_2}{\partial \zeta} & \frac{\partial f_2}{\partial v} \\ \frac{\partial f_3}{\partial i} & \frac{\partial f_3}{\partial \zeta} & \frac{\partial f_3}{\partial v} \end{bmatrix}\right|_{\mathbf{x}_{eq}} \tag{3.9}$$

Now, by analyzing the matrix around the equilibrium point, the nonlinear system can be written in the same form as in Equation (3.3). This linear system can be analyzed through well-established linear system theory. It must be mentioned that even for systems with very nonlinear terms, the Jacobian matrix gives a pretty accurate impression of the system near the equilibrium point.

3.1.2 Modal Transformation

In order to obtain information about systems such as the linearized DC/DC converter system, multiple techniques have been established, all depending on what information is wanted about the system. For eigenvalue-analysis investigating the stability, the modal transformation is a very fundamental technique. The concept of the modal transformation is to transform the states into a domain of modes. Hence the equations representing the states will be represented as a linear combination of the modes of the system [42]. The resulting modal matrix is very practical in the analysis of the eigenvectors and eigenvalues of the modes of the system. The modes of the system, $z(t)$, are defined as in Equation (3.10) or (3.11).

$$z(t) = \Psi \cdot \Delta x(t) \tag{3.10}$$

$$\Delta x(t) = \phi \cdot z(t) \tag{3.11}$$

Where $x(t)$ is the states, $z(t)$ is the modes which are directly associated to one of the variables, and Ψ and ϕ are defined in Equation (3.7) and (3.8) above.

By utilizing the relationship from Equation (3.11), Equation (3.3) can be expressed as in Equation (3.12) below.

$$\phi \cdot \dot{z} = A \cdot \phi \cdot z \implies \dot{z} = \phi^{-1} \cdot A \cdot \phi \cdot z \tag{3.12}$$

As a consequence, the description becomes like in Equation (3.13) below.

$$\dot{z} = D \cdot z \tag{3.13}$$

For an 3x3 matrix the result would be as in Equation (3.14).

$$\frac{d}{dt}\begin{bmatrix} z_1 \\ z_2 \\ z_3 \end{bmatrix} = \begin{bmatrix} \lambda_1 & 0 & 0 \\ 0 & \lambda_2 & 0 \\ 0 & 0 & \lambda_3 \end{bmatrix} \cdot \begin{bmatrix} z_1 \\ z_2 \\ z_3 \end{bmatrix} \tag{3.14}$$

The system in Equation (3.14) has the generic solution shown below.

$$z(t) = \begin{cases} z_1(t) = z_1(0) \cdot e^{\lambda_1 t} \\ z_2(t) = z_2(0) \cdot e^{\lambda_2 t} \\ z_3(t) = z_3(0) \cdot e^{\lambda_3 t} \end{cases}$$

Hence, the solution and dynamics of the modes can easily be found. But, the main purpose of analyzing a dynamic system, is to relate the dynamics of the system to the state variables of the system. The modes are hence of no interest, and for practical and analytical reasons, the relationship between the modes and the states must be found [43]. This relationship is found through the participation matrix, which is expressing how much each of the state variables is related to each of the eigenvalues of the modes. The generic participation matrix is seen in Equation (3.15) below.

$$\mathbf{P} = \begin{bmatrix} p_1 & p_2 & \dots & p_n \end{bmatrix} \tag{3.15}$$

Here, each of the p_i's have the relationship from Equation (3.16).

$$p_i = \begin{bmatrix} p_{1i} \\ p_{2i} \\ \vdots \\ p_{ni} \end{bmatrix} = \begin{bmatrix} \phi_{1i}\Psi_{i1} \\ \phi_{2i}\Psi_{i2} \\ \vdots \\ \phi_{ni}\Psi_{in} \end{bmatrix} \tag{3.16}$$

By calculating the participation matrix, it is hence possible to obtain information about the eigenvalues of the state-system and thereof also information about the dynamics of the system [44].

3.1.3 Block-triangular Matrices

A particular type of linear matrices that will be useful for our purposes, is one with a block-triangular structure [45]. The block triangular matrix can either be lower or upper triangular, as shown in respectively Equation (3.17) and (3.18).

$$A_L = \begin{bmatrix} A_{11} & 0 \\ A_{21} & A_{22} \end{bmatrix} \tag{3.17}$$

$$A_U = \begin{bmatrix} A_{11} & A_{12} \\ 0 & A_{22} \end{bmatrix} \tag{3.18}$$

Each A_{ij} is representing a sub-matrix of the original matrix, and have the dimensions of $A_{11} \in \mathbb{C}^{n\times n}$ and $A_{22} \in \mathbb{C}^{m\times m}$. One example of upper block triangular matrix, is seen below.

$$A = \begin{bmatrix} 3 & 2 & 4 \\ 1 & 5 & 2 \\ 0 & 0 & 1 \end{bmatrix} = \left[\begin{array}{ccc:c} 3 & 2 & 4 \\ 1 & 5 & 2 \\ \hdashline \dots & \dots & \dots \\ \hdashline 0 & 0 & 1 \end{array}\right] = \begin{bmatrix} A_{11} & A_{12} \\ 0 & A_{22} \end{bmatrix} = A_U$$

which can be divided into sub-matrices as demonstrated above, hence becoming as in Equation (3.18).

If the original matrix A can be divided into sub-matrices as described, with a null matrix either on the upper or lower triangle, it can be formulated as a block triangular matrix, and it holds the properties that now will be explained.

The main advantage of the block triangular matrices is that the eigenvalues of the sub-matrices are also eigenvalues of the original matrix, A. In other words, if a matrix can be divided into a block triangular one, it is possible to determine the eigenvalues of the original matrix only by calculating the eigenvalues of the diagonal sub-matrices. This is a

very useful property that can simplify the analysis and calculations of the eigenvalues of a big system [45].

3.1.4 Gershgorin Circle Theorem

Sometimes, when the eigenvalues are too complex and hard to calculate, a possible way to obtain information about the eigenvalues is by calculating some bounds for them [46]. Gershgorin circle theorem is one way of bounding the eigenvalues for a square matrix. The theorem returns circles in the complex plane which contain the eigenvalues of the system. Hence it is not possible to determine the exact value of the eigenvalues. But if some criteria are fulfilled, it is possible to determine the location or scale of the eigenvalues.

The theorem can easily be mathematically proven, as in [46], and the result can be seen in Equation (3.19).

$$|\lambda - A_{ii}| \leq \sum_{c \neq i} |A_{ic}| \tag{3.19}$$

Here, λ is the eigenvalue, A_{ii} is the diagonal element of row i, and the sum over A_{ic} is representing the summation of the absolute value of all the other elements on that specific row, i.

The more important part is the understanding of the theorem and its practical applications. The theorem states that, for an arbitrary matrix, it can be created circles for all of the n rows in the matrix. The circle representing each row should have its center in a_{kk} and a radius equal to the sum of the absolute values of the other elements in that row. Then, the resulting circles are representing the domain of the eigenvalues of the modes. In other words, the eigenvalues of the modes of the system will be within the created circles.

The issue with this theorem is that it is unknown where within the circles the eigenvalues are. Hence, a further extension of the theorem will be explained. First, if one Gershgorin circle is by itself, meaning not overlapping or including any other circles or points, exactly one eigenvalue will be within that circle. Secondly, if two circles are intersecting, or overlapping, there must be exactly two eigenvalues in the union of the circles. As a consequence, if n circles are overlapping, there must be exactly n eigenvalues within the union of the circles.

As a consequence of this extension, it would be possible to distinguish the different eigenvalues into different places in the complex plane, if the Gershgorin circles are not overlapping.

3.2 Control Design and Stability

When designing the control and topology of a converter, there are many challenges. For the DC/DC converter in focus, the nonlinear contributions are demanding to handle. From the specialization project, it is known that a Lyapunov analysis can be carried out for some

criteria. The most critical criterion is the TSS between current and voltage, also described in the specialization project. To sum it up, the TSS is making sure that the current-state is reaching its steady-state much faster than the voltage-state is. Hence it is possible to only focus on the dynamics from the voltage equation. In Chapter 4 the TSS is taken more into account, and some derivations and calculations regarding how to ensure it is presented. Further on some theory that is essential for reaching the objectives of the control design for a stability-preserving converter with plug-and-play features will be presented. In order to be able to analyze the nonlinear system, the Lyapunov theory will first be presented, then the passivity theory that can ensure stability for interconnections will be explained.

3.2.1 Lyapunov

To determine the stability for a nonlinear system, a couple of methods have been suggested. Both Vidiasagar (1993) and Khalil (1996) have created a work frame for analyzing nonlinear stability [47, 48]. Some of the most acknowledged theories are Lyapunov stability and input-output stability, and a plurality of theorems based on these to prove or disprove stability for nonlinear systems. Since Lyapunov stability was investigated in [1] and proved itself to be very useful, it will be of great interest for this project as well.

Lyapunov stability is a theory for describing and determining equilibrium stability for nonlinear systems. A stable equilibrium point is a point in which solutions starting close to this point, stay near to this point. By "close to" the point is it meant that when time goes towards infinity, the solution is equal to or nearby the equilibrium point, and not increasing or decreasing towards $\pm\infty$. If the solution after some time is equal to the equilibrium values, the system is said to be asymptotically stable.

Assume an autonomous system as described in Equation (3.1). **x**(t) is assumed continuous, and to have a different solution for every starting conditions. This can, for instance, be the case if **f** is Lipschitz continuous, as defined in Equation (3.20),

$$||\mathbf{f}(t, \mathbf{x}) - \mathbf{f}(t, \mathbf{y})|| < k||\mathbf{x} - \mathbf{y}|| \tag{3.20}$$

where **x** and **y** are defined for all values within a ball of a given radius from the starting conditions. k is defined as a Lipschitz constant. Further on in the analysis of the equilibrium point, the point will be assumed to be in the origin for simplicity reasons. This will not cause any kind of loss of generality. A definition of the stability of the equilibrium is needed, as the one mentioned by Khalil [48] (p.112).

Definition 1. *The equilibrium point at x = 0 of Equation* (3.1) *is:*
stable if, for every $\epsilon > 0$, there is a $\delta = \delta(\epsilon) > 0$, s.t

$$||x(0)|| < \delta \implies ||x(t)|| < \epsilon, \forall\, 0 \leq t$$

and asymptotically stable if, defined as stable, and in addition a δ can be chosen s.t.

$$||x(0)|| < \delta \implies \lim_{t \to \infty} x(t) = 0$$

and unstable if not defined as stable.

With this ϵ-δ way of analyzing the stability of an equilibrium point, the Lyapunov theorem can be stated as in [48](p.114).

Lyapunov's Stability Theorem. *If x = 0 is an equilibrium point of Equation* (3.1)*, and $D \subset R^n$ is a domain including x = 0. Now, $V : D \rightarrow R$ is a continuous and differentiable function s.t.*

$$V(0) = 0, \text{ and } V(x) > 0 \text{ in } D - \{0\} \tag{3.21}$$

$$\dot{V}(x) \leq 0 \text{ in } D \tag{3.22}$$

Then x = 0 is a stable equilibrium. Further on, if in addition

$$\dot{V}(x) < 0 \text{ in } D - \{0\} \tag{3.23}$$

Then x = 0 is an asymptotically stable equilibrium point.

The Lyapunov theorem has through history been proven to be an essential part of nonlinear analysis and will be so in this thesis as well. *Lyapunov's indirect method* is another well established nonlinear theorem. The theorem generally states that by linearizing a continuous and differentiable function, $\dot{x} = f(x)$, in the equilibrium point, some conclusions regarding the stability can be drawn. If the real parts of all eigenvalues are negative, the equilibrium point is asymptotically stable [48] (p.139). In Appendix B.1 the requirements of a Lyapunov function are explained and derived mathematically for the inner-loop dynamics of the relevant converter-system. An extension of Lyapunov theory called passivity, that will be very central for the later control-design, will further on be explained.

3.2.2 Passivity

Some specialists are proposing a new way to treat the control of physical systems [49, 8]. The idea is for some systems to move away from the signal-processing viewpoint, which is by far the standard way to do it today, and to do the controller design based on more physical concepts. The main reason why this traditional control theory for some electrical power systems must be renewed is that numerous of the assumptions for model-based signal theory will not be valid for future applications. Some of the most common ones are the linearity of the dynamics and interconnections of subsystems. Another concern is that through the signal-processing analysis there is only a focus on the stability, and not very much on the physical background of the system. Of course, the most important element is to determine if the system is stable or not, but for industrial applications, the actual performance is important as well. By integrating physical properties such as energy into the system-models, more physical information about the system could be obtained [7].

In general, the control of a system can be seen as multiple interconnections between passive elements. Analyzing the "energy" of these passive elements is then a way of interpreting the stability and stabilization of the system. The one fundamental property for this

way of analyzing stability is called passivity. Passivity is highly related to another important term, namely energy-shaping. The general idea of the passivity based control (PBC) is to consider the system from an energy processing viewpoint. A dynamic complex and nonlinear system can be analyzed in terms of the energy of its subsystem and through the physical energy laws as energy-transformation, and then by interconnecting and adding up the energies of the sub-systems to determine the performance of the total system. Most physical systems often have a relationship describing the energy-conservation of the systems, including supplied energy and dissipation. For PBC the control objective is to preserve these energy-conservation laws, but with some new functions for dissipated energy and supplied energy. Summed up the idea is to shape the energy to be considered at the controller by creating a new energy function and to change the dissipation structure. A huge advantage is that it not only can analyze stability but also the dynamic performances while stabilizing [49, 7]. Additionally, the need for nonlinear cancellation with high gain and feed-back and feed-forward terms are not needed. One third and very prominent advantage is that energy is a concept understood by professionals within control, power, and mechanics, etc. and can hence work as a "lingua franca", i.e. a common language, for different disciplines [7].

More specifically, the system is seen as dynamic sub-port-systems, interconnected with each other through ports that have the unit of power. For the converter system or a DC-microgrid bus-bar, the power is a result of the multiplication of current and voltage. The first actual control objective is regarding the steady-state behavior, i.e. controlling the equilibrium-values. These values are mainly determined by the shape of an energy-function. It is assumed that the system fulfills the energy-balancing relationship, as described in Equation (3.24).

$$H[x(t)] - H[x(0)] \leq \int_0^t u^\top(s)y(s)ds - d(t) \tag{3.24}$$

The left-hand-side of the equation is the stored energy within the system, while the term $d(t)$ is representing the non-negative dissipated energy. The integral-term is representing the energy that is supplied to the system, where u and y is representing the power variables, for instance the voltage and current, or the output-variable and the control-variable. This equation implies two essential points; first that the energy of an uncontrolled system is non-increasing. Secondly, if the energy storage function $H(x)$ is positive the total possible energy that can be extracted from the passive system is bounded.

A definition for a passive system is a system in which there can't be extracted more energy from the system than what it was supplied with [50]. This relationship can be described for electric power applications through a mathematical expression, as seen in Equation (3.25) [51].

$$\int_{-\infty}^{\tau} P_{in}(t)dt = \int_{-\infty}^{\tau} u(t)^\top y(t)dt \geq 0 \tag{3.25}$$

In general, passivity and stability are highly related, since they both are related to poles and zeroes in the left-hand-side of the complex plane [51]. The reason why the

theory of passivity is of great interest related to the control of converters is, hence, because it can ensure stability for the converter. This is only if an energy-function such as a Lyapunov-function candidate and the input/output variables fulfill the previously mentioned demands.

One type of system that automatically will fulfill the mentioned demands, is a port-Hamiltonian (pH) system. A formulation of such a system is defined as seen in Equation (3.26) and (3.27) below [52].

$$\dot{x} = [J(x) - R(x)]\nabla H + G(x) \cdot u \tag{3.26}$$

$$y = G^{\top}(x)\nabla H \tag{3.27}$$

The vector x is the system states and u is the control mechanism. J is defined as $-J^{\top}$, which is the structure/interconnection matrix and R is the dissipation/damping matrix. G is the system input matrix and H is the Hamiltonian energy storage function. Typically, the (shifted) Hamiltonian function is a natural candidate for a Lyapunov function of the system, which is based on the physical quantity of energy. As presented in [52], it follows that the equilibrium hence can be stabilized with a PI-controller, and that stability can be achieved even in the case of an uncontrolled system [53], even for the shifted, ie. incremental, system.

The procedure for applying passivity to the converter-system in order to ensure the stability of it will now be described. First, the passivity of the system must be provided. By this is it meant to find an energy storage function that follows Equation (3.24), and hence makes sure that the mapping of $u \rightarrow y$ is passive. This can be done by showing that the output is greater or equal to the change of the energy in the system. When passivity is proven, the system can be shifted in such a way that the minimum energy of the system will be at the steady-state, i.e., equilibrium value. In [53] it has been proven that for nonlinear RLC-circuits, such as the DC/DC converter, the system can be stabilized globally with a straightforward PI controller, as long as the electric energy storage function is convex. Hence stability for a passive system is obtained, with operating conditions at the wanted operating point.

3.2.3 Properties of Passive Systems

A commonly applied property of passive systems is related to *interconnection* [54]. There are plenty of theorems stating the fact that the interconnection of two passive systems H_1 and H_2, is also passive. The different theorems all depend on the way the two systems are connected. Say that a system is obtained by the feedback interconnection, then it can easily be proven that the new system is passive. Say that

$$S(x) = S_1(x_1) + S_2(x_2)$$

where S_1 and S_2 are representing the energy functions of the two passive systems H_1 and H_2, and $S(x)$ hence is the total system. Then the energy of the feedback interconnection

can be expressed as

$$S(x(T)) - S(x(0)) \leq \int_0^T (u_1^\top y_1 + u_2^\top y_2) ds$$

For an interconnected feedback-system y_1=u_2 and $u_1 = U_{ref} - y_2$ which simplifies to

$$S(x(T)) - S(x(0)) \leq \int_0^T U_{ref}^\top y_1 ds$$

which proves that the feedback interconnection is also passive [55].

A natural question is what happens if a system does not mathematically fulfill the passivity-demands. This can be the case for instance if the definition of the system, as in Equation (3.26), has a negative dissipation matrix R. This leads to a *lack of passivity*. It is possible to compensate for this lack of passivity, by enforcing it via an output feedback. This is demonstrated for a shifted system in [56] Proposition 7. For the case of interest in this thesis, it will be shown that by changing the power direction of the converter, the dissipation matrix of the system becomes positive, and thus the system will have a lack of passivity. By taking this into account and compensate for it through output feedback, i.e. for instance an outer loop controller, it is possible to compensate for the lack of passivity and stabilize the system.

The lack of passivity might arise due to many different reasons. In [57] shortage and excess of passivity are formulated as a mathematical problem. By letting Equation (3.24) be the base, it can be reformulated as in Equation (3.28).

$$H[x(t)] - H[x(0)] \leq \int_0^t u^\top(s) y(s) ds - (\gamma - k) \cdot \int_0^t u^\top(s) u(s) ds \tag{3.28}$$

By definition, this system is passive as long as γ is greater or equal than k.

Chapter 4

Time-Scale Separation of Inner-Loop Dynamics

This chapter is analyzing the TSS of the inner-loop system. It is of great interest that the TSS is ensured by design and not by chance, which was the case in the specialization project [1]. By designing the converter-system and the control-system in such a way that the TSS is ensured, the derived Lyapunov function in Appendix B.1 is valid, and the non-linear voltage-dynamics can be analyzed. A direct eigenvalue-method will first be applied, before the theory from Chapter 3.1 will be utilized to develop a control design for the inner-loop.

For some dynamic systems, the system itself can be divided into subsystems, each with different time-scales of the dynamics. For a generic converter-system, this can imply different order of magnitude on the rate of convergence of the dynamics for the current and the voltage. For the relevant DC/DC converter-system, the system parameters and the control parameters can be chosen and designed to ensure this time-scale separation (TSS) between the dynamics of the current and the dynamics of the voltage.

The DC/DC converter model with the PI-regulator with feed-forward term and under compensated modulation and in current-control mode has been presented in Chapter 2.4, and the descriptive equations are repeated in Equation (4.1)-(4.3) for convenience.

$$L\frac{di}{dt} = -R_s \cdot i + K_p(i_{ref} - i) + K_i \cdot \zeta \tag{4.1}$$

$$\frac{d\zeta}{dt} = i_{ref} - i \tag{4.2}$$

$$C\frac{dv}{dt} = -I_s + i \cdot \frac{V_s - K_p(i_{ref} - i) - K_i \cdot \zeta}{v} \tag{4.3}$$

If the dynamics of the current is approximately 10 times faster than the dynamics of the voltage, the TSS between the voltage and current is a reality. This is implying that the

current dynamics are significantly faster than the voltage dynamics, hence it is possible to consider the current equation at first, and subsequently assume that the current has stabilized and only consider the voltage dynamics. This second step is instrumental for this thesis and is equivalent to restricting the Lyapunov analysis to the so-called *zero-dynamics manifold*; i.e., Equation (4.3) with $i = i_{ref}$. This will significantly simplify both the stability analysis and the outer loop control design methodology. However, the validity of the results will depend on whether the TSS exists between current and voltage dynamics. Thus, it is key to ensure via parametric tuning of the controllers that the TSS is always achieved.

The third-order dynamical system of interest consists of two linear equations, (4.1) and (4.2), and one nonlinear equation, (4.3), it has 8 parameters and 3 unknown variables or states. The goal is to determine some limitations or restrictions for the parameters in such a way that the current dynamics have a faster response than the voltage dynamics. For a linear system, an eigenvalue analysis of the system would be useful to obtain information about the dynamics. Even though the system is partly nonlinear, an eigenvalues analysis will be completed for the system. But, the approach is not as straight-forward as for a linear system.

The objective is to find some restrictions or relationships between the parameters, in such a way that it is possible to obtain the TSS by design, i.e. by changing the system parameters. In other words, to be able to design the converter and tune the controller in a way that the TSS always is present. The approach is to apply the theory presented in Chapter 3.1 and step-wise obtain some mathematical relationships for how the TSS can be achieved.

4.1 Eigenvalue Analysis

For nonlinear systems, there are some different approaches for the purpose of analyzing the system dynamics and stability. As commonly known, nonlinear system analysis is often very complex and it is hard to obtain any relevant information about the system. It is hence necessary to do linearizations and to approach the problem in a simplified, yet efficient, way. In [58] different methods and approaches for solving such nonlinear systems are suggested and presented. The main methods are by Lyapunov theory, orbital stability such as Poincaré, the method of successive approximations, and the point transformation method. One possible approach, and the one chosen in this thesis, is to simplify the system by linearization and analyze the eigenvalues of the system in a small-signal manner. By analyzing the eigenvalues of the simplified system, some conclusions can be drawn about the rate of convergence for the different variables. Since the objective is to ensure a TSS between the fast current dynamics and the slower voltage dynamics, the ζ variable will be of the least interest.

The system from Equation (4.1)-(4.3) can be formulated in matrix-form as in Equation (4.4)

$$\dot{\vec{x}} = \begin{bmatrix} \dot{i} \\ \dot{\zeta} \\ \dot{v} \end{bmatrix} = \begin{bmatrix} f_1(i,\zeta) \\ f_2(i) \\ f_3(i,\zeta,v) \end{bmatrix} \tag{4.4}$$

where f_1, f_2 and f_3 represents respectively Equation (4.1), (4.2) and (4.3). It is essential to notice that only the differential voltage-equation is dependent on the voltage-state, while all three equations are dependent on the current-state.

To linearize the system the Jacobian matrix A (explained in Chapter 3.1.1) is calculated, in order to present the system as

$$\dot{\vec{x}} = \mathbf{A} \cdot \vec{x}$$

For the DC/DC converter, when the relevant equations are inserted and calculated, the linearized system is evaluated around the equilibrium point

$$\vec{x}^* = \begin{bmatrix} i_{ref} \\ \zeta^* \\ v^* \end{bmatrix}$$

and becomes as in equation (4.5).

$$A = \begin{bmatrix} \frac{-R_s - K_p}{L} & \frac{K_i}{L} & 0 \\ -1 & 0 & 0 \\ \frac{V_S + K_p \cdot i_{ref} - K_i \cdot \zeta^*}{C \cdot v^*} & -\frac{i_{ref} \cdot K_i}{C \cdot v^*} & \frac{i_{ref} \cdot (K_i \cdot \zeta^* - V_s)}{C \cdot {v^*}^2} \end{bmatrix} \tag{4.5}$$

Since this is a PI-controller in current-mode it can be noted that the current is reaching its reference value in the equilibrium.

When starting the eigenvalue analysis, the characteristic equation is important. The matrix in Equation (4.5) has the following general characteristic equation

$$0 = a\lambda^3 + b\lambda^2 + c\lambda + d \tag{4.6}$$

where

$$a = -1$$

$$b = \left(\frac{i_{ref}}{C \cdot {v^*}^2}\right) \cdot (K_i \cdot \zeta^* - V_s) - \frac{R_s + K_p}{L}$$

$$c = \left(\frac{R_s + K_p}{L}\right) \cdot \left(\frac{i_{ref}}{C \cdot {v^*}^2}\right) \cdot (K_i \cdot \zeta^* - V_s) - \frac{K_i}{L}$$

$$d = \left(\frac{K_i \cdot i_{ref}}{L \cdot C \cdot {v^*}^2}\right) \cdot (K_i \cdot \zeta^* - V_s)$$

It can be noted that it is a very complex equation with very many parameters that affect the solution. By doing the modal transformation of this system, explained in Chapter 3.1.2,

the resulting solution can give much information about the rate of convergence of the linearized system. This means that the value of the eigenvalue is directly saying something about the rate of convergence for the different variables. The generic solution of Equation (3.14) from Chapter 3.1 is justifying this. Of course, all of them must be negative, to obtain a stable system. But a negative yet high amplitude value for one of the eigenvalues would mean that this state variable has a fast rate of convergence and is reaching its "solution" or steady-state value very quickly.

By solving Equation (4.6) for λ_i, the different eigenvalues can be found. These are important for the modal transformation, hence for the final goal of obtaining information about the rate of convergence. It was attempted to analytically obtain any information about the correlation between the parameters. But due to a very complex solution where the relationship is arduous to conclude with, this was not possible. A MATLAB-script was created with the purpose of solving Equation (4.6). Both the MATLAB-script and the resulting solution can be found in Appendix B.2.

Since it is hard to obtain any information from the solution in Appendix B.2, another approach is to solve and analyze the eigenvalues numerically. By numerically testing for different parameter values in MATLAB it is possible by trial-and-error to obtain a much larger negative eigenvalue for the current than for the voltage, hence the TSS. A MATLAB script was created for this purpose, and it can be found in Appendix A.1.

A numerical approach is great for the purpose of validating or observing the system dynamics, but it is a poor tool when the goal is to obtain analytical insight in the system such that design criteria can be decided. To obtain a more analytical relationship between the parameters, first, some interesting properties of block-triangular matrices were used in order to simplify the mathematical expressions.

It can be observed that matrix A from Equation (4.5) has the form

$$A = \begin{bmatrix} A_{1,1} & A_{1,2} & 0 \\ A_{2,1} & 0 & 0 \\ A_{3,1} & A_{3,2} & A_{3,3} \end{bmatrix}$$

where the matrix can be rewritten and modified to become as in Equation (4.7).

$$A = \begin{bmatrix} \vec{A}_{11} & \vec{0} \\ \vec{A}_{21} & \vec{A}_{22} \end{bmatrix} \tag{4.7}$$

In this case,

$$\vec{A}_{11} = \begin{bmatrix} A_{1,1} & A_{1,2} \\ A_{2,1} & 0 \end{bmatrix}, \vec{0} = \begin{bmatrix} 0 \\ 0 \end{bmatrix}, \vec{A}_{21} = \begin{bmatrix} A_{3,1} & A_{3,2} \end{bmatrix}, \vec{A}_{22} = A_{3,3}$$

By applying theory from Chapter 3.1 it is known that the eigenvalues of the sub-matrix $\vec{A}_{11}$ will be eigenvalues to the matrix A. The eigenvalue of the other sub-matrix, $\vec{A}_{22}$, will also be an eigenvalue of A. In other words, the eigenvalues of A will be the *union* of the

eigenvalues of $\vec{A}_{11}$ with those of $\vec{A}_{22}$. This is justified by the theory of block-triangular matrices. This leads to the following three eigenvalues:

$$\lambda_1 = -\frac{R_S + K_P}{2 \cdot L} - \sqrt{\left(\frac{R_S + K_P}{2 \cdot L}\right)^2 - \frac{K_i}{L}} \tag{4.8}$$

$$\lambda_2 = -\frac{R_S + K_P}{2 \cdot L} + \sqrt{\left(\frac{R_S + K_P}{2 \cdot L}\right)^2 - \frac{K_i}{L}} \tag{4.9}$$

$$\lambda_3 = \frac{i_{ref}}{C \cdot V^{*^2}}(K_i \cdot \zeta^* - V_s) \tag{4.10}$$

In Equation (4.8)-(4.10) a direct relationship between the parameters and the eigenvalues is obtained, and some trends and relations between the parameters can be concluded. But still, it is unknown which eigenvalues are related to which states, and additionally, the expressions are complex and not very easy to analyze.

The problem with these eigenvalues is that they are representing the rate of convergence of the different *modes*. For the purpose of this project, it is interesting to know the relationship between each of the eigenvalues and the different *states*, because it says something about the rate of convergence of the current and voltage. As a consequence of the block-triangular property, the eigenvalue λ_3 in Equation (4.10) is corresponding directly to the voltage-state. Consequently, the participation factors of the eigenvalues must be calculated to relate the two remaining eigenvalues to the current-state and the ζ-state.

A MATLAB script was created for the purpose of calculating the participation matrix and the eigenvalues. This MATLAB script can be found in Appendix A.1. It was tested for different, yet realistic, values of the parameters. The values applied for this case, and for some of the coming physical representations and tests of the converter which is being presented below, the parameter values are as in Table 4.1.1. The values are highly inspired by [59, 60, 61], and are similar to the values from [1].

Table 4.1.1: Values applied for the analysis of the TSS of the inner-loop.

Parameter	**Value**
V_s, voltage source	700 V
R_s, resistance	1.1 Ω
C, capacitance	0.001 F
L, inductance	0.01 H
I_s, current source	20 A
K_p, inner loop P-gain	30
K_i, inner loop I-gain	10
i_{ref}, reference current	40 A

The resulting normalized participation matrix can be seen in Equation (4.11) below.

$$P = \begin{bmatrix} 0 & 0.0010 & 0.9990 \\ 0 & 0.9990 & 0.0010 \\ 1 & 0 & 0 \end{bmatrix} \tag{4.11}$$

The resulting vector consisting of the eigenvalues of the modes can be seen below.

$$\vec{\lambda} = \begin{bmatrix} -15.2439 \\ -0.3216 \\ -3109.678 \end{bmatrix}$$

It can be observed that all eigenvalues are real and negative, hence providing stability. The most interesting part is to compare the eigenvalues to the participation matrix. It can be concluded that the first eigenvalue from $\vec{\lambda}$ is belonging to the voltage-state, the second eigenvalue mainly to the ζ-state, and the third one mainly to the current-state. This basically means that all of the eigenvalues of the modes are belonging to each one state. As a consequence of MATLAB rearranging the order of the eigenvalues, each of the eigenvalues from $\vec{\lambda}$ have to correspond to one of the equations above. From Equation (4.8)-(4.10), this connects λ_1 to the current, λ_2 to the ζ-state, and λ_3 to the voltage.

It can be seen that the eigenvalue of the current is more than a hundred times as big in amplitude as the eigenvalue of the voltage. This means that for our case the rate of convergence, or in other words the response-time of the current, is way faster than for the voltage. The two solutions can be plotted to state this, and the two different functions are visualized in Figure 4.1.1.

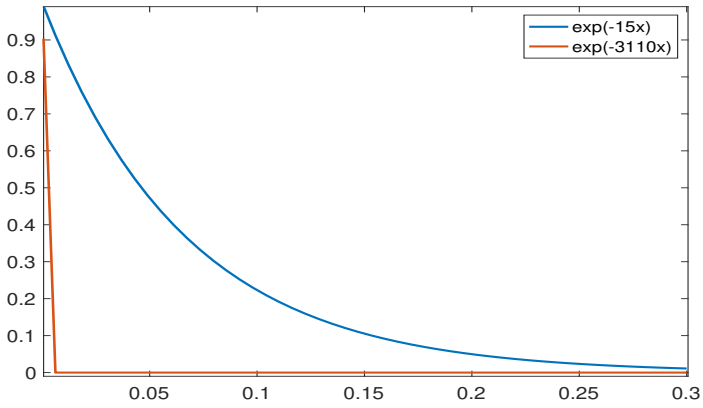

Figure 4.1.1: The solutions of the differential equations for current in red and voltage in blue for a given set of parameters, to emphasize the significant difference between the two eigenvalues and the corresponding rate of convergence.

This is visualized in order to truly understand that the time-scale of the current response is much faster than the voltage response, in the converter. But in order to find some

heuristic restrictions of the parameter values, the eigenvalue-expressions from Equation (4.8)-(4.10) must be evaluated. Through analysis of the participation matrix and the corresponding MATLAB-script, it has been concluded that Equation (4.8) is the eigenvalue dominated by the current-state, Equation (4.9) by the ζ-state, and Equation (4.10) by the state of voltage. Since the goal is to obtain a TSS between the current and the voltage, the eigenvalue dominated by the current-state must be "much bigger" than the eigenvalues dominated by the voltage. By "much bigger", a relationship where the current-eigenvalue is at least 10 times more negative than the voltage-eigenvalue is approved.

Assuming that both eigenvalues are negative, this basically means that

$$|\lambda_{current}| \geq 10 \cdot |\lambda_{voltage}|$$

where $\lambda_{current}$ corresponds to λ_1 from Equation (4.8) and $\lambda_{voltage}$ to λ_3 from Equation (4.10). When the expressions are inserted this gives the relationship in Equation (4.12).

$$-\frac{R_S + K_P}{2 \cdot L} - \sqrt{\left(\frac{R_S + K_P}{2 \cdot L}\right)^2 - \frac{K_i}{L}} \leq \frac{10 \cdot i_{ref}}{C \cdot V^{*2}}(K_i \cdot \zeta^* - V_s) \tag{4.12}$$

By making some justified assumptions, the inequality can be rewritten. The assumptions are as following:

$$\frac{R_S + K_P}{2 \cdot L} > 0$$

$$\left(\frac{R_S + K_P}{2 \cdot L}\right)^2 > \frac{K_i}{L}$$

$$\frac{10 \cdot i^*}{C \cdot V^{*2}} > 0$$

All of these assumptions will be fulfilled for any carefully chosen values of K_p and K_i. If the assumptions are all fulfilled the following relationship, that is a rewrite of Equation (4.12), would ensure a TSS.

$$V_s \leq \frac{\sqrt{\left(\frac{R_S+K_P}{2 \cdot L}\right)^2 - \frac{K_i}{L}} + \frac{R_S+K_P}{2 \cdot L} + \frac{10 \cdot i^* \cdot (K_i \cdot \zeta^*)}{C \cdot V^{*2}}}{\frac{10 \cdot i^*}{C \cdot V^{*2}}}$$

This is a pretty perplexing inequality that is containing many parameter-relationships and can still be considered as complicated to base the design criteria on. Without any more assumptions, this is the best that can be done with this direct eigenvalue method. For a more simple expression, another approach must be taken.

4.2 Gershgorin Circles Analysis

In order to view the problem from a different angle, the theory of Gershgorin circles is applied. This theory was explained in Chapter 3.1.4 and is essential for simplifying the

parameter-relationship and being able to interpret the relationship between the parameters. A MATLAB-script that visualizes the three Gershgorin circles from the equations in (4.5) was created. The script can be found in Appendix A.2. The resulting plot can be seen in Figure 4.2.1 below. The black circle is representing the current-row, the red circle is the voltage-row, and the blue one is the ζ circle. The ζ-circle is actually just a dot (radius = 0) and additionally very close to the red center, hence it is hard to see. The values for this plot are the same as the ones from Table 4.1.1.

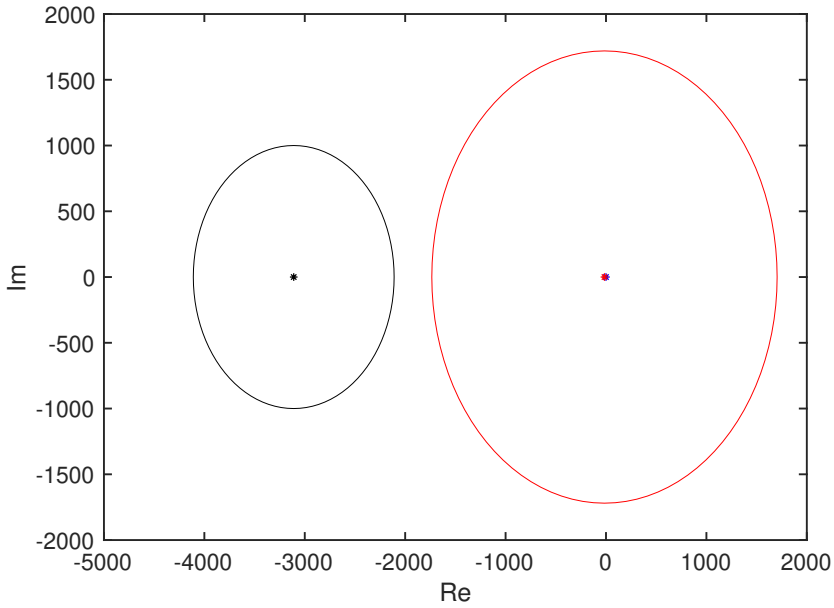

Figure 4.2.1: Gershgorin circles for the matrix A, showing TSS. The black circle is representing the domain of the location of the current-eigenvalue, and the red circle is representing the same for the voltage-eigenvalue.

From Figure 4.2.1 is it possible to conclude that there is in fact a TSS between the current and the voltage. This is true since the circles are separated, and the highly current-dominated circle is to the left of the voltage-dominated circle. Therefore, the eigenvalue has to be more negative for the current than for the voltage.

In order to obtain an analytical relationship between the parameters to ensure the TSS, the theory explained in Chapter 3.1.3 about block triangular properties was utilized. By exploiting the block-triangular structure shown in Equation (4.7), $\vec{A}_{11}$ and $\vec{A}_{22}$ can be analyzed separately. A direct consequence of this is that $\vec{A}_{22}$ has one single element ($A_{3,3}$), and therefore the radius of the voltage circle is zero and the eigenvalue representing the voltage-state is shown as a single point in the Gershgorin analysis. This can be seen in Figure 4.2.2. The values from Table 4.1.1 were applied, but the inductance was increased

to be 0.1 H in order to decrease the distance between the circles. Hence, for lower values of the inductance, the TSS is even greater.

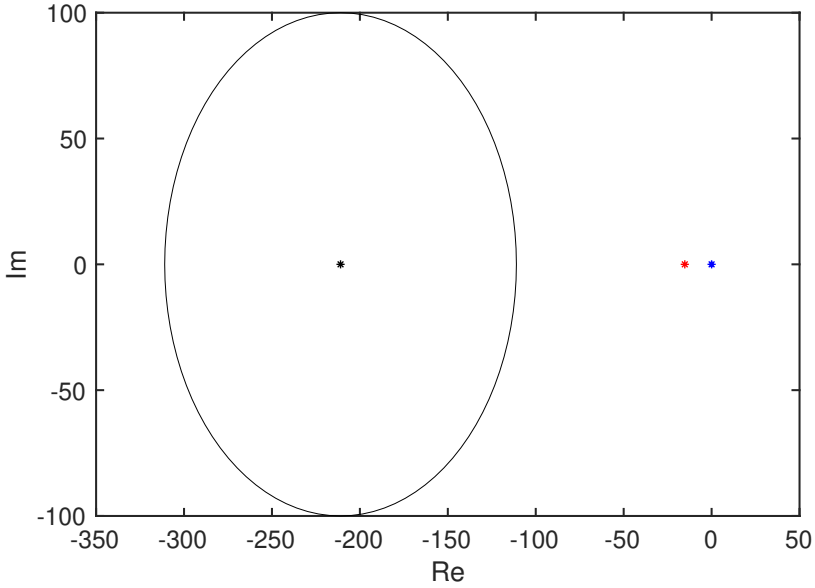

Figure 4.2.2: Gershgorin circles of the matrix A, when utilizing the block triangular properties. The red dot is the voltage-eigenvalue, the blue dot is the ζ-eigenvalue, and the black circle is representing the domain of the location of the current-eigenvalue.

Now, the objective is to separate the current-circle from the voltage-dot, and that the current-circle is located to the left of the voltage-dot. This demand is given by Equation (4.13) below, which forces the current circle center plus its radius to be less than the voltage eigenvalue.

$$-\frac{R_s + K_p}{L} + \frac{K_i}{L} < \frac{i_{ref}}{C \cdot V^{*2}} \left(K_i \cdot \zeta^* - V_S\right) \tag{4.13}$$

The terms to the left are representing the right-most point of the current-circle, and the term to the right is representing the voltage-dot. It can be seen that the parameters with the major influence on the center and radius of the circles are the inductance, the capacitance, and the tuning constants K_i and K_p. To further simplify the expression, some practical assumptions can be done. It is assumed that R_s is neglected, that $K_i\zeta^* - V_S \approx -V_S$, and that the inductance is greater than the capacitance by a generic constant, i.e. that $L = \alpha C$. These are relatively accurate assumptions, since both R_s and $K_i\zeta^*$ often are small. A direct consequence of neglecting R_s is that $K_i\zeta^*$ is zero as well, since $K_i\zeta^*$ is representing the voltage drop on R_s. Then the mathematical expression in Equation (4.13) simplifies to the expression in Equation (4.14).

$$\frac{-K_p}{\alpha} + \frac{K_i}{\alpha} < \frac{-V_s \cdot i_{ref}}{V^{*2}} \tag{4.14}$$

This gives the relationship between the two tuning parameters, as can be seen in Equation (4.15).

$$K_p > K_i + \alpha \cdot \frac{V_s \cdot i_{ref}}{V^{*2}} \tag{4.15}$$

The first interesting finding from this is that in order to guarantee through Gershgorins theorem that the system has a TSS between its current and voltage dynamics, the K_p must be greater than K_i plus a term dependent on the operating conditions and the design of the converter. It must be bared in mind that the resulting Equation (4.15) is based on some simplifications. But yet, the main result is somehow valid due to the assumptions being realistic. The second interesting finding is that by increasing the proportional tuning parameter, K_p, the center of the current-disk will be moved to the left. This basically allows us to separate the discs by increasing K_p. The question is how big the tuning parameter must be. As seen in Equation (4.15) K_p must be greater than K_i plus a term dependent on the converter-design and the operating conditions. The fraction in the last term is the reference current multiplied with the voltage source, divided by the obtained steady-state voltage squared. In general, this term will be small in magnitude, and for the values in Table 4.1.1 in the order of 10^{-2}. This small term is multiplied with the relationship factor α. It can hence be concluded that for very big inductance relatively to the capacitance, K_p needs to be very big relative to the K_i in order to separate the circles. It can be noted that as long as

$$L \leq 100 \cdot C$$

the last term of Equation (4.15) is in the same order of magnitude as the values of the tuning parameters. So for any greater relationship, i.e. bigger inductance's, the TSS might be destroyed.

4.3 Analysis and Discussion

By adding a safety margin to the expression in Equation (4.13) the TSS between current and voltage can be assured. The first term on the left-hand side of Equation (4.13) is representing the center of the Gershgorin circle, while the second term is representing the radius of the circle. On the right-hand side the equilibrium point of the voltage-state is represented. This equation can be interpreted in a logical way to explain the relationship between the parameter values and the TSS of current and voltage.

- First of all, it can be noted that the bigger K_P is, the better it is for the TSS. It forces the center of the Gershgorin disk of the current to the left, while it doesn't affect the voltage disk in any way, neither the radius of the current disk. So a high K_P is good in order to ensure a TSS.
- The R_S is also only affecting the center of the current-disk, and it is pushing it to the left. Hence an increasing R_S is also good for the TSS. However, in practical applications it is expected that this value is negligible.

- The inductance, L, is both affecting the radius and the center of the current-disk. A lower inductance will force the disk to the left, but at the same time increase the radius of the disk. In order for it not to overlap with the voltage-equilibrium point, the relationship between the other parameters is essential, in order to determine what has the most influence on the dimensions of the disk.
- It is wanted to not have a too big radius of the current-disk, and it is hence of interest that K_i is not too big. K_i is also affecting the voltage-equilibrium, and it is of interest that this equilibrium point is not too negative, to stay out of the current-disk. It can be seen that an increase in the K_i is good for the TSS because it moves the voltage-equilibrium to the right. But at the same time, since ζ^* is (normally) pretty small, the main wish is to keep K_i small in order to keep the radius of the current-disk small.
- The capacitance, C, is preferred to be big, to move the equilibrium of the voltage to the right. It is also wanted that the C is not many times lower than L because than the equilibrium of the voltage would be greater than the current-equilibrium. The most essential part in determining the value of the capacitance is to determine it in correlation with the inductance. The goal is not to get a too big α, i.e. L/C, because this would need to be compensated for with a great increase in K_p. A value of the capacitance approximately 10 times lower than the inductance is a good rule of thumb. This is adding a safety margin to the above derived expression of an inductance less or equal to 100 times the capacitance.

It is clear that it is a trade-off between the different parameters. Some of the most important relationships are highlighted above, but in the physical world, the design of converters is a battle between price, space, and operation among others. A very high C and L would be expensive to implement. So the cheapest and preferable solution is to be able to set the tuning parameters for the inner-loop, K_P and K_i, to obtain the TSS. But it is also clear that it is a good option to keep these findings/relationships in mind when designing the converter itself as well.

First, an approach with the direct eigenvalue-method was tested. The resulting equations and expressions were really hard to interpret, so no analytical insight was obtained from this approach. Then an approach with the Gershgorin theorem was tested, and gave a much more straight-forward result. Analytical insight was obtained, and therefore a design criterion could be derived. But this approach, exploiting the Gershgorins theorem, has some limitations/disadvantages. First of all, since the theorem is based on a linear system theory, the converter-dynamics had to be linearized around the equilibrium point. This is very precise around the equilibrium point, but for large signal-analysis it might not be that precise. Additionally, some assumptions were done while deriving the final relationship in Equation (4.15). It was mentioned that the assumptions were realistic, and that the result wasn't affected too much by them. The neglect of the resistance, R_S, was the first assumption. R_S is in reality small in value. The issue is that even though R_S is small, it is divided by an even smaller value, the inductance L. So the overall impact might actually be big. But, it can be seen from Equation (4.13) that an increasing R_S actually is good for the TSS, since it is pushing the center of the current-circle to the left. The neglect of the

the term $K_i\zeta^*$ immediately seems more unrealistic, due to the relatively high value of it. It must be emphasized that $K_i\zeta^*$ is representing the voltage drop on R_S, so by neglecting the resistance, $K_i\zeta^*$ becomes zero as a consequence. For the parameter values from Table 4.1.1 the term $K_i\zeta^*$ becomes equal to 44 V. But seen in relation to the term it is subtracted from, it is only 6 % of the voltage from the voltage source. So relatively speaking, this assumption is also precise. It can from Equation (4.13) be seen that the term $K_i\zeta^*$ actually is pushing the voltage-circle to the right, hence that it is good for the TSS. This means that if the result from Equation (4.15) which is neglecting the resistance and the term $K_i\zeta^*$ is giving a TSS, then the system without these assumptions would definitely give a TSS.

Since simplifications have been carried out in the process of determining the restrictions of the parameters in order to obtain a TSS, validation that the conclusions are correct must be carried out. This has been done by comparing the results with plots created by the computational tool from the specialization project [1] that was calculated numerically using *phase portraits*. The phase portrait will give an insight in the large-signal dynamics of the converter. For the values in Table 4.1.1 the resulting phase portrait of the converter dynamics is clearly showing a TSS between the current and the voltage. This can be seen in figure 4.3.1.

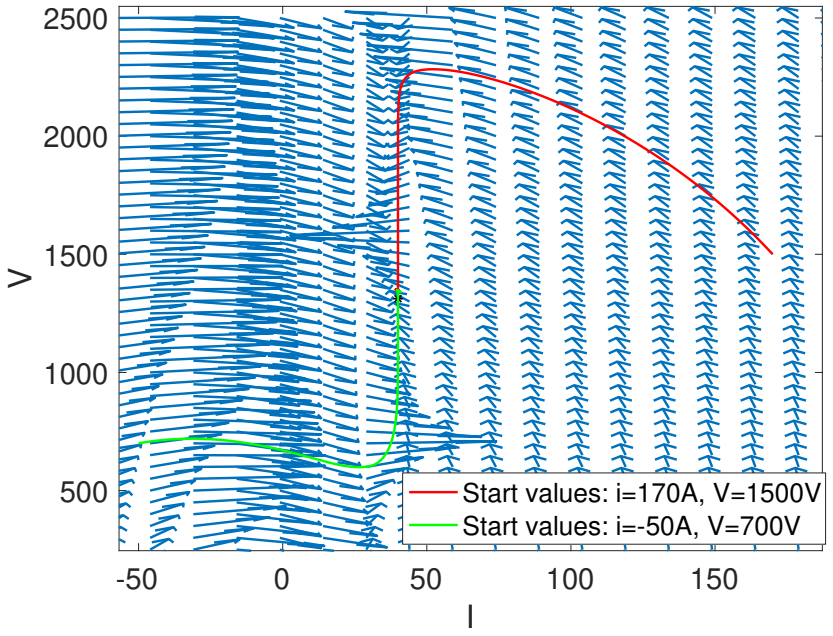

Figure 4.3.1: Phase portrait of a single DC/DC converter, clearly showing stability and a TSS in the case of large-signal disturbances. Current is on the x-axis and voltage on the y-axis, and the two streamlines represents two starting conditions.

It can be seen that in a large-signal analysis the zero-dynamics manifold of current

is present, i.e. the vertical “wall” appearing when the current is equal to the reference current. The streamlines for the two starting conditions are both reaching the steady state value of 40 A and 1310 V. Hence, the system is stable and the TSS is ensured.

Chapter 5

Passivity-Based Design of Unidirectional DC/DC Converter

The goal of this chapter is to add an outer-loop to the converter system, where the design is based on passivity. First, the mathematical derivations related to the passivity-based control-loop will be done. The reason why it is of great interest that the control is passivity-based, is because it then supports the plug-and-play features, i.e. it has the interconnection property. Then the system will be simulated and validated, to see if the findings match the reality. The converter, previously in current-control mode, will now be voltage-controlled via the implementation of an outer loop. The implementation of the outer-loop may be in conflict with the findings from the previous chapter, hence, if possible, some new design criteria for the system to obtain the TSS will be analyzed.

5.1 Derivation of PI-PBC

Assuming that the TSS between current and voltage is present, and hence that the current due to the PI-control already has reached the steady-state (reference) value, the inner-loop system dynamics can be represented by Equation (5.1).

$$C\frac{dv}{dt} = -I_s + \frac{i^* \cdot (V_S - K_i \cdot \zeta^*)}{v} = -I_s + \frac{e^*}{v} \cdot I^{ref} \tag{5.1}$$

The internal voltage, e, is described in Chapter 2.4, and $e^* = V_s - K_i \cdot \zeta^*$. The proportional-gain term is equal to zero because the current is equal to the reference-current due to the PI-control. Further on, by introducing the reference control-current

$$\tilde{I}^{ref} = I^{ref} - I_*^{ref}$$

and inserting it into Equation (5.1), Equation (5.2) below shows the new behavior of the dynamics.

$$C\frac{dv}{dt} = -I_s + \frac{e^* \cdot I_*^{ref}}{v} + \frac{e^* \cdot \tilde{I}^{ref}}{v} \tag{5.2}$$

Referred to Chapter 3.2, it is wanted to present the system in terms of energy. Accordingly, by exploiting that the charge in a capacitor (which is directly related to the energy stored in the capacitor) can be expressed as the product of the voltage and the capacitance, i.e., $q = C \cdot v$. Then the system-description in terms of charge can be presented as in Equation (5.3).

$$\dot{q} = -I_s + \frac{e^* \cdot I_*^{ref}}{v} + \frac{e^* \cdot \tilde{I}^{ref}}{v} \tag{5.3}$$

Further on, by introducing the incremental model, and exploiting the fact that

$$I_s = \frac{e^* \cdot I_*^{ref}}{v^*}$$

in steady-state, the relevant equation becomes as Equation (5.4).

$$\dot{\tilde{q}} = e^* \cdot I_*^{ref} \cdot \left(\frac{1}{v} - \frac{1}{v^*}\right) + \frac{e^*}{v} \cdot \tilde{I}^{ref} \tag{5.4}$$

By applying the Lyapunov function from the specialization project, which can be found derived and proven in Appendix B.1, the equation can be rewritten in a pH-way [62] as seen in Equation (5.5).

$$\dot{\tilde{q}} = -e^* \cdot I_*^{ref} \cdot \nabla V(v) + \frac{e^*}{v} \cdot \tilde{I}^{ref} \tag{5.5}$$

Here, the negative gradient of the shifted Hamiltonian, which will also serve as the Lyapunov-function, is inserted with $V(v)$ equal to

$$V(v) = \left(\frac{v}{v^*} - ln(v)\right) + (ln(v^*) - 1)$$

and hence the gradient is

$$\nabla V(v) = \frac{1}{v^*} - \frac{1}{v}$$

The second partial derivative of $V(v)$ is then equal to

$$\nabla^2 V(v) = \frac{1}{v^2}$$

which always is greater than zero, and therefore fulfilling the requirement to be global stable.

The time derivative of the system, expressed by the total derivative, is expressed in Equation (5.6).

$$\dot{V} = -\nabla V^\top \cdot e^* I_*^{ref} \cdot \nabla V + \nabla V^\top \cdot \frac{e^*}{v} \cdot \tilde{I}^{ref} \tag{5.6}$$

From Equation (5.6) it is possible to obtain information about the passivity of the system, hence also the control which can contribute to this passivity. Equation (5.6) can be divided into different parts to clarify the terms.

$$\dot{V} = -\nabla V^\top \cdot \underbrace{e^* I_*^{ref}}_{\mathrm{K}} \cdot \nabla V + \underbrace{\nabla V^\top \cdot \frac{e^*}{v}}_{y(v)^\top} \cdot \underbrace{\tilde{I}^{ref}}_{\tilde{u}}$$

$\dot{V}$ must be negative for it to fulfill the Lyapunov criterion mentioned in Chapter 3.2.1. From the expression above, K is a constant that needs to be positive to make the first term negative. This is done by selecting a reference direction for the current and then chose the current in that direction. This will always be the case as long as the converter is unidirectional, i.e. the reference current only is positive. In Chapter 6, the bidirectional converter will also be investigated. In that case, some other criteria need to be fulfilled, in order to provide the asymptotically stable Lyapunov function. From the above expression, $y(v)$ is the passive output equal to

$$y(v) = \frac{e^*}{v} \cdot \left(\frac{1}{v^*} - \frac{1}{v} \right) \tag{5.7}$$

and $\tilde{u}$ is the control signal. For a simple P-control, the $\tilde{u}$ can easily be set to $-K_p y$ and be shown to be negative, hence that the system is passive. The system is passive if Equation (5.8) is fulfilled.

$$\dot{V} \leq y^\top \cdot \tilde{u} \tag{5.8}$$

A solution more realistic and relevant from an industry point of view is the *PI-control*. By designing u correctly as a PI-controller, the control loop can assure global asymptotic stability. For PI-control, the terms added to the system is as in Equation (5.9) below.

$$\begin{aligned} u &= -K_{po} \cdot y - K_{io} \cdot \zeta_2 \\ \dot{\zeta}_2 &= y \end{aligned} \tag{5.9}$$

K_{po} is the outer-loop P-gain, and K_{io} is the outer-loop I-gain. At the equilibrium of the system, the states have the following values

$$\begin{aligned} u^* &= -K_{io} \cdot \zeta_2^* \\ y^* &= 0 \end{aligned} \tag{5.10}$$

It is still assumed that K is greater than 0 thus the system fulfills Equation (5.8), where $\tilde{u} = u - u^*$. V is only considering the proportional part of the control, so by applying a PI-control, the ζ-state of the system must also be included in the Lyapunov-function. This is done by adding the energy of the integrator state. The resulting proposal for a Lyapunov-function of the new system is seen in Equation (5.11)

$$W(v, \zeta) = V(v) + \frac{1}{2}(\zeta_2 - \zeta_2^*)^\top K_{io} (\zeta_2 - \zeta_2^*) \tag{5.11}$$

where $\dot{W} \leq 0$ is the criteria to be verified to use W as the new Lyapunov function. Now, it must be shown that this new energy-function $W(v, \zeta)$, is negative semi-definite, hence fulfilling this criterion. By calculating the total derivative and exploiting Equation (5.8)-(5.10), the following can be proven

$$\begin{aligned}
\dot{W} &= \dot{V} + [K_{io}(\zeta_2 - \zeta_2^*)]^\top \cdot \dot{\zeta}_2 \\
&= \dot{V} + [K_{io}\zeta_2 - K_{io}\zeta_2^*]^\top \cdot y \\
&= \dot{V} + [-K_{po}y - u - K_{io}\zeta_2^*]^\top \cdot y \\
&= \dot{V} - y^\top K_{po} y - u^\top y - (K_{io}\zeta_2^*)^\top y \\
&\leq y^\top \tilde{u} - y^\top K_{po} y - y^\top u + y^\top u^* \\
&= -y^\top K_{po} y \leq 0
\end{aligned} \tag{5.12}$$

which always is less than zero. In the last transition it is exploited that $\tilde{u} = u - u^*$. For the relevant system y is just a scalar, hence the last line of the derivation consists of y squared, which always is greater than zero, and K_{po} which is chosen to be a positive value. The last step is to show that the system is detectable, since it until now only has been proven global stability. This is done by analyzing the last term of the derivation in Equation (5.12), and to show that this expression only is zero when y is zero. y can be zero in two cases; first if v=v^*, and second if v is equal to infinity. However, since v equal to infinity imply an unstable system, it is proven that the system is stable and the only possibility is when v=v^*. This is proving asymptotic convergence, and consequently global asymptotic stability. Hence, the system is globally stable and the Lyapunov function is proper and fulfilling all the demands.

When designing this PI-PBC the determination of the control tuning-parameters K_{po} and K_{io} for the outer loop, is the essential choice. Positive values are a must, with respect to the above stability proof. One problem that remains to be solved is to obtain the correct parameter values to achieve a good performance of the converter.

The complete model considering the dynamics of the whole system and with a PI-PBC can be seen in Equation (5.13)-(5.16) below.

$$L\frac{di}{dt} = -R_s \cdot i + K_p(i_{ref} - i) + K_i \cdot \zeta_1 \tag{5.13}$$

$$C\frac{dv}{dt} = -I_s + \frac{(V_s - K_p(i_{ref} - i) - K_i \cdot \zeta_1) \cdot i_{ref}}{v} \tag{5.14}$$

$$\frac{d\zeta_1}{dt} = i_{ref} - i \tag{5.15}$$

$$\frac{d\zeta_2}{dt} = y = \frac{V_s}{v} \cdot \left(\frac{1}{v^*} - \frac{1}{v}\right) \tag{5.16}$$

From Equation (5.13) the inner loop control signal, earlier expressed as e, is equal to

$$e = V_s - K_p(i_{ref} - i) - K_i \cdot \zeta_1$$

and the term i_{ref}, or the reference current control signal, is equal to

$$i_{ref} = -K_{po}y - K_{io}\zeta_2$$

where y is the passive output signal, expressed as in Equation (5.7), with one small adjustment. From Equation (5.7) the term e^* was a part of the output, but for the chosen control system this term is modified to V_S. This is done mainly because this is a constant value that is independent in the system description, unlike the e^*-term. Additionally, the two values are pretty similar by definition, and the substitution will not influence the dynamics in a significant way, given that this change will only scale the control parameters K_{po} and K_{io}, without compromising the stability proof.

5.1.1 Outer Loop Dynamics

A SIMULINK model was created for the converter, assuming that the TSS is present, for the purpose of visualizing and verifying the above result about the passive outer loop. This was done in order to see if the outer loop is stabilizing with the same assumptions as the derivation is based on, and that the result is as concluded above. The values from Table 5.1.1 below were used. The converter-values, i.e. not the control parameters, are similar to the once chosen in [1], and highly inspired by [59, 60, 61].

Table 5.1.1: Values for the voltage outer-loop model.

Parameter	**Value**
V_s, voltage source	700 V
C, capacitance	500 μ F
L, inductance	5 mH
K_p, inner loop P-gain	15
K_i, inner loop I-gain	10
I_s, current source	20 A
V_{ref}, voltage reference	800 V
ζ_1^*, inner loop ζ_1-steady-state	2.6
K_{po}, outer loop P-gain	24/12
K_{io}, outer loop I-gain	10000/5000

In Figure 5.1.1 the resulting dynamics of the voltage from the model and script in Appendix A.4 is shown for two different sets of outer-loop tuning parameters. In the derivation of the passive output above, the e^* appeared, but for the control of the converter, this term is substituted with V_s, for reasons earlier explained. The chosen values of K_{io} and K_{po} are not tuned, but only randomly chosen. This is because the main purpose of this simulation is to show that the system is stable. K_p and K_i are chosen such that the

findings from the previous chapter related to the TSS for the inner-loop holds. The inner-loop parameters must be chosen in order to determine the steady-state of the ζ_1, since that term is appearing in the outer loop voltage equation.

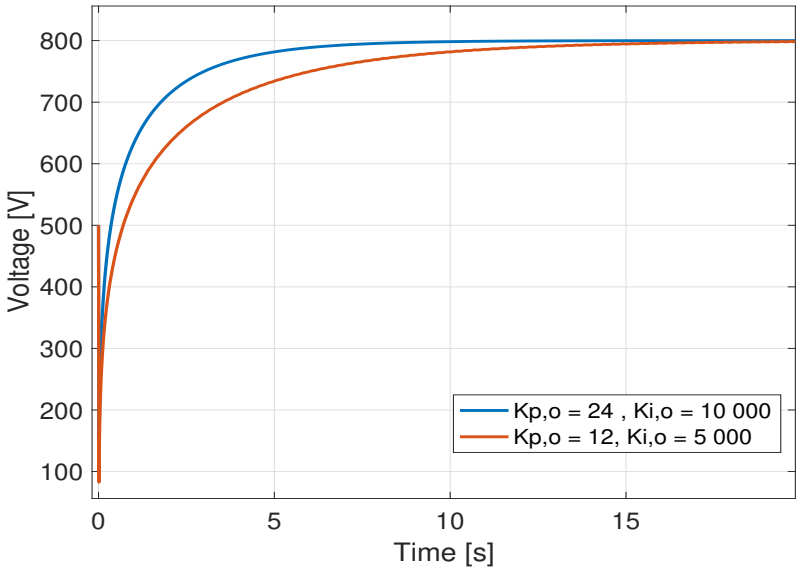

Figure 5.1.1: Voltage evolution with respect to time for two different values of K_{po} and K_{io} for the voltage outer-loop. TSS is assumed for this model and the resulting plot.

The tuning parameters must be very large to stabilize within the magnitude of seconds, and not minutes. As seen from Figure 5.1.1 the voltage is reaching its reference value and is hence stable. This complies with the above deviation of the PI-PBC. In the figure, the voltage dynamics are shown for two sets of tuning parameters. The parameters for the red graph are lower than for the blue graph, and as expected the blue graph is reaching its steady-state value faster than the red. Another thing that must be noted is that the response time is relatively slow, especially compared to the response time of the current. From the specialization project [1], a response time in the scale of milliseconds for the current was often present. This is also as expected due to the assumption of TSS between the current and voltage. But the model which only includes the outer loop and the voltage dynamics is simplified. A concern is that the design of the outer loop, even though it has a much slower response time, will break or destroy the assumption of the TSS. Even though the current in the inner loop has really fast dynamics, and the voltage dynamics are really slow as seen in the figure above, the concern is regarding the reference current. For the inner loop considered alone, the reference value is a constant current. But, when adding the PI-PBC for the outer loop, the reference current becomes dependent on the voltage dynamics. Hence it might not be correct to represent the voltage and current dynamics separately, because the influence of the new reference current on the current dynamics is unknown.

5.1.2 Dynamics of the Full System

Therefore, to make sure that the additional outer-loop doesn't destroy the TSS, another model that is showing both the current and the voltage dynamics has been created, in such a way that the overall dynamics can be analyzed. The SIMULINK model and the corresponding MATLAB code can be seen in Appendix A.5. The values chosen for the simulations can be seen in Table 5.1.2.

Table 5.1.2: Values for the full model.

Parameter	**Value**
V_S, voltage source	700 V
C, capacitance	500 μF
L, inductance	5 mH
R_s, resistance	1.1 Ω
K_p, inner loop P-gain	15
K_i, inner loop I-gain	10
I_s, current source	20 A
V_{ref}, voltage reference	800 V
K_{po}, outer loop P-gain	24
K_{io}, outer loop I-gain	10 000

The resulting current and voltage rate of change, i.e. derivatives, of the full converter can be seen in Figure 5.1.2 below, and the current and voltage evolution with respect to time can be seen in Figure 5.1.3.

It can be observed from Figure 5.1.2 that the current rate of change is very fast, compared to the voltage rate of change, which is slower. This is relevant since the dynamics are faster for the current compared to the voltage. The tuning parameters have to be very large in this case as well, in order to stabilize the system within seconds and not minutes. Also for smaller values of the outer loop tuning parameters the rate of change is way faster for the current compared to the voltage. From Figure 5.1.3 it can be seen that both voltage and current are reaching steady-state at approximately the same time. So it can be concluded that the dynamics of the current are faster than for the voltage, but due to the PI-PBC-loop the current is dependent on the voltage and they are reaching steady-state approximately at the same time.

One concern regarding the development of the outer loop is that it destroys, or complicates, the expressions to ensure the TSS that was found in Chapter 4. So, an analysis of the new system using the Gershgorin circle theorem will now be completed.

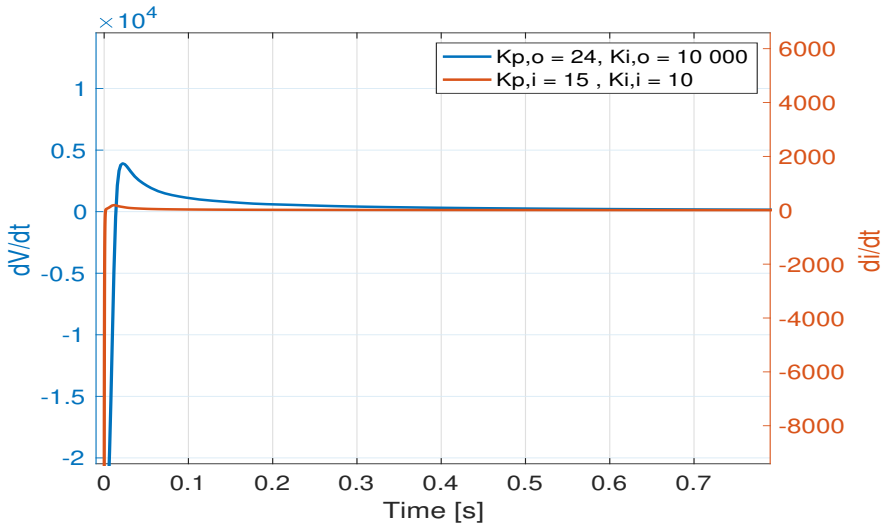

Figure 5.1.2: Voltage and current rate of change for the respectively outer-loop and inner-loop converter system. The rate of change for the voltage is shown in blue and is corresponding to the left y-axis, while the rate of change for the current is shown in red and is corresponding to the right y-axis.

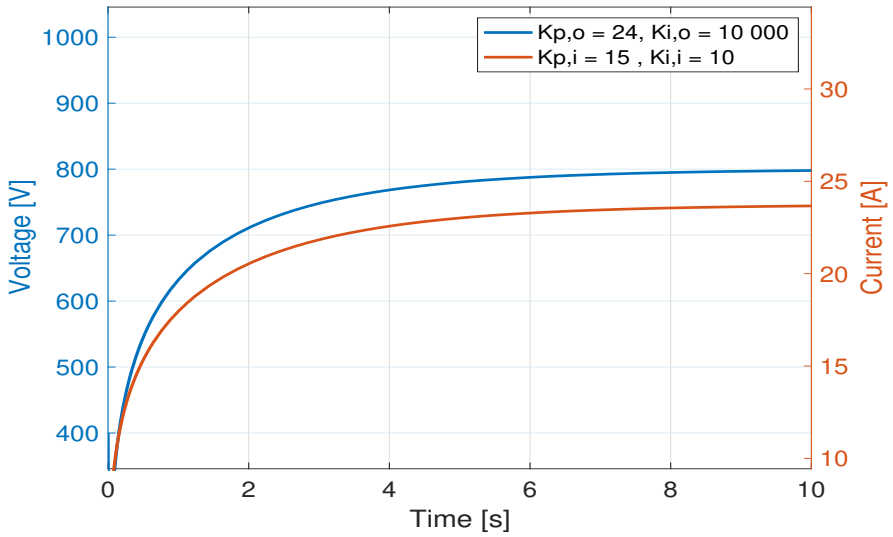

Figure 5.1.3: Voltage and current evolution with respect to time for the outer-loop and inner-loop converter system. The voltage is shown in blue and corresponds to the left y-axis, and the current is shown in red and corresponds to the right y-axis.

5.2 Design Criteria and Gershgorin Analysis

The first step of the Gershgorin analysis is to simplify the nonlinear and complex converter-system described in Equation (5.13)-(5.16) above. This is done by calculating the Jacobian matrix through a created MATLAB-scrip found in Appendix A.3. Then the Jacobian matrix is evaluated near the equilibrium point

$$\vec{x}^* = \begin{bmatrix} i^* \\ V_{ref} \\ \zeta_1^* \\ \zeta_2^* \end{bmatrix}$$

and the resulting A-matrix is seen in Equation (5.17) below.

$$A = \begin{bmatrix} -\frac{R_s+K_p}{L} & -\frac{K_p \cdot K_{po} \cdot V_s}{L \cdot V_{ref}^3} \\ \frac{K_p \cdot K_{io} \cdot \zeta_2^*}{C \cdot V_{ref}} & \frac{K_{po} \cdot K_p \cdot V_s \cdot K_{io} \cdot \zeta_2^*}{C \cdot V_{ref}^4} + \frac{K_i \cdot \zeta_1^* - V_S - K_p \cdot i^* + K_p \cdot K_{io} \cdot \zeta_2^*}{C \cdot V_{ref}^2} \cdot \left(\frac{K_{po} \cdot V_s}{V_{ref}^2} + K_{io} \cdot \zeta_2^* \right) \\ -1 & -\frac{K_{po} \cdot V_s}{V_{ref}^3} \\ 0 & -\frac{V_s}{V_{ref}^3} \end{bmatrix} \tag{5.17}$$

$$\begin{bmatrix} \frac{K_i}{L} & \frac{K_{io} \cdot K_p}{L} \\ -\frac{K_i \cdot K_{io} \cdot \zeta_2^*}{C \cdot V_{ref}} & -\frac{K_{io}^2 \cdot K_p \cdot \zeta_2^* - K_{io} \cdot (V_s - K_i \cdot \zeta_1^* + K_p \cdot (i^* - K_{io} \cdot \zeta_2^*))}{C \cdot V_{ref}} \\ 0 & K_{io} \\ 0 & 0 \end{bmatrix}$$

Further on some relationships will be exploited to simplify the expressions. First of all, $i^* = K_{io} \cdot \zeta_2^*$, and secondly, $e^* = V_s - K_i \cdot \zeta_1^*$. In steady-state, both of these relationships are valid. Then, the A matrix from Equation (5.17) can be rewritten as the A_1 matrix seen in Equation (5.18) below.

$$A_1 = \begin{bmatrix} -\frac{R_s+K_p}{L} & -\frac{K_p \cdot K_{po} \cdot V_s}{L \cdot V_{ref}^3} & \frac{K_i}{L} & \frac{K_{io} \cdot K_p}{L} \\ \frac{K_p \cdot i^*}{C \cdot V_{ref}} & \frac{K_{po} \cdot K_p \cdot V_s \cdot i^*}{C \cdot V_{ref}^4} - \frac{e^*}{C \cdot V_{ref}^2} \cdot \left(\frac{K_{po} \cdot V_s}{V_{ref}^2} + i^* \right) & -\frac{K_i \cdot i^*}{C \cdot V_{ref}} & -\frac{K_{io} \cdot K_p \cdot i^* - K_{io} \cdot e^*}{C \cdot V_{ref}} \\ -1 & -\frac{K_{po} \cdot V_s}{V_{ref}^3} & 0 & K_{io} \\ 0 & -\frac{V_s}{V_{ref}^3} & 0 & 0 \end{bmatrix} \tag{5.18}$$

This is the matrix describing the linearized dynamics that will be used for this analysis. Further on, the constant e^* will be replaced by V_s to further simplify the expressions. This is considered a good approximation for practical applications with low R_s, which result in voltages which are very similar in magnitude.

First, a mathematical analysis of the A_1 matrix will be done. The Gershgorin theory, presented in Chapter 3.1.4 is essential. The main goal, is to ensure the TSS. This can be done if the current-circle is to the left of the voltage-circle, and additionally, that the two

circles are not overlapping. The worst-case scenario with respect to the TSS is for the current eigenvalue to be the point most to the right within the current-circle. Likewise, the worst case for the voltage-eigenvalue is to be the point most to the left within the voltage-circle. These two points are expressed in respectively Equation (5.19) and (5.20), where the sub-indexes i and v represents the *current* and *voltage*, and the sub-indexes r and l represents the most *right* and most *left* point within the circles.

$$\lambda_{i,r} = -\frac{R_s + K_p}{L} + \frac{K_p \cdot K_{po} \cdot V_s}{L \cdot V_{ref}^3} + \frac{K_i}{L} + \frac{K_{io} \cdot K_p}{L} \tag{5.19}$$

$$\begin{aligned}\lambda_{v,l} =& \frac{K_{po} \cdot K_p \cdot V_s \cdot i^*}{C \cdot V_{ref}^4} - \frac{V_s}{C \cdot V_{ref}^2} \cdot \left(\frac{K_{po} \cdot V_s}{V_{ref}^2} + i^* \right) - \frac{K_p \cdot i^*}{C \cdot V_{ref}} \\ & - \frac{K_i \cdot i^*}{C \cdot V_{ref}} - abs\left(\frac{K_{io} \cdot (Vs - K_p \cdot i^*)}{C \cdot V_{ref}} \right)\end{aligned} \tag{5.20}$$

Since both eigenvalues are negative, the goal is to obtain the relationship in Equation (5.21).

$$\lambda_{i,r} < \lambda_{v,l} \tag{5.21}$$

If that is the case, it is through the Gershorins theorem proved that the eigenvalue of the current is more negative than the eigenvalue of the voltage. Later, after this mathematical analysis, the participation factors will be calculated and analyzed in order to prove that the eigenvalues of the *modes*, i.e. the eigenvalues in this Gershorin analysis, can be correlated to the eigenvalues of the *states*. The expression is Equation (5.21), can be simplified, by neglecting the terms with the lowest order of magnitude. Assuming a voltage, inductance, and capacitance in the same order as in Table 5.1.2, then all the terms that are proportional to the inverse of the reference-voltage cubed, mathematically expressed

$$t(V_{ref}) \propto \frac{1}{V_{ref}^3}$$

or higher order of the reference voltage, can be neglected. Additionally, to get rid of the absolute sign, it is assumed that V_s is greater than $K_p \cdot i^*$. Then Equation (5.19) and Equation (5.20) can be simplified to respectively Equation (5.22) and (5.23).

$$\lambda_{i,r} = \underbrace{-\frac{R_s + K_p}{L}}_{\text{center}} + \underbrace{\frac{K_i + K_{io} \cdot K_p}{L}}_{\text{radius}} \tag{5.22}$$

$$\lambda_{v,l} = \underbrace{-\frac{V_s \cdot i^*}{C \cdot V_{ref}^2}}_{\text{center}} - \underbrace{\frac{i^* \cdot (K_i + K_p)}{C \cdot V_{ref}} - \frac{K_{io} \cdot (Vs - K_p \cdot i^*)}{C \cdot V_{ref}}}_{\text{radius}} \tag{5.23}$$

Assuming that the conclusions from Chapter 4 holds, i.e. that the inductance is approximately ten times the capacitance, and that K_p is bigger than K_i, some interesting analytical relationships can be observed. First of all, it can be seen that the center of the

current-circle in Equation (5.22) is greater in order of magnitude than the voltage-circle center in Equation (5.23), and that both are negative. Further on, the K_p is pushing the current-circle to the left, and at the same time it is increasing the radius of the current-circle, as seen in Equation (5.22). But, if the K_{io} is chosen to be small, the effect of the increasing K_p with respect to the radius can be canceled out. This also counts for the last term of Equation (5.23) from above. Additionally, the K_p is increasing the radius of the voltage circle, seen in the second term of Equation (5.23), so the inner-loop tuning parameter can not be chosen to be as big as possible because it will lead to an overlap of the Gershgorin circles. This means that the K_p has an upper limit before it is destroying the possibility to ensure TSS by analytical design.

K_i must still be lower than the K_p, but the question is by how much. By analyzing the order of magnitude of the terms in the expressions of the circles, it can be seen that for very big values of the inner-loop parameters, the radius of the circles gets very big. So, if the parameters K_p and K_i are in the order of tens, and not hundreds, and at the same time K_p is approximately 3 times bigger than K_i, this will not be a problem. It was mentioned that K_{io} must be small in magnitude. Assuming that the earlier mentioned criteria are valid, then by small is it meant in the order of 10^{-1}, in order to cancel out the effect of K_p. This can be observed in the radius term of Equation (5.22).

It can be observed that the outer-loop parameter of K_{po} is not of great interest since it only appears in the terms with the smallest order of magnitude. But this finding is actually really important as well, since this implies that K_{po} has a high degree of freedom (DOF). K_{po} can be a really high value before it is affecting the result, and even then, it can be fixed by increasing K_p. This is of great interest for later, when investigating the bidirectional converter.

5.2.1 Analytical Interpretation

Since an analytical expression has been obtained, it is possible to obtain a deeper understanding of the impact of the parameter values with respect to the voltage and the current in the converter. The different terms in the analytical expressions and the parameters in these terms all have a different effect on the total result, where the goal is to achieve a design leading to a stable converter with the presence of TSS such that the mathematical derivations are guaranteed to apply.

The first topic is regarding the design of the converter itself, i.e. the resistance, inductance, and capacitance. The resistance is in most cases small and doesn't have too much influence in the analysis. But as seen in Equation (5.18), a higher Rs will lead to a more negative eigenvalue for the current, implying faster dynamics. The more interesting part is regarding the inductance and the capacitance. When analyzing the previously mentioned equation, it can be observed that the inductance is appearing in the denominator of all the current-related terms, while the capacitance is doing the same for all the voltage-related terms. It is not that surprising that the capacitance is related to the voltage dynamics and inductance related to the current dynamics, but what's interesting is the effect the two parameters have on the location and development of the Gershgorin circles. Since the goal

is to ensure the TSS, it can be seen that by designing L and C respectively low and high, the center of the circles can be separated in order of magnitude. A concern is to not exaggerate the low value of the inductance, leading to a very big radius of the current-circle, hence an overlap of the circles. So to sum it up, even though it is not always physically possible to do this, a low value of the inductance compared to the capacitance is helpful in obtaining the TSS. As mention in Chapter 4, an appropriate relationship between the two is an inductance approximately ten times the capacitance. This is a realistic physical relationship as well. But, to ensure that the Gershgorin circles are separated, a smaller difference between the L and C would be preferred. It can also be mentioned that the higher V_{ref} is, the smaller and more to the right is the voltage-circle. But by changing the reference voltage, other parameters such as the equilibrium current, i^* will change as well. So the net effect of an increasing reference-voltage is complex and depends on the change of the steady-state value for the current.

For instance, by setting the value of the inductance equal to the value of the capacitance, the K_{po} has an even higher DOF than earlier, meaning that it can be even higher in value. Additionally, the K_{io}, K_i and K_p can be increased more, and still obtaining the TSS. If on the contrary the inductance is lower than the capacitance, the parameters would have an even higher freedom still ensuring the TSS. So by changing the relationship between the L and C the total DOF for the design of the control-loops can be rapidly increased. This might be practical for some situations, for instance if the converter has very fluctuating and different operating conditions. But the concern is related to the practical consequences this has for the converter.

Further on, the control-parameters will be inspected analytically. Equation (5.22) and (5.23) will be the foundation when looking further into what terms the different parameters affect. For the mentioned terms all the current-relevant terms are divided by the inductance, while the voltage-related equations are divided by the capacitance times the reference voltage, possibly squared.

The first tuning variable is the P-gain for the inner loop, K_p. K_p is appearing in all terms, except for the term determining the voltage-circle center. This implies that K_p is both contributing to the TSS by moving the current-circle to the left, and counteracting it by increasing the radius of both circles; which might lead to an overlap of the circles. The next variable is the I-gain for the inner-loop, K_i. K_i is appearing in the voltage-radius term, scaled with a factor equal to the steady-state current. It is also appearing in the radius of the current-circle. Hence, the K_i is contributing to an increase in the radius of the circles. Further on the P-gain of the outer-loop, K_{po}, is up. K_{po} is not appearing in Equation (5.22) or (5.23), for reasons earlier explained. Hence, the A_1 matrix in Equation (5.18) must be investigated to obtain more information about it. From A_1 it can be observed that K_{po} is affecting the voltage-circle center. Since V_S in most cases is greater than the product of K_p and i^*, an increase in K_{po} is moving the voltage-circle to the left. But as can be seen, K_{po} must be really big in magnitude in order to actually affect the center. K_{po} also appears in the current-circle radius term, but yet again it must be really big to influence it. The last tuning parameter is the I-gain for the outer-loop, K_{io}. K_{io} is appearing in both

the radius of the voltage-circle and the current-circle. For the current-circle it is multiplied with K_p, while for the voltage-circle it is multiplied with the difference between V_S and $K_p i^*$.

By applying some approximations to Equation (5.22) and (5.23), an even more simplified expression will now be gone through. For simplicity reasons, it is assumed that $L = \alpha C$, where α is the relationship between the inductance and capacitance with the units of [H/F]. Additionally K_{io} and R_S are assumed to be very small in value, so they can be neglected. Since V_S is in the same order as V_{ref}, the two quantities will be chosen to be equal. Then the expression in Equation (5.24) will guarantee TSS and consequently stability.

$$\frac{-K_p + K_i}{\alpha} < -\frac{i^*}{V_{ref}} - \frac{i^*(K_i + K_p)}{V_{ref}} \tag{5.24}$$

Since the relationship between the reference voltage and the steady-state current is a number in the order of 10^{-2}, it will be neglected, and the expression in Equation (5.24) can be further simplified to the below expression.

$$\frac{K_p}{\alpha} > \frac{i^*(K_i + K_p)}{V_{ref}} + \frac{K_i}{\alpha}$$

This basically means that the TSS can be guaranteed for this example as long as

$$K_p > K_i \cdot \left(\frac{1 + \frac{i^* \alpha}{V_{ref}}}{1 - \frac{i^* \alpha}{V_{ref}}} \right)$$

or even shorter as

$$K_p > K_i \cdot \left(\frac{1 + \beta}{1 - \beta} \right) = K_i \cdot \kappa \tag{5.25}$$

where β is defined as $\frac{i^* \alpha}{V_{ref}}$. Of course this relationship is influenced by a lot of assumptions and will not be a hundred percent correct, but it catches the essence of the different control parameters. That is that the most important relationship is the relationship between K_p and K_i to achieve TSS, which is arguably not an intuitive one.

5.2.2 Visualization and Verification

In order to visualize and validate these findings, a MATLAB-script was created for the purpose of plotting the Gershgorin disks for different parameter values. The script can be found in Appendix A.6. The values chosen for these visualizations are all based on the findings mentioned in the previous section. For the plots, the values in Table 5.2.1 will be the base, and it will then be observed what the consequences of changing the parameter values are.

It can be seen that the relationship between the inductance and capacitance is 10, which referred to the example above implies that $\alpha = 10$. When calculating the reference current

Table 5.2.1: Values applied for the Gershgorin analysis of the full model.

Parameter	**Value**
V_S, voltage source	700 V
C, capacitance	500 μF
L, inductance	5 mH
R_s, resistance	1.1 Ω
K_P, inner loop P-gain	15
K_i, inner loop I-gain	5
I_s, current source	20 A
V_{ref}, voltage reference	800 V
K_{Po}, outer loop P-gain	10
K_{io}, outer loop I-gain	0.2

a $\beta \approx 0.3$ is obtain from Equation (5.25) , and a factor $\kappa \approx 2$. In the table the relationship between K_p and K_i is sat a bit higher, i.e. to 3 as a safety margin. For the parameter values in Table 5.2.1, where all of the findings are taken into account, the resulting Gershgorin circles can be seen in Figure 5.2.1 below.

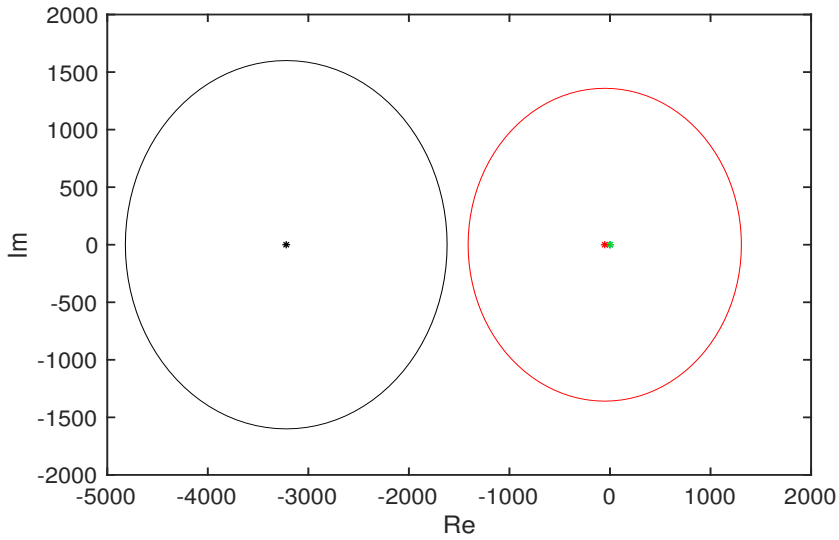

Figure 5.2.1: Gershgorin circles for the parameter values fulfilling the derived TSS design criteria. The domain of the current-eigenvalue is within the black circle, and the domain of the voltage-eigenvalue is within the red circle.

The black circle and dot are representing the current circle and center. The red circle and dot are representing the voltage circle and center. The green dot is representing the Gershgorin circle for the ζ_1 and ζ_2 states. These circles are centered around (0,0), and

have a very small radius compared to the voltage and current circles. Hence, they are only represented as a small dot. As expected with the chosen parameter values, designed by the Gershgorin disk theorem, it resulted in two separate disks. From the expansion of the Gershgorins theorem, it can hence be concluded that the current-eigenvalue (given that the participation-factor, later to be investigated, confirms that the state and modes are related) is within the black circle. In the same way, the voltage-eigenvalue is within the red circle. It can then be observed that the eigenvalue of the current is many times more negative than the voltage eigenvalue, hence the TSS is present. Even though it looks from the figure that the circles are pretty close, the difference between them is in the order of hundreds. This is actually a big difference when it comes to the eigenvalue, and as described, the difference between the actual eigenvalues is probably much greater, since the distance between the disks is representing the worst-case scenario when it comes to the eigenvalues positioning within the circles. Since the voltage circle spans both the positive and negative domain of the real axis, and it is known that only negative eigenvalues are stable, it is of great interest that the actual eigenvalue of the voltage is in the negative part of the circle. This is a decent assumption to make since it from the simulations earlier was shown that the voltage is stabilizing towards its reference value. The eigenvalues will also be investigated in a bit when the participation matrix is analyzed.

The eigenvalues and the corresponding participation matrix for this system will now be analyzed in order to obtain more information about the system. As written earlier, the participation factor for the eigenvalues is really essential in this analysis, since they are connecting the eigenvalues of the modes, to the states of the system. This means that for the Gershgorin analysis the eigenvalues obtained can be connected to the states, i.e. voltage and current, in such a way that the result gets a practical meaning. A MATLAB script was created for this purpose. The resulting script can be seen in Appendix A.7. When the script is run with the parameters from Table 5.2.1, representing the Gershgorin circles in Figure 5.2.1 above, the following eigenvalues are obtained

$$\vec{\lambda} = \begin{bmatrix} -3219.7 \\ -51.96 \\ -0.3106 \\ -8.86 \cdot 10^{-6} \end{bmatrix}$$

It can be observed that all eigenvalues are negative, which implies that the system is stable. Further on, it is clear that the first eigenvalue is much bigger in magnitude than the second, the second bigger than the third, and the third bigger than the fourth. It is wanted that the first eigenvalue can be correlated to the current-state, in order to ensure the TSS. Compared to the Gershgorin circles in Figure 5.2.1, it seems like the center of the black circles is very close to the first eigenvalue of the vector, and that the red center is very close to the second eigenvalue. Up to now it has been assumed that the black circle can be correlated to the current-state, and that the red circle can be correlated to the voltage-state. The participation factor will be useful for the purpose of determining if this assumption is correct. Further on the script calculated the normalized participation matrix, which is seen in Equation (5.26) below.

$$P = \begin{bmatrix} 0.9999 & 0 & 0.0001 & 0 \\ 0 & 1 & 0 & 0 \\ 0.0001 & 0 & 0.9999 & 0 \\ 0 & 0 & 0 & 1 \end{bmatrix} \tag{5.26}$$

This means that the first eigenvalue above is almost completely described by the current-state. Additionally, the second eigenvalue is described by the voltage-state. This is very good for the analysis made this far because it confirms that the findings and conclusions regarding the TSS described through Gershgorin circles were correct.

In Figure 5.2.2 it is shown what happens with the Gershgorin circles in the case of violations of the design criteria mentioned above. In Figure 5.2.2a, K_i is changed from 5 to 10. This is rapidly increasing the radius of both of the circles, leading to an overlap of the Gershgorin disks. In this case, it can not through Gershgorins theorem be stated that the TSS is present, since it is unknown where the eigenvalues are located. It is only known that all of the eigenvalues have to be located within the union of the circles. It was mentioned that this problem could be solved by increasing K_p to about 3 times the values of K_i. By doing this, the circles are again totally separated.

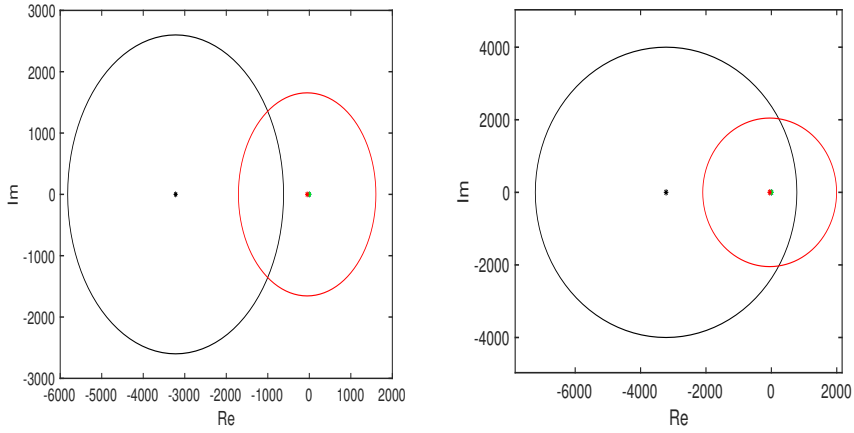

(a) K_i increased to 10.

(b) K_{io} increased to 1.

Figure 5.2.2: Gershgorin circles for two cases that are violating the design criteria. The circles are overlapping, and consequently it is not possible to ensure the TSS.

In Figure 5.2.2b, the outer-loop integral gain is increased from 0.2 to 1. Since K_{io} is counteracting the inner-loop gains to reduce the radius of the circles, increasing it would also increase the radii rapidly. This is leading to an overlap of the circles, and the conclusion from the previous paragraph applies here as well. The only way to separate the circles again is by increasing the capacitance and lowering the inductance, hence designing the converter all over again. So arguably the most important design criterion is to keep the K_{io} as low as possible.

The system with the modifications in parameter values from Figure 5.2.2 that were in conflict with the design criteria, was tested in the script calculating the eigenvalues and the participation-matrix from Appendix A.7. For both cases, the conclusion was the same. The eigenvalue representing the current was much larger than the eigenvalue representing the voltage. So even though it was not possible to ensure TSS through the Gershgorin analysis, the TSS was still present. The reason for this is that the result of the Gershgorin circles always is based on the worst-case scenario, further discussed below.

5.3 Analysis and Discussion

By designing the control of the converter based on passivity, it has been shown that the operation is stable and that the voltage is reaching the reference value, and additionally that TSS could be ensured by design.

The models that were created in SIMULINK had some simplifications involved since they were numerically calculated, and based on the Eulers method. The result can hence be influenced by the step length. For the simulations the SIMULINK standard step-length was chosen, and by varying it the result did not change much. It is known that for non-linear systems these types of tools are relatively precise, and it is to be believed that the findings still are valid. First of all, the PI-PBC outer loop is stabilizing towards the reference voltage, as wanted. Secondly, regarding the full converter model, the rate of change for the current is of greater magnitude than for the voltage, even though they reach steady-state approximately at the same time. This means that the current is reaching its reference value way faster than the voltage is. This may be potentially confusing to understand, but one way to interpret it is to say that while the voltage is changing, the current is reaching many temporary equilibrium points. But since the current reference is dependent on the voltage, the current can't reach the final equilibrium point that is matching the reference voltage before the voltage has reached its equilibrium point. It is shown that they do that approximately at the same time, or actually the current some milliseconds after the voltage.

When actually designing the control-loop parameters based on passivity, the Gershgorin theorem was the foundation for doing the eigenvalue-analysis. For the derivation of the PBC to definitely hold, or to be proven mathematically, the TSS needs to be present. In other words this means that if the TSS is present, the system is stable. This implies that the Gershgorin circle for the current must be to the left of the Gershgorin voltage circle, and also that the two circles don't overlap. In order to do the Gershgorin analysis, the Jacobian A-matrix must be calculated. This matrix is based on linearizations around the equilibrium point. Since the relevant converter system has some very nonlinear terms, this kind of linearization will not give a precise image of the converter in the whole domain, but for a small-signal analysis the result is pretty accurate.

Since the analytical insight and the design criteria are derived based on the Gershgorin theorem, a concern related to microgrids occurs. To find the Jacobian matrix, the equilibrium point must be available. For one converter with a given operating condition, this might be fine. But for a microgrid, the operating conditions might be dynamic and chang-

ing, implying trouble for the Jacobian matrix. One possibility is to analyze the system for the two most extreme values, i.e. the highest and lowest voltage equilibrium value, and do the control design based on this. Another possibility is to create some sort of adapting control design that is changing for different modes/operations of the converter. At last, a possibility is that the change of the steady-state value of the voltage actually doesn't influence the control design that much. Either way, this must be considered for the control design of a stability-preserving microgrid with plug-and-play features.

A drawback with the use of the Gershgorin theorem to predict the eigenvalues is regarding the condition of necessity and sufficiency. The Gershgorin theorem can only state a sufficient solution to the problem, i.e. if the circles are separated the TSS is present, while on the contrary if TSS is present it doesn't necessarily mean that the circles are separated. This can in theory lead to a big difference between the Gershgorin eigenvalue-circles and the actual eigenvalues that are necessary to get the TSS. But as shown in Chapter 4, it was very difficult to extract any kind of information from the eigenvalue-expressions that were obtained when analyzing the system by actually calculating the eigenvalues. Hence, in order to obtain some insight into the system and being able to relate both converter-parameters and control-parameters to the stability-analysis, a perspective such as Gershgorin is a great tool. By analyzing the equations of the Gershgorin circles it was possible to find some relationship between the parameter values, such that the previously mentioned relationship between the Gershgorin circle holds. These findings were also verified by plotting the Gershgorin circles for different parameter values. The main control design findings were:

- The conclusions from Chapter 4 holds. This means that K_p must be bigger than K_i, and that the inductance is approximately 10 times higher than the capacitance. It was developed a simplified expression, describing the relationship between L, C, K_i and K_p. From this expression, i.e. Equation (5.25), the design of the converter and inner-loop control can be inspired.

- K_p must be within the order of 10, and not bigger. This will lead to an overlap of the circles. If this is the case, then the K_i must be no higher than one-third of the K_p. Additionally, the sum of K_p and K_i must not be big, such that the radius of the voltage-circle is controlled. This is achieved if the previously mentioned demands are fulfilled.

- K_{io} must be small. This is in order to compensate for the bigger K_p, such that the circles don't overlap. K_{io} must be in the order of 10^{-1} and approximately 1/100 of the value of K_p.

- K_{po} is only appearing in the terms with a small order of magnitude, hence not affecting the result. This high DOF for this tuning variable is something that will be useful in the coming section. But for these results, as long as K_{po} does not have an order of magnitude in the range of 10^4-10^5 or higher, it will not affect the results.

Additionally, the findings were also verified by calculating the eigenvalues and the participation factors for the different sets of parameter values.

Equation (5.25) is very useful for designing the control of especially the inner-loop. But, the expression is based on some assumptions that now will be discussed. The first assumption, and the same assumption that was applied in Chapter 4, was the neglect of the resistance R_S. The same conclusion applies for this expression as for the one in the previous chapter. This means that by neglecting the resistance, the situations related to the TSS gets worsen since an increasing R_S is contributing to moving the current-center to the left. Hence, this is a good assumption to make in terms of the validity of the result. The next assumption done in order to derive Equation (5.25) is to neglect the outer-loop I-gain, K_{io}. Since K_{io} by design should be small in value this assumption can be done. But, as this tuning-parameter is affecting the radius of both the circles, just a small K_{io} might lead to an overlap of the circles. In addition, the terms containing K_{io} have a small denominator, such that even a small tuning-gain could actually lead to a big value. Hence, neglecting it might be a relatively imprecise assumption. But on the contrary, since K_{io} is designed to be small, the terms that mainly are determining the order of magnitude for the radius of the circles are not the terms containing K_{io}. So, some information about the radius of the circles gets lost with this assumption, but the main trends showing the big picture are safeguarded. Overall, it is a relatively reasonable assumption to do. The last simplification done, was to assume that V_S and V_{ref} can be seen as the same value since they are very similar in value. In this way the two terms can be removed from the expressions if they appear in both the denominator and numerator. For bigger differences between the two parameters than what is chosen in this project, this assumption might be imprecise. But roughly speaking, this is a fair assumption to do, especially when considering how much the resulting expression simplifies.

Based on these results, one important issue to discuss is the importance of K_{io}. From converter-control theory is it known that K_{io} should be great in order to rapidly reach zero steady state error. This was also tested in the SIMULINK-models, and verified. But from the Gershgorin analysis the conclusion was to keep K_{io} low. This will have consequences in the operation of the converter, where the outer-loop voltage slowly will reach its steady-state value. For higher values of K_{io} the eigenvalues were calculated from the MATLAB-script in Appendix A.7. The result was still that the current-eigenvalue was way more negative than the voltage-eigenvalue, i.e. that the system was stable and TSS present. So, a consequence of the Gershgorin analysis, and its sufficient-based conclusions, is that a lot of information gets lost. This means that Gershgorins theorem states that K_{io} must be low, but in reality it can be much higher than the theorem states. Hence, a more realistic and optimal control of the converter can in reality be achieved. So yet again it is seen that the Gershgorin theorem is powerful, but its results are clearly conservative.

Chapter 6

Passivity-Based Design of Bidirectional DC/DC Converter

From the previous chapter it has now been shown that it is possible to design a unidirectional converter based on passivity, such that the dynamics are stable. But in the physical world, and for all practical reasons, it is not very realistic nor of interest to have a DC-microgrid only consisting of unidirectional converters. Hence, it is of interest to investigate the bidirectional converter, in order to ensure that power can both be delivered and received for the converter. A consequence of this is that the current, more precisely the reference current, can be both positive and negative. This leads to some consequences for the passivity based derivations of the control, where the main problem is that this can lead to a lack of passivity. The solution is to quantify this lack of passivity, and then to compensate for it.

6.1 Mathematical Derivation and Analysis

The foundation for investigating the bidirectional converter is Equation (5.1)-(5.6). These are the equations that were part of deriving the passivity-property for the converter system. Equation (5.5) can be reformulated in a more convenient way for further analysis, as in Equation (6.1) below.

$$\dot{\tilde{q}} = -K \cdot \nabla V(v) + g(v) \cdot \tilde{I}^{ref} \tag{6.1}$$

K is a constant equal to the product of e^* and I_*^{ref}, i.e. a power, and $g(v)$ is the input vector equal to

$$g(v) = \frac{e^*}{v}$$

This leads to the derivative of the Lyapunov function of this energy-based (i.e. charge-based) system. This is the function that needs to provide passivity and is a reformulation of Equation (5.6). The resulting time-derivative energy-storage function that needs to be passive, is seen in Equation (6.2) below.

$$\dot{V}(v) = -\nabla V^{\top}(v) \cdot K \cdot \nabla V(v) + y^{\top} \cdot \tilde{I}^{ref} \tag{6.2}$$

where

$$y^{\top} = \nabla V^{\top}(v) \cdot g(v) \tag{6.3}$$

As a reminder $\tilde{I}^{ref}$ is the control signal. In Chapter 5.1 this clearly fulfilled the demand to be passive and had a relationship as expressed in (6.4).

$$\dot{V} \leq y^{\top} \cdot \tilde{I}^{ref} \tag{6.4}$$

Both e^* and I_*^{ref} were always positive, hence making the K from Equation (6.2) positive. This is the mathematical reasoning why the change of sign for the control signal, i.e. reference current, will lead to a lack of passivity. This lack of passivity is causing the Lyapunov function not to be proper. But, as suggested in [57] and [56], a solution exists. The first part is to quantify the lack of passivity, and the second part is to compensate for this lack with the help of the control-parameters. But, the first part is to quantify the lack of passivity, and that will be done by adding a zero term to Equation (6.2), and obtaining Equation (6.5). Both V, y and g are functions of the voltage v, but for practical reasons it is not included in the next equations.

$$\dot{V} = -\nabla V^{\top} \cdot K \cdot \nabla V + y^{\top} \cdot \tilde{I}^{ref} + \nabla V^{\top} \left[\gamma \cdot g \cdot g^{\top} - \gamma \cdot g \cdot g^{\top}\right] \nabla V \tag{6.5}$$

Further on, by rearranging the equation and extracting the negative part from the last term and inserting it with the K, it can be formulated as in Equation (6.6).

$$\dot{V} = -\nabla V^{\top} \cdot [K + \gamma \cdot g \cdot g^{\top}] \cdot \nabla V + y^{\top} \cdot \tilde{I}^{ref} + \nabla V^{\top} \cdot \gamma \cdot g \cdot g^{\top} \cdot \nabla V \tag{6.6}$$

Then, by exploiting the relationship from Equation (6.3), and formulating

$$y^{\top} \cdot y = ||y||_2^2$$

then the equation can be rewritten in a more convenient way, as in Equation (6.7).

$$\dot{V} = -\nabla V^{\top} \cdot [K + \gamma \cdot g \cdot g^{\top}] \cdot \nabla V + y^{\top} \cdot \tilde{I}^{ref} + \gamma \cdot ||y||_2^2 \tag{6.7}$$

Now, it is possible to achieve a negative first term, even though K is negative. This is done by finding a γ such that

$$K + \gamma \cdot g \cdot g^{\top} \geq 0 \tag{6.8}$$

If this is accomplished, an expression of the passivity such as in Equation (6.4) can be achieved. The new derivation of the control hence becomes as shown below in Equation (6.9), for a simple P-controller.

$$\begin{aligned}\dot{V} &\leq y^{\top} \cdot \tilde{I}^{ref} + \gamma \cdot ||y||_2^2 \\ &\leq -y^{\top} \cdot K_{po} \cdot y + \gamma \cdot y^{\top} \cdot y \\ &\leq -y^{\top} \cdot (K_{po} - \gamma) \cdot y\end{aligned} \tag{6.9}$$

Hence, the demand for the system to be stable is for

$$K_{po} \geq \gamma$$

where γ is the quantity representing the lack of passivity. So it can be seen that it is the outer-loop P-gain parameter that needs to compensate for the lack of passivity due to the negative reference current.

So, the next step is to investigate Equation (6.8), to find the correct γ. The inequality can be written as

$$\gamma \cdot g \cdot g^{\top} \geq -K$$

assuming the worst case for the passivity, meaning that the current is going in the wrong direction. Then

$$\gamma \cdot \left(\frac{e^*}{v}\right)^2 \geq e^* \cdot |I_*^{ref}|$$

since the output vector is only a scalar. Further on, solely expressing it in terms of the γ, the result gets as in Equation (6.10).

$$\gamma \geq \left|I_*^{ref}\right| \cdot \frac{v^2}{V_S} \tag{6.10}$$

Here it is assumed that $e^* \approx V_S$, which is a reasonable assumption utilized previously. From Equation (6.10) two different approaches can be taken towards the goal. The first approach, and the simplest one, is to determine some worst-case values for the current and the voltage, i.e. making v in addition to I_*^{ref} constant, and then determine γ and K_{po}. The second approach is to only consider I_*^{ref} constant and let the voltage vary. Since this leads to γ being a function of the voltage, the consequence of this is that the design of the outer-loop P-gain, K_{po}, also becomes a function dependent on the voltage.

The simplest case will be investigated, and the first step is to determine some maximal values for the voltage and current. The current value represents the maximum current the system can operate with before being destroyed, and the same counts for the voltage. One example is that for currents higher than the maximum current the cables will start to melt, and for voltage the insulation will break. Insulation and protection is a complex and important topic related to both converters and the power system, but it will not be in focus in this project. Since the exact rated values are not the importance of this project, while on the contrary the order of magnitude is, some literature was the foundation for determining the maximum voltage and current [63, 64, 65]. It must be emphasized that the values are not necessarily correct, but they do not have to be since the focus is the worst-case values

and not the actual rated values. Additionally, compensating for the lack of passivity is the focus, and the concept is shown here regardless of the accuracy of the mentioned values. Hence, the chosen worst-case values for the current and voltage can be seen in Table 6.1.1.

Table 6.1.1: Maximal values for the current and the voltage while determining γ.

Parameter	**Value**
V_{max}, maximal voltage	$3{\cdot}V_{ref}$ [V]
I_{max}^{ref}, maximal current	$3{\cdot}I_S$ [A]

When applying the values from Table 6.1.1, the following rule counts for the lack of passivity and the tuning parameter

$$K_{po} \geq \gamma \geq 27 \cdot I_S \cdot \frac{V_{ref}^2}{V_S}$$

When inserting the values applied in the previous chapter, i.e. from Table 5.2.1, the following limitation is obtained for the outer-loop tuning variable

$$K_{po} \geq 27 \cdot 20 \cdot \frac{800^2}{700} = 493714$$

This basically means that if K_{po} is sat that high, then it would definitely compensate for the lack of passivity in the case of negative current, i.e. power entering the system. If this is the case, then the converter would be bidirectional and the lack of passivity would be compensated for, and global asymptotic stability would be achieved. It can be observed that the value of K_{po} must be relatively high. As found in the previous chapter when doing the Gershgorin analysis of the converter system, it was shown that K_{po} had a high DOF and could take relatively high values. But, this was in the case of a positive reference current. The next step is to check if the converter will be stable for such high values of the tuning parameter. The same approach as in the previous chapter will be applied, implying that first only the outer-loop voltage dynamics will be analyzed, and then the full system will be investigated.

6.1.1 Outer Loop Dynamics

The dynamics of the outer-loop is now in focus. This implies that the current already has reached its steady-state value, such that the TSS is present. This is not a realistic event since the states are affecting each other, but it opens up the possibility to analyze the voltage dynamics in an isolated way. The goal is to test if the compensation for the lack of passivity is possible, and if so, what the consequences of it are. When simulating the system, the values in Table 6.1.2 below are applied. The values are matching the findings from the previous chapter, and the K_{po} is sat to match the finding from above.

The script from Appendix A.4 is the relevant one. This is the same script as applied earlier, but the difference is the direction of the current source. By making it negative, the

Table 6.1.2: Values applied for the bidirectional outer-loop validation.

Parameter	**Value**
V_S, voltage source	700 V
C, capacitance	500 μF
L, inductance	5 mH
R_s, resistance	1.1 Ω
K_p, inner loop P-gain	15
K_i, inner loop I-gain	5
I_s, current source	-20 A
ζ^*_{inner}, ζ_{inner}-steady state value	-4.86
V_{ref}, voltage reference	800 V
K_{po}, outer loop P-gain	500 000/300 000
K_{io}, outer loop I-gain	0.2

power is entering the converter, making the current direction negative. The resulting plot of the voltage with the values from Table 6.1.2 can be seen in Figure 6.1.1 below.

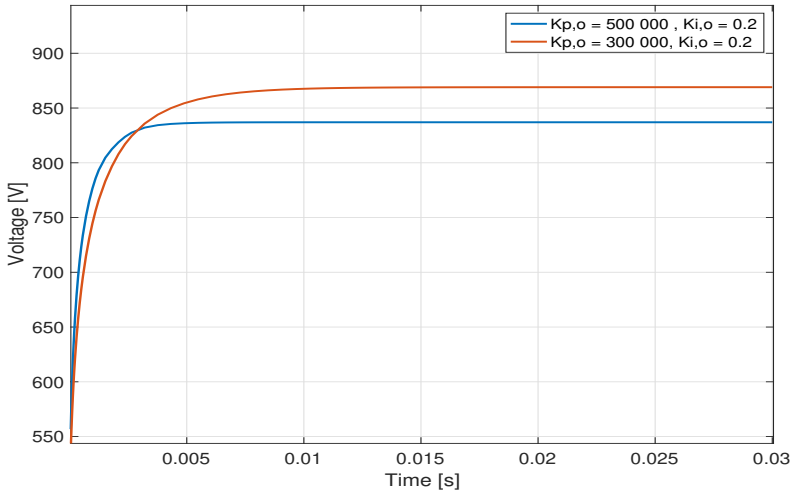

Figure 6.1.1: Voltage in the outer-loop of the bidirectional converter when compensating for the lack of passivity. It is assumed a TSS and that the current has already reached the equilibrium value, and it is tested for two different values of K_{po}.

It can be observed that the voltage stabilizes. While simulating the system, this was not always the case. For the two voltage evolutions in Figure 6.1.1, one K_{po} greater than the derived value above was chosen, and one K_{po} a bit lower than the derived value was chosen. Both of these tuning parameters led to stability. For even lower values of K_{po}, i.e. values lower than 136 500, the voltage dynamics got unstable due to the lack of passivity.

It can be noted that the limit between stable and unstable voltage dynamics are at K_{po} equal to 136 500 and that the derived value was 493 714. This means that the derived K_{po} is pretty accurate and that the safety margin at around 3.2 times the real minimum value. The steady-state time of the system is pretty low. This is a consequence of the high K_{po}. Since a higher P-gain is leading to a more robust, i.e. faster responding, system.

The second observation is that the voltage-equilibrium value is not equal to the voltage-reference value, i.e. $800\,V$. When running the script in Appendix A.7 with the values from Table 6.1.2 to calculate the equilibrium point, the result was an equilibrium value of the voltage equal to $800\,V$, as expected, and an equilibrium value of the current equal to $-22.09\,A$. But the simulations tell a different story, and the dynamics of the system doesn't manage to reach the correct value. But the higher the value of K_{po}, the closer the steady-state value of the voltage is to the reference value. This can be seen in Figure 6.1.1. The reason for this might be the high value of the proportional gain. The system might actually act as a P-controller, due to the high value of the P-gain. The only way of obtaining the exact reference value is to increase the outer-loop I-gain, K_{io}. The model was tested with different values of K_{io}, and the result is that a very big value is needed in order to obtain the reference voltage. By very big, it is meant that a K_{io} in the order of 10^4-th is necessary. Figure 6.1.2 below is showing the voltage for two different values of K_{io}, both very high in magnitude. It can be observed that both of the voltages reach the reference-voltage. But, such high values of the outer-loop I-gain is a clear violation of the findings from the previous chapter, regarding the limitation of the tuning parameter.

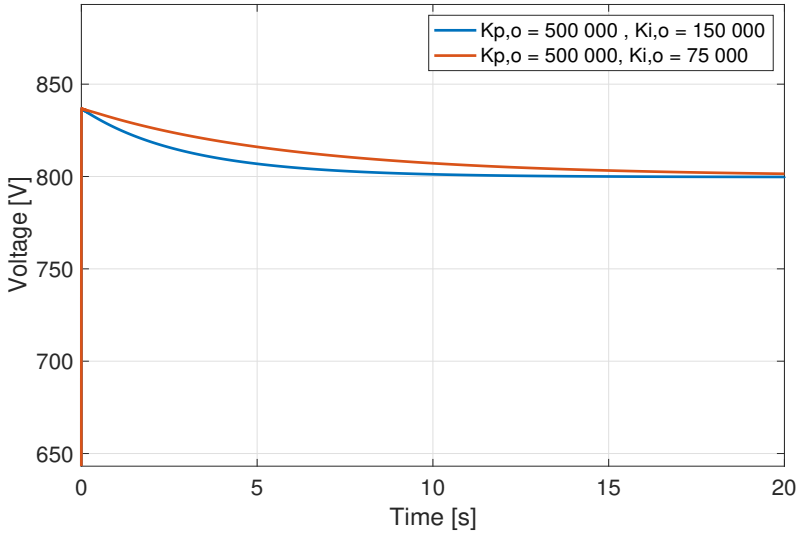

Figure 6.1.2: Voltage in the outer-loop of the bidirectional converter when compensating for the lack of passivity. High values of K_{io} is needed to reach the steady-state voltage of 800 V.

It is hence possible to obtain the reference voltage when assuming TSS and that the current has stabilized. But, the consequence is a non-tolerable high K_{io} with respect to the findings from Chapter 5. Further on, the dynamics of the full system will be investigated, before a more analytical approach to the analysis of the converter will be done to examine the consequences of this high K_{io} needed to reach the reference-voltage.

6.1.2 Dynamics of the Full System

In order to validate if the findings regarding the compensation for the lack of passivity is correct, i.e. that this compensation is leading to a stable system, the SIMULINK model from Appendix A.5 is applied. The states of voltage and current are affecting each other, especially since the reference-current is a function of the voltage, and it is hence of great interest to simulate the dynamics of the full system. The values in Table 6.1.3 are used for the simulations with the mentioned model.

Table 6.1.3: Values applied for the validation of the bidirectional converter.

Parameter	**Value**
V_S, voltage source	700 V
C, capacitance	500 μF
L, inductance	5 mH
R_s, resistance	1.1 Ω
K_p, inner loop P-gain	15
K_i, inner loop I-gain	5
I_s, current source	-20 A
V_{ref}, voltage reference	800 V
K_{po}, outer loop P-gain	250 000
K_{io}, outer loop I-gain	0.2

As mentioned, the model from Appendix A.5 will be the one in focus. This is the same model as applied in Chapter 5.1.2, except for the changes of parameter-values and the change of sign of the current source. The resulting voltage and current dynamics can be seen in Figure 6.1.3.

It must be emphasized, to avoid any confusion, that the current-axis in Figure 6.1.3, i.e. the right-hand axis, is mostly negative. It can from the figure be seen that both the voltage and the current are stabilizing. The reference value for the current is $-22.09\ A$, while the steady-state value of the voltage is $904\ V$. It can also be seen that the P-gain is set to 250 000, which is a bit lower than the above-derived minimum value.

First of all, the reason why the P-gain of the outer-loop is set to 250 000 is by trial-and-error. Meaning, first a value of 500 000 was chosen, but as the simulation led to an unstable voltage the value of K_{po} was changed. First the value was sat even higher, as it was natural that maybe the P-gain was too small to compensate for the lack of passivity. This also gave an unstable voltage. Then the value of K_{po} was chosen to be half of the

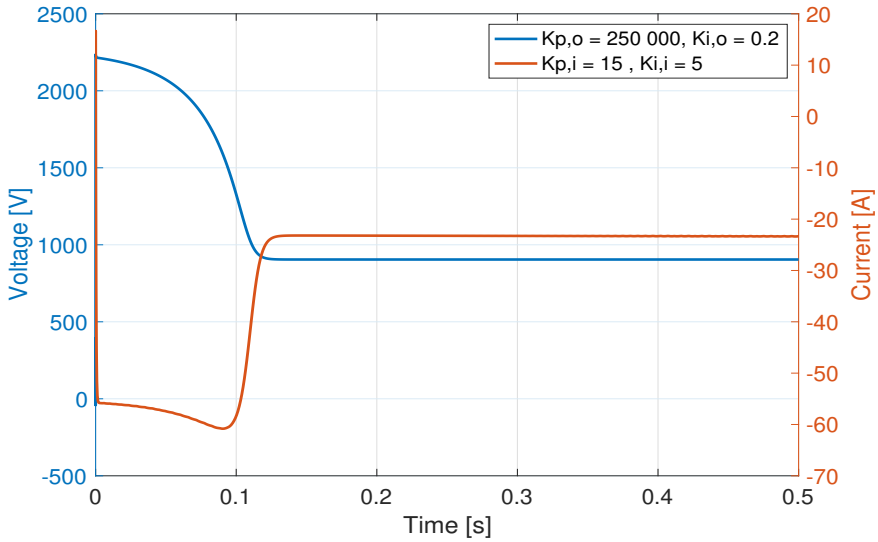

Figure 6.1.3: Voltage and current for the bidirectional converter when compensating for the lack of passivity. The voltage is shown in blue and corresponds to the left y-axis, and the current is shown in red and corresponds to the right y-axis.

starting one, i.e. 250 000. This led to a stable result. It can also be mentioned that for even lower values of K_{po} the voltage again got unstable. This is due to the lack of passivity which, for small values of K_{po}, doesn't get compensated enough for. The more curious part is what happens with the voltage for very high values of the tuning constant. In order to answer this question a more analytical approach to the problem will be done in the next section.

For the simulation of the full bidirectional converter system in Figure 6.1.3, on the same level as for the simulation of only the outer-loop in Figure 6.1.1, the voltage is not reaching its reference value. The deviation between the reference and the obtained steady-state value is 13 %, which is pretty high. Since the converter is in voltage-control mode, it would at first be expected that the voltage should be able to reach the reference value. But again it is not that surprising that it doesn't since this also was the case for the simple simulation that only was considering the voltage-dynamics.

For the outer-loop dynamics the result was that for higher values of the I-gain, it was possible to reach the reference-voltage. This was also done for the full converter-system. Additionally, it is necessary to use higher values of the inner-loop tuning parameters to stabilize the current. The resulting voltage and current dynamics can be seen in Figure 6.1.4, when the power is going in the negative direction.

From the figure can it be noted that the current is closing in on the equilibrium value

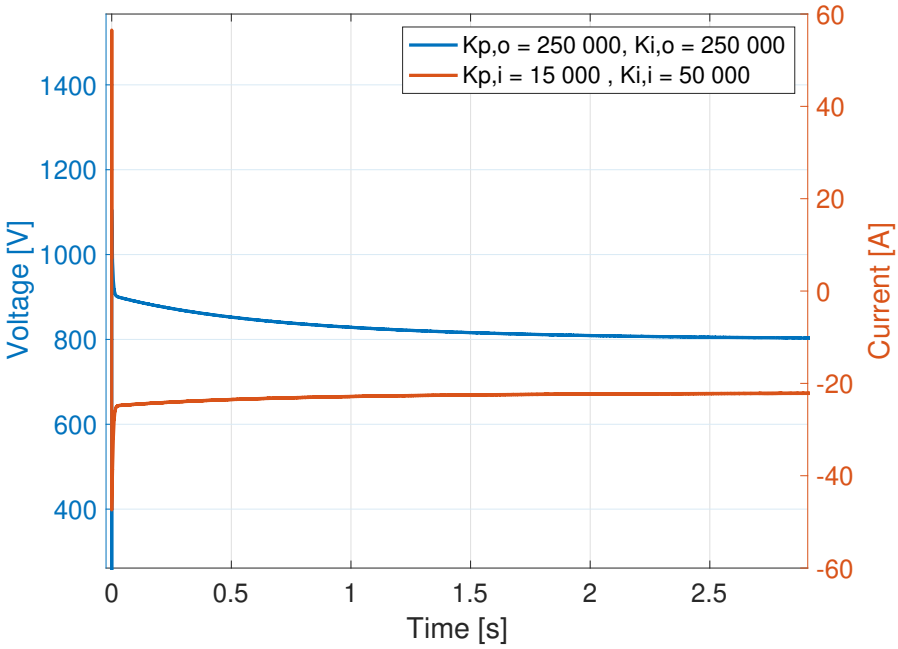

Figure 6.1.4: Voltage and current for the bidirectional converter when power is transferred in the negative direction. The reference values get obtained. The voltage is shown in blue and corresponds to the left y-axis, and the current is shown in red and corresponds to the right y-axis.

faster than the voltage is. This might indicate a TSS. It can also be seen that both the current and voltage have a transient behavior at first. This is a consequence of the non-tuned parameters, which battles in order to ensure the correct value of the states, and it might affect the robustness of the states. Since this converter is bidirectional, Figure 6.1.5 below shows the voltage and current for the same values as for Figure 6.1.4 above, but now for power going in the positive direction.

It can be seen from Figure 6.1.5 that the voltage reaches its reference-value also in the positive direction. The steady-state voltage is now $23.4\ A$. Compared to Figure 6.1.4, it can be seen that the stabilizing time is very similar, which is as expected due to similar tuning-parameters. Since the voltage and current is stabilizing for the positive power direction as well as the negative, it can be concluded that the converter is, in fact, bidirectional, and that it is stable and reaching the reference voltage.

It can be observed that for the full converter system, the consequence of obtaining the exact reference-voltage is to use a very high K_{io}, hence violating the restrictions found in Chapter 5. Additionally, the inner-loop tuning parameters are scaled up by many factors compared to the ones in the previous chapter. This might also affect the converter model,

but in order to be able to interpret and analyze it an analytical study will be completed next.

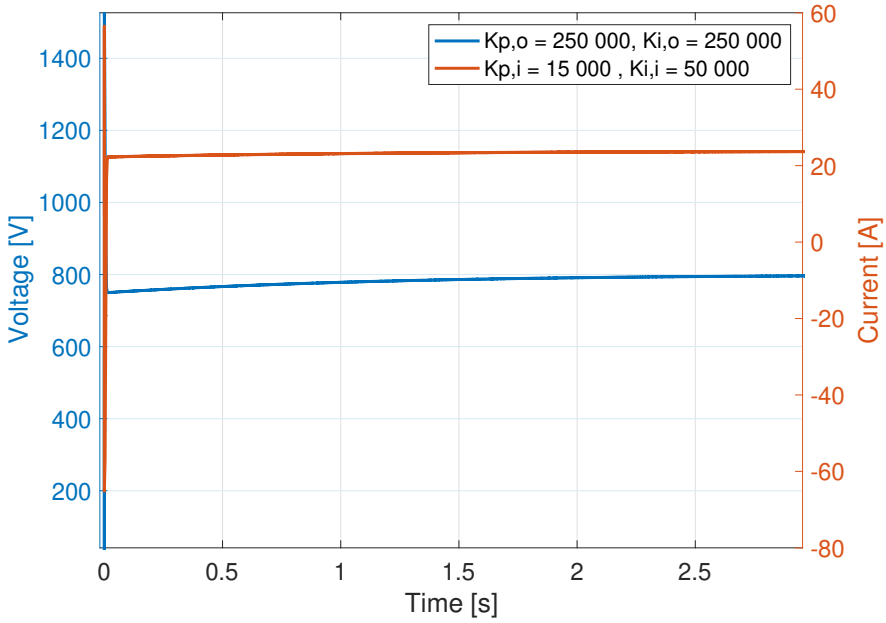

Figure 6.1.5: Voltage and current for the bidirectional converter when power is transferred in the positive direction. The reference values get obtained. The voltage is shown in blue and corresponds to the left y-axis, and the current is shown in red and corresponds to the right y-axis.

6.2 System Analysis, Interpretation, and Discussion

The Gershgorin theorem will yet again be exploited. The Jacobian matrix in Equation (5.18) from Chapter 5 will be important, and is hence repeated in Equation (6.11) below. It is assumed that e^* can be approximated to V_s for reasons earlier explained.

$$A_1 = \begin{bmatrix} -\frac{R_s+K_p}{L} & -\frac{K_p \cdot K_{po} \cdot V_s}{L \cdot V_{ref}^3} & \frac{K_i}{L} & \frac{K_{io} \cdot K_p}{L} \\ \frac{K_p \cdot i^*}{C \cdot V_{ref}} & \frac{K_{po} \cdot K_p \cdot V_s \cdot i^*}{C \cdot V_{ref}^4} - \frac{V_s}{C \cdot V_{ref}^2} \cdot \left(\frac{K_{po} \cdot V_s}{V_{ref}^2} + i^* \right) & -\frac{K_i \cdot i^*}{C \cdot V_{ref}} & -\frac{K_{io} \cdot K_p \cdot i^* - K_{io} \cdot V_s}{C \cdot V_{ref}} \\ -1 & -\frac{K_{po} \cdot V_s}{V_{ref}^3} & 0 & K_{io} \\ 0 & -\frac{V_s}{V_{ref}^3} & 0 & 0 \end{bmatrix} \tag{6.11}$$

Yet again it is the current-row and the voltage row, respectively row 1 and 2 of matrix A_1, that are of interest. Some of the tuning parameters applied in the simulations explained

above, have been relatively large in value. Consequently, since the range of the tuning parameters have been so big, none of the terms in the matrix can be neglected in the further analysis. The goal is a TSS, where the eigenvalue of the current is bigger, i.e. more negative, than the eigenvalue of the voltage. This can be assured through the Gershgorin theorem if the furthermost right point of the current-circle is to the left of the furthermost left point of the voltage circle. These values were expressed mathematically in Equation (5.19) and (5.20) in Chapter 5. They are repeated in Equation (6.12) and (6.13) below, but since the equilibrium current now is negative, the terms containing this variable have changed the sign.

$$\lambda_{i,r} = -\frac{R_s + K_p}{L} + \frac{K_p \cdot K_{po} \cdot V_s}{L \cdot V_{ref}^3} + \frac{K_i}{L} + \frac{K_{io} \cdot K_p}{L} \tag{6.12}$$

$$\begin{aligned}\lambda_{v,l} = &- \frac{K_{po} \cdot K_p \cdot V_s \cdot |i^*|}{C \cdot V_{ref}^4} - \frac{V_s}{C \cdot V_{ref}^2} \cdot \left(\frac{K_{po} \cdot V_s}{V_{ref}^2} - |i^*| \right) - \frac{K_p \cdot |i^*|}{C \cdot V_{ref}} \\ &- \frac{K_i \cdot |i^*|}{C \cdot V_{ref}} - \frac{K_{io} \cdot (Vs + K_p \cdot |i^*|)}{C \cdot V_{ref}}\end{aligned} \tag{6.13}$$

For the unidirectional converter it was concluded that the K_{po} had a high DOF, and that this also would count for the bidirectional converter. The DOF of the parameter is high also for the bidirectional converter, but way lower than for the unidirectional one. For the values in Table 6.1.3 when testing for different values of K_{po} in the MATLAB-script from Appendix A.6, the value of K_{po} that separated the two circles was approximately 5 000. As derived above a K_{po} at almost 500 000, i.e. 100 times higher than the Gershgorin circles allow, is a must to compensate for the lack of passivity.

In order to understand the system properly and be able to interpret the effect of the different tuning parameters, the influence of the different tuning parameters will sequentially be investigated through Equation (6.12) and (6.13). As a reminder, it is wanted to separate the circles to be able to ensure TSS between current and voltage in the converter, such that the Lyapunov stability proof holds. Yet again, the Gershgorin circle theory can ensure the TSS, but if the circles are overlapping it can not guarantee that the TSS is present. In other words, the circles can overlap and TSS can still be present, but it can not be proven.

The first tuning parameter in focus is the outer-loop P-gain, K_{po}. This parameter is controlling the current radius. So a high K_{po} implies a large radius of the current circle which might lead to an overlap of the circles. K_{po} is also controlling the voltage center. For current in the negative direction, an increasing K_{po} will push the voltage-circle to the left on the real axis. This is also not good for the TSS since it is wanted that the voltage circle is placed to the right of the current circle. It was noted when simulating the full converter system, that for low and very high values of K_{po} the voltage got unstable. The reason for this is that for low values of the K_{po} the eigenvalues of the voltage becomes positive and it is a lack of passivity. For too big values of the outer-loop P-gain, the eigenvalue of the voltage becomes much greater than the eigenvalues of the current, and this is destroying the TSS and therefore also the stability proof. The next outer-loop tuning

parameter in focus is the I-gain, K_{io}. This parameter is controlling both the voltage radius and the current radius. So a high K_{io}, which was shown to be needed in order for the voltage to reach the reference value, will increase both of the circles and be leading to an overlap between them.

Also the inner-loop parameters must be scaled up in order to stabilize both the current and the voltage. The P-gain of the inner-loop, K_p, controls both the voltage center and the current center. A higher K_p will move both circles to the left. This is a consequence of the negative current-direction, leading to a negative sign in front of the K_p term representing the voltage-center. The order of magnitude depends on the other tuning-parameters, but in the case of compensating for lack of passivity with a high K_{po} the voltage-center will increase faster than the current-center. Hence the ability to move the current-circle to the left experienced in the previous chapter, is now lost when the current in the bidirectional converter is negative. K_p is additionally controlling both of the circles radius. The inner-loop I-gain, K_i, is controlling the radius of both circles. So the requirement of a big K_i to stabilize the current, is forcing an overlap between the current and voltage Gershgorin circles.

To sum it up, it is not possible to separate the Gershgorin circles, and hence mathematically be proving that the TSS is present for the bidirectional converter when the current is in the negative direction. But even though the Gershgorin theorem can't prove the TSS, the TSS might be present. By calculating the eigenvalues in the script from Appendix A.7 with the values used in Figure 6.1.4, the current-eigenvalue is still more than 10 times more negative than the voltage-eigenvalue. But for these values of the tuning-parameters the participation factor changes, and 15 % of the most negative eigenvalue is now explained by the voltage, while the remaining 85 % is explained by the current. But, when increasing the outer-loop tuning parameters, especially K_{po}, more and more of the most negative eigenvalue is explained by the voltage. This is also in compliance with the conclusion above, stating that for very high values of K_{po} the voltage-circle is being pushed to the left of the current-circle. In other words, it exists an interval of K_{po}'s which will provide both TSS and stability.

Another point to discuss is regarding the full converter model with the negative reference current. A set of tuning parameter-values was observed to give a stable system where the voltage reached its reference value. But when changing the values of the tuning-parameters by only a few thousandths, instabilities occurred. For instance a set of tuning-parameters very similar to the one mentioned above, would give a stable system but with a positive current steady-state and a voltage steady-state at a couple of negative thousands of volts. So small changes in tuning-parameters gave very different results. Two different causes might be behind this type of action. The first one is related to the SIMULINK-model and the solver used. For such high values of the tuning parameters the robustness of the system can be fragile for small changes. More information related to the solver chosen for the simulations can be found in Appendix A.4. The second cause might be that this is just how the nonlinear behavior of the system actually is in that range of the tuning-parameters. Since an analytical insight can't be obtained for the system with these high tuning-parameters such as in the previous chapter, the dynamics are hard to interpret.

Since this PI-PBC of the converter in the negative direction was pretty challenging, even though it seemed to work for some tuning-parameters, another type of control can be applied for the current in the negative direction. From similar cases, especially for bigger systems, it is known that a droop-control can be applied for the voltage. Hence, by using a passivity-based droop-control the plug-and-play features would still apply, and still let us add up the Lyapunov functions of the different systems. Of course, in order to use this type of passivity-based droop-control, a new mathematical proof related to the passivity of the control must be carried out.

The reason why a droop-control is a good replacement for the converter in the negative direction is that it doesn't require the large tuning-parameter values of the outer-loop that is making the system hard to stabilize and analyze. As a consequence, the I-gain of the voltage-loop will not be present. This could lead to a small tuning constant K_1 of the droop control compared to the K_{po} for the PI-control, and no K_{io}. This might again lead to two separate Gershgorin circles and a TSS that can be proven. A direct consequence of the missing I-gain is that the system encounters a robustness problem. This robustness problem can be explained from Equation (5.8) in Chapter 5.1. It was written that $\tilde{u}$ is a function of the control signal u and the reference u^*. This implies that the control signal u is a function of voltage, current and control references, i.e.

$$u = f(v^*, i^*, u^*)$$

It is only possible to determine one of these values exactly, and then let the other two be a consequence, i.e. predicted through equilibrium analysis. For the unidirectional converter this was not a problem, since the TSS naturally gave the i^* and the I-gain of the PI-controller gave the u^*. But when removing the I-gain, the u^* is no longer induced and connected to a chosen reference-voltage. Since only one of the values can have the exact correct value, the system is not perfectly described, and hence suffers from a robustness problem. Many suggestions on how to fix this problem for similar systems have been suggested [66], and additionally, many new techniques and procedures on how to fix this problem are being researched at this moment. So a passivity based droop-control is recommended for the bidirectional converter, particularly for the challenging power flow direction, given that the derivation first has been completed correctly, and while keeping the mentioned robustness problem in mind.

Chapter 7

Conclusion and Further Work

In this chapter the findings throughout this thesis will be summarized shortly, with a focus on the key findings and the essential discussion points. A conclusion will be formulated, before suggestions for future work will be presented.

7.1 Conclusion and Key Findings

Throughout this thesis several mathematical derivations and results, analytical analysis and interpretation, and validations through simulations, have been presented. The key-findings and main conclusions will now be highlighted. The overall goal of the thesis is to contribute towards a goal of a microgrid with stability-preserving plug-and-play features, i.e., with fully decentralized local measurements and guarantees of stability, for any future topology change in the microgrid. The way this thesis is contributing is by investigating the stability of DC/DC converters with compensated modulation and with passivity-based control, and suggesting control designs according to this.

As a part of this contribution, first of all the TSS must be ensured for the inner-loop dynamics, such that the findings related to the Lyapunov function from [1] are ensured by design and not by chance. The inner-loop system consists of the DC/DC converter with a PI-controller in current-control-mode, and under compensated modulation. In order to ensure the TSS, an eigenvalue-analysis was done, while exploiting the block-triangular matrix properties. This direct eigenvalue approach didn't contribute to the analytical insight that was wanted in order to suggest some design criteria for the inner-loop, hence another approach was necessary.

Therefore, the *Gershgorin circle theorem* was exploited in order to come up with design criteria for the inner loop. With help from the theorem it was possible to obtain an analytical expression, which gave the possibility to interpret the dynamics of the inner loop and the relation to the different controlling parameters. The main finding was related to the relationship between the inductance and capacitance, and the tuning parameters K_p and

K_i. The main conclusion was that an increasing K_p would push the current-circle to the left, and eventually to the left of the voltage-circle, hence guaranteeing TSS. Additionally, it was concluded that K_i had to be smaller than K_p, and that the greater the value of the inductance is compared to the value of the capacitance, the higher the value of K_p must be in order to guarantee the TSS. Hence, a design criterion to ensure TSS in the inner-loop based on the Gershgorins theorem was provided, summarized in Equation (4.15). Some assumptions had to be done in order to derive the design criteria. These assumptions were discussed, and the conclusion was that they were realistic for practical applications.

The mentioned theorem of Gershgorin proved itself to be a very useful tool for this kind of problem, but related to the practical aspects of the converter some disadvantages occurred. The first issue is related to the linearizations that are necessary in order to apply the theorem. A great amount of information related to the large-signal behavior of the converter gets lost. However, linearizations and simplifications are a common practice for analyzing nonlinear systems, so for most practical applications the conclusions and results are still valid. The second issue is related to the condition of necessity and sufficiency. The theorem can state a sufficient solution for TSS, but not a necessary one. As a consequence of this it was concluded that by relaying the control design on the Gershgorin circle theorem, you would have to accept that the design is rather conservative. This implies that the control design is not optimal in terms of operation, i.e., the tuning parameter-values are exaggerated either up or down in order to guarantee the TSS. Hence, much higher/lower tuning variables are actually necessary to get the TSS, but in that case, the Gershgorin circle theorem can't prove it.

Further on, a mathematical derivation of PI-PBC for the added outer-loop in voltage-mode was done for the DC/DC converter. The effectiveness of this outer loop control proposal requires the TSS to be present. The goal is a passivity based converter with TSS, which will guarantee global asymptotic stability. The challenge is the control design, ensuring these properties. Since the system now is even more complex than for the inner-loop analysis, the direct-eigenvalue method would definitely not give any theoretical insight. Therefore, yet again, the Gershgorin circle theorem was applied. By mathematically describing the separation of the voltage-disk and the current-disk, i.e. the TSS, analytical insight of the converter-model was obtained. This gave the possibility to interpret the dynamics of the converter related to the tuning parameters, such that a control design ensuring stability and preserving plug-and-play features could be provided. This led to some new design criteria related to the outer-loop tuning parameters. The main conclusion was first of all that K_{po} had a really high DOF and did not affect the circles when in the same order of magnitude as the other tuning variables. Secondly the K_{io} was the most sensitive tuning parameter. It had to be really small compared to the other parameters in order to not lead to an overlap between the circles. It was seen through calculations of eigenvalues and participation matrices that the center of the Gershgorin circles often was very in compliance with the actual eigenvalues of the states. So from a practical point of view, higher values of K_{io} would probably also give TSS, but it would not be possible to prove it analytically. A new control design criteria was derived for the inner-loop of the new system, summarized in Equation (5.25). This result was based on some assumptions.

These assumptions were discussed, and the conclusion was that they were realistic. Hence, a control design for the full-converter model was preserved such that stability is ensured and the voltage-reference is obtained, still preserving the plug-and-play features.

Regarding the Gershgorin theorem, the same restriction as mentioned above counts, meaning it is a powerful tool but it has its practical disadvantages. Two SIMULINK-models were created in order to validate the mathematical derivations mentioned above; one assuming TSS and only analyzing the passivity based outer-loop dynamics, and one with the full converter-system. Both models validated the mathematical results. One challenge related to the models was the choice of solver in the SIMULINK-models. Due to zero-crossing derivatives and nonlinear equations, some problems occurred. But by applying the *ode45*-solver, these problems got fixed.

Design criteria for the full converter-model have been suggested, but only for power transferred in one direction. Due to an increasing share of ES such as batteries in the power system, a bidirectional converter is essential. From the mathematical analysis earlier provided, it is known that for negative current some constraints related to the Lyapunov-function and the passivity requirements get violated. One possible way of solving this, is to quantify the lack of passivity and then compensating for it. It was proven that this can be done, but the consequence is that the values of K_{po} must be really big, i.e. in the order of 10^5. If this was the case, the system got stable for power transferred in both directions, preserving the TSS. But, since the design criteria for the outer-loop indicates to have a really big K_{po} and a very small K_{io}, the reference-voltage does not get obtained. To reach the reference-voltage the K_{io} must increase comparably in magnitude. But, this violates the suggested design criteria for the outer-loop. In this case, the TSS cannot be mathematically proven to be ensured. Additionally, the inner-loop tuning parameters had to be increased, such that the current stabilized. This is also violating the created design criteria for the inner-loop. By analyzing the system through Gershgorins theorem, the conclusion was that it was not possible to separate the circles for such high values of the tuning parameters, for power transferred in the negative direction.

But even though Gershgorins theorem, as we know is a bit conservative, can't prove the TSS between current and voltage, it has through simulations of the earlier mentioned SIMULINK-models been showed that the system actually manages to stabilize. Hence, the bidirectional passivity-based converter has the ability to stabilize to the correct voltage-reference, but not by design. On the contrary, a proposal for the converter control design for the power in the negative direction was given. The proposal was to investigate the possibility of a passivity-based droop-control for the outer-loop in the negative power direction, such that the stability-preserving plug-and-play features also is maintained for the bidirectional converter. If this is done, it would be possible to construct a pretty realistic DC-microgrid with interconnections of DC-units, all based on passivity. This gives the opportunity for plug-and-play features, such that the DC-microgrid would be stable in the case of any future change in topology without any adjustments related to the exciting control. This can be accomplished for instance by exploiting mathematical graph theory to interconnect multiple converters. This has been done for similar systems [67, 68], so a

similar approach could be tested also for converter interconnections.

Throughout this thesis some simulations have been carried out. The availability of data has been a minor challenge. The values chosen for the converter model etc. have been based on papers with similar situations, and are therefore not completely practical realistic. The chosen values are accurate and could represent a physical DC/DC converter, since the order of magnitude of the parameter values is pretty precise.

At the very end, it must be emphasized that the findings from this thesis related to the design of the tuning-parameters and the converter-parameter can be generalized. Throughout the thesis much information about the relationships between the design-parameters has been provided, and how the design-parameters affect the dynamics. This was made possible because of the analytical insight obtained from the Gershgorin theorem. So for similar converter models, even though the topology is different from the one in focus in this project, it would be possible to obtain the same insight into the dynamics. The descriptive equations will of course be different, but by using the same procedure as in this thesis similar insight can be obtained.

So a control design, or suggestions for control, has been provided for a DC/DC converter under compensated modulation. The control is based on passivity such that the converter can be part of a DC-microgrid with stability-preserving plug-and-play features. The design was very successful for a unidirectional power flow, while some challenges occurred for the bidirectional case, and a recommendation for how to solve the challenges was mentioned.

7.2 Further Work

This master thesis has taken part in contributing to construct the future power grid. The potential is tremendous and has almost no limits. Directly related to this thesis, some itemized suggestions for further work are presented below.

- Investigate the mentioned suggestion of a passivity-based droop-control for the bidirectional converter. The first step would be to mathematically derive/prove that it is possible. Secondly to look at the analytical expressions, for instance with help from Gershgorins theorem, to develop some design criteria.
- Examine the interconnection of multiple DC/DC converters, in order to design a full DC-microgrid. This can for instance possibly be done with mathematical graph theory. This would create the opportunity to create a passivity-based DC-microgrid that is stability-preserving with plug-and-play features.
- A natural next step is to follow the scientific method, and do laboratory experiments. Multiple of the findings would be interesting to test in the lab. Firstly, the TSS for the inner-loop control. Secondly, the PI-PBC design criteria. Thirdly, for the bidirectional converter maybe more insight could be obtained from experimental tests. Additionally, the two above bullet-points could be tested and verified.

- The focus in this project has been the DC/DC converter under a compensated modulation. It could be of great interest to investigate the same possibilities for an uncompensated modulation.
- Another possible step is to explore converters without the TSS, to see if the passivity-property still could be satisfied.
- A possible approach is to linearize the voltage, instead of the current as in this project. A feedback linearization with respect to the voltage could give a simpler analysis of the converter for power in the negative direction.
- This thesis has only dealt with DC/DC converters. In order to manage to design a full microgrid of any type with the stability preserving plug-and-play features, other types of converters must also be analyzed. Inverters, or other types of converters, should be analyzed related to passivity. The first step would be to focus on one converter and mathematically derive some sort of passivity-based control. Then to find some design criteria such that this always is fulfilled. And thirdly to look at the interconnections of different converters with this property.
- It is also possible to review if a more optimal control design for the DC-DC converter can be achieved, still guaranteeing stability and TSS. In other words look into if other tools such as the Gershgorin circle theorem can be utilized to guarantee these kinds of features.

If these, or some of these, bullet-points were to be done, it could contribute to shaping the future electric power grid.

Bibliography

[1] E. H. Lillefosse. Development of a computational tool for assessing uninterrupted microgrid operation. Master's thesis, Faculty of Information Technology and Electrical Engineering, NTNU, Trondheim, 2019.

[2] United Nations Climate Change. The paris agreement (2016). https://unfccc.int/process-and-meetings/the-paris-agreement/the-paris-agreement, accessed: 04.05.2020.

[3] BP. Statistical review of world energy, 2019, 68th edition. https://www.bp.com/content/dam/bp/business-sites/en/global/corporate/pdfs/energy-economics/statistical-review/bp-stats-review-2019-full-report.pdf, accessed: 20.05.2020.

[4] M. Vaziri, S. Vadhva, T. Oneal, and M. Johnson. Distributed generation issues, and standards. In *2011 IEEE International Conference on Information Reuse Integration*, pages 439–443, 2011.

[5] E. Rodriguez-Diaz, M. Savaghebi, J. C. Vasquez, and J. M. Guerrero. An overview of low voltage dc distribution systems for residential applications. In *2015 IEEE 5th International Conference on Consumer Electronics - Berlin (ICCE-Berlin)*, pages 318–322, Sep. 2015.

[6] F. Dörfler, J. W. Simpson-Porco, and F. Bullo. Plug-and-play control and optimization in microgrids. In *53rd IEEE Conference on Decision and Control*, pages 211–216, 2014.

[7] R. Ortega, A. J. Van Der Schaft, I. Mareels, and B. Maschke. Putting energy back in control. *IEEE Control Systems Magazine*, 21(2):18–33, April 2001.

[8] R. Ortega, A. van der Schaft, F. Castanos, and A. Astolfi. Control by interconnection and standard passivity-based control of port-hamiltonian systems. *IEEE Transactions on Automatic Control*, 53(11):2527–2542, Dec 2008.

[9] T. S. Hermansen. Finding smart grid driving forces and how they affect smart grid development, december 2019. https://blog.sintef.com/uncategorized-en/finding-smart-grid-driving-forces-smart-grid-development/, accessed: 06.04.2020.

[10] J. Dickert and P. Schegner. Evolution and future prospects of electricity demand for residential customers. In *2015 IEEE Power Energy Society General Meeting*, pages 1–5, 2015.

[11] A. Ghosh and V. Aggarwal. Shared autonomous electric vehicles, december 2018. `https://web.ics.purdue.edu/~vaneet/publi_grid.htm`, accessed: 23.09.2019.

[12] Ramakrishna Kappagantu and S. Arul Daniel. Challenges and issues of smart grid implementation: A case of indian scenario. *Journal of Electrical Systems and Information Technology*, 5(3):453 – 467, 2018.

[13] M. AL-NUSSAIRI, R. Bayindir, P. Sanjeevikumar, L. MIHET-POPA, and P. Siano. Constant power loads (cpl) with microgrids: Problem definition, stability analysis and compensation techniques. *Energies*, 10, 10 2017.

[14] Li Fusheng, Li Ruisheng, and Zhou Fengquan. Chapter 1 - overview of microgrid. In *Microgrid Technology and Engineering Application*, pages 1 – 10. Academic Press, Oxford, 2016.

[15] David Wenzhong Gao. Chapter 1 - basic concepts and control architecture of microgrids. In *Energy Storage for Sustainable Microgrid*, pages 1 – 34. Academic Press, Oxford, 2015.

[16] Li Fusheng, Li Ruisheng, and Zhou Fengquan. Chapter 2 - composition and classification of the microgrid. In Li Fusheng, Li Ruisheng, and Zhou Fengquan, editors, *Microgrid Technology and Engineering Application*, pages 11 – 27. Academic Press, Oxford, 2016.

[17] Manuela Sechilariu and Fabrice Locment. Chapter 4 - direct current microgrid power modeling and control. In *Urban DC Microgrid*, pages 133 – 170. Butterworth-Heinemann, 2016.

[18] M. Sahoo and K. S. Kumar. High gain step up dc-dc converter for dc micro-grid application. In *7th International Conference on Information and Automation for Sustainability*, pages 1–5, 2014.

[19] M. d. S. Neves, M. A. Aredes, H. Khezri, E. T. H. Ida, and M. Aredes. Advantages of grid-tied dc microgrid. In *2017 Brazilian Power Electronics Conference (COBEP)*, pages 1–6, 2017.

[20] B. Kroposki, C. Pink, R. DeBlasio, H. Thomas, M. Simões, and P. K. Sen. Benefits of power electronic interfaces for distributed energy systems. *IEEE Transactions on Energy Conversion*, 25(3):901–908, 2010.

[21] Vagelis Vossos, Karina Garbesi, and Hongxia Shen. Energy savings from direct-dc in u.s. residential buildings. *Energy and Buildings*, 68:223 – 231, 2014.

[22] Piotr Biczel. Power electronic converters in dc microgrid. In *2007 Compatibility in Power Electronics*, pages 1 – 6, 05 2007.

[23] H. Bevrani, B. Francois, and T. Ise. Chapter 5: Hierarchical microgrid control. In *Microgrid Dynamics and Control*. Wiley, 2017.

[24] Rajeev Chauhan. Challenges and opportunities for dc micro grid. *School of Computing Electrical Engineering Indian Institute of Technology Mandi, India*, 10.13140/RG.2.1.1923.6240, 2016.

[25] S. Mirsaeidi, X. Dong, S. Shi, and D. Tzelepis. Challenges, advances and future directions in protection of hybrid ac/dc microgrids. *IET Renewable Power Generation*, 11(12):1495–1502, 2017.

[26] K. A. Corzine and R. W. Ashton. A new z-source dc circuit breaker. *IEEE Transactions on Power Electronics*, 27(6):2796–2804, 2012.

[27] D. Paul. Dc traction power system grounding. *IEEE Transactions on Industry Applications*, 38(3):818–824, 2002.

[28] T. L. Nguyen, E. Guillo-Sansano, M. H. Syed, V. H. Nguyen, S. Blair, L. Reguera, T. Tran-Quoc, R. Caire, G.M. Burt, C. Gavriluta, and Ngoc-An Luu. Multi-agent system with plug and play feature for distributed secondary control in microgrid—controller and power hardware-in-the-loop implementation. *Energies*, 11:3253, 11 2018.

[29] S. Dasgupta, S. N. Mohan, S. K. Sahoo, and S. K. Panda. A plug and play operational approach for implementation of an autonomous-micro-grid system. *IEEE Transactions on Industrial Informatics*, 8(3):615–629, 2012.

[30] A. Bubovich. The comparison of different types of dc-dc converters in terms of low-voltage implementation. In *2017 5th IEEE Workshop on Advances in Information, Electronic and Electrical Engineering (AIEEE)*, pages 1–4, 2017.

[31] Priyabrata Shaw. Chapter 2.6: Bidirectional dc dc converters. In *Modeling and Control of a Battery Connected Standalone Photovoltaic System*. PhD thesis, 2015.

[32] Dileeka Dias. Chapter 3 - dc to dc converters. In Nihal Kularatna, editor, *Power Electronics Design Handbook*, EDN Series for Design Engineers, pages 55 – 98. Newnes, Woburn, 1998.

[33] Y. Liu, Y. Han, C. Lin, P. Yang, and C. Wang. Design and implementation of droop control strategy for dc microgrid based on multiple dc/dc converters. In *2019 IEEE Innovative Smart Grid Technologies - Asia (ISGT Asia)*, pages 3896–3901, 2019.

[34] Y. Du, A. Q. Huang, X. Yu, and J. Li. Droop controller design methods for isolated dc-dc converter in dc grid battery energy storage applications. In *2013 Twenty-Eighth Annual IEEE Applied Power Electronics Conference and Exposition (APEC)*, pages 1630–1637, 2013.

[35] D. Vasanthakumar and Srikanth V. Dc-dc converter control using ip controller. In *2014 International Conference on Computation of Power, Energy, Information and Communication (ICCPEIC)*, pages 245–249, 2014.

[36] Aidan O'Dwyer. *Handbook Of Pi And Pid Controller Tuning Rules (3rd Edition).*, volume 3rd ed. Imperial College Press, 2009.

[37] G. Bergna Diaz, J. A. Suul, and S. D'Arco. Small-signal state-space modeling of modular multilevel converters for system stability analysis. In *2015 IEEE Energy Conversion Congress and Exposition (ECCE)*, pages 5822–5829, 2015.

[38] Issa Amadou Tall. Feedback and partial feedback linearization of nonlinear systems: A tribute to the elders. In Dongbin Lee, Tim Burg, and Christos Volos, editors, *Nonlinear Systems*, chapter 2. IntechOpen, Rijeka, 2016.

[39] P. Kundur. Chapter 12: Small-signal stability. In *Power System Stability and Control*. McGraw-Hill Inc, 1994.

[40] J. G. Balchen, T. Andresen, and B. A Foss. Chapter 8: Stabilitet. In *Reguleringsteknikk*, NTNU, Trondheim, 2016. Institutt for teknisk kybernetikk.

[41] L. K. Timothy and B. E. Bona. *State space analysis: and introduction*. McGraw-Hill Book Company, 1968.

[42] M. Dahleh, M. A. Dahleh, and G. Verghese. *Lectures on Dynamic Systems and Control*. Department of Electrical Engineering and Computer Science, Massachuasetts Institute of Technology, 2011.

[43] I. J. Perez-Arriaga, G. C. Verghese, and F. C. Schweppe. Selective modal analysis with applications to electric power systems, part i: Heuristic introduction. *IEEE Power Engineering Review*, PER-2(9):29–30, Sep. 1982.

[44] Roman Prytula. Power system participation factors for real and complex eigenvalues cases. *Poznan University of Technology Academic Journals: Electrical Engineering*, pages 369–381, 01 2017.

[45] J. Pestana. On the eigenvalues and eigenvectors of block triangular preconditioned block matrices. *SIAM Journal on Matrix Analysis and Applications*, 35:517–525, 04 2014.

[46] E. Kreyszig. *Advanced Engineering Mathematics*. John Wiley & sons, inc, 1967.

[47] M. Vidiasagar. *Nonlinear system analysis*. Prentice Hall, Englewood Cliffs, New Jersey, 1993.

[48] H. K. Khalil. *Nonlinear systems*. Prentice Hall, Upper Saddle River, New Jersey, 2002.

[49] R. Ortega and E. García. *Energy-Shaping Stabilization of dynamical systems*. Laboratoire des Signaux et Systèmes, 2003.

[50] A. Loriá. Passivity in control systems. *C.N.R.S, UMR 5228, Laboratoire d'Automatique de Grenoble, ENSIEG, St. Martin d'H'eres, France,*.

[51] J. C. Mayo-Maldonado, J. E. Valdez-Resendiz, J. C. Rosas-Caro, O. F. Ruiz-Martinez, D. Guillen-Aparicio, and G. Escobar-Valderrama. Passivity-based stabilization of dc-dc converters with constant power loads. In *2019 IEEE Texas Power and Energy Conference (TPEC)*, pages 1–6, 2019.

[52] Pooya Monshizadeh, Juan E. Machado, Romeo Ortega, and Arjan van der Schaft. Power-controlled hamiltonian systems: Application to electrical systems with constant power loads. *Automatica*, 109:108527, 2019.

[53] B. Jayawardhana, R. Ortega, E. Garcia-Canseco, and F. Castanos. Passivity of nonlinear incremental systems: Application to pi stabilization of nonlinear rlc circuits. In *Proceedings of the 45th IEEE Conference on Decision and Control*, pages 3808–3812, Dec 2006.

[54] R. Ortega, A. Loría, P. J. Nicklasson, and H. Sira-Ramírez. Appendix a: Dissipativity and passivity. In *Passivity-based Control of Euler-Lagrange Systems*, pages 475–482. Springer London, London, 1998.

[55] P. Lee and J. Bao. Chapter 2: Dissipativity and passivity. In *Process Control: The Passive Systems Approach*, pages 5–41. Springer-Verlag, London, 2007.

[56] Nima Monshizadeh, Pooya Monshizadeh, Romeo Ortega, and Arjan [van der Schaft]. Conditions on shifted passivity of port-hamiltonian systems. *Systems Control Letters*, 123:55 – 61, 2019.

[57] Dr R. Sepulchre, M. Janković, and P. V. Kokotović. *Passivity Concepts as Design Tools*, pages 25–69. Springer London, London, 1997.

[58] S. Vojtášek and K. Janáč. *Solutions of Non-Linear Systems*. Iliffe Books LTS, 1969.

[59] P. Shaw, P. K. Sahu, S. Maity, and P. Kumar. Modeling and control of a battery connected standalone photovoltaic system. In *2016 IEEE 1st International Conference on Power Electronics, Intelligent Control and Energy Systems (ICPEICES)*, pages 1–6, July 2016.

[60] A. Ali, P. Shanmugham, and S. Somkun. Single-phase grid-connected voltage source converter for lcl filter with grid-current feedback. In *2017 International Electrical Engineering Congress (iEECON)*, pages 1–6, March 2017.

[61] D. Marx, S. Pierfederici, B. Nahid-Mobarakeh, and B. Davat. Contribution to determination of domain of attraction in power systems: Application to drives with input filter. In *2009 IEEE Industry Applications Society Annual Meeting*, pages 1–8, Oct 2009.

[62] B. M. Maschke, A. J. van der Schaft, and P. C. Breedveld. An intrinsic hamiltonian formulation of the dynamics of lc-circuits. *IEEE Transactions on Circuits and Systems I: Fundamental Theory and Applications*, 42(2):73–82, Feb 1995.

[63] F. De Stasi. Know your limits. *Texas Instruments Application Report*, SNVA736, May 2016.

[64] Technical Bulletin. Voltage and current ratings. *Camesa, Technical Bulletin 014*, February 2012.

[65] Ieee recommended practice for 1 kv to 35 kv medium-voltage dc power systems on ships. *IEEE Std 1709-2010*, pages 1–54, 2010.

[66] Chunxia Dou, Zhanqiang Zhang, Dong Yue, and Hanxiao Gao. An improved droop control strategy based on changeable reference in low-voltage microgrids. *Energies*, 10:1080, 07 2017.

[67] Daniele Zonetti, Romeo Ortega, and Abdelkrim Benchaib. Modeling and control of hvdc transmission systems from theory to practice and back. *Control Engineering Practice*, 45:133 – 146, 2015.

[68] S. Fiaz, D. Zonetti, R. Ortega, J.M.A. Scherpen, and A.J. [van der Schaft]. A port-hamiltonian approach to power network modeling and analysis. *European Journal of Control*, 19(6):477 – 485, 2013. Lagrangian and Hamiltonian Methods for Modelling and Control.

[69] E. Hairer, G. Wanner, and S.P Nørsett. *Solving Ordinary Differential Equations I: Nonstiff Problems*, chapter II. Runge-Kutta and Extrapolation Methods. Springer Series in Computational Mathematics, vol. 8, 1993.

[70] G. Bergna-Diaz. Energy modelling and control of mmc-mtdc grids in a time-invariant framework: Part ii: Energy modelling and control for large-signal stability guarantees. Presentation p. 4-5, NTNU, Trondheim, 20.03 2019.

[71] A. H. Nayfeh and B. Balachandran. *Applied Nonlinear Dynamics*. Wiley-VCH, 2004.

Appendices

A MATLAB Scripts

A.1 Eigenvalues and Participation-Matrix for Inner-Loop Dynamics

The created script is using the built-in MATLAB-functions *solve()* to solve the set of non-linear equations and finding the equilibrium point, and *eig()* to calculate the eigenvalues of the linearized matrix.

```
%Script that calculates the eigenvalues, eigenvectors and
    participation factors
Vs=700;
Rs=1.1;
C=0.001;
Is=20;
Kp=15;
Ki=10;
i_ref=40;
L=100*C;

%calculate the equilibrium:
syms x1 x2 x3
eq_point1 = solve((-Rs*x1) +Vs-(Vs-Kp*(i_ref-x1)-Ki*x3) ==
    0, ...
    (-Is)+((Vs-Kp*(i_ref-x1)-Ki*x3)*x1)/(x2) == 0, i_ref-x1
        ==0);
f1=double(eq_point1.x1); %i-equilibrium
g1=double(eq_point1.x2); %v-equilibrium
h1=double(eq_point1.x3); %zeta-equilibrium

%calculate the eigenvectors and eigenvalues:
A=[(-Rs-Kp)/L, Ki/L, 0; -1, 0, 0; (Vs+Kp*i_ref-Ki*h1)/(C*g1
    ), ...
    (-f1*Ki)/(C*g1), ((f1)/(C*(g1)^2))*(Ki*h1-Vs)];
[V,D,W]=eig(A); %D is only including the eigenvalues
V; %Right eigenvectors
W=transpose(W); %Left eigenvectors
Eigenvalues=eig(A) %Eigenvalues

%Participation factor
for i=1:3
    for k=1:3
    P(k,i)=abs(V(k,i)*W(i,k));
    k=k+1;
    end
    i=i+1;
end

```

```
36 %Normalized P-matrix
37 for j=1:3
38     for g=1:3
39         G(g,j)=P(g,j)/sum(P(:,j));
40         g=g+1;
41     end
42     j=j+1;
43 end
44 P;
45 G;
```

A.2 Gershgorin Circles for the Inner-Loop Dynamics

The created script is using the built-in MATLAB-function *solve()* to solve the set of non-linear equations and finding the equilibrium point.

```
1  Vs=700;
2  L=0.1;
3  Rs=1.1;
4  C=0.001;
5  Is=20;
6  Kp=15;
7  Ki=10;
8  i_ref=40;
9  % L=10*C;
10
11 syms x1 x2 x3
12 eq_point1 = solve((-Rs*x1) +Vs-(Vs-Kp*(i_ref-x1)-Ki*x3) ==
       0, (-Is)+((Vs-Kp*(i_ref-x1)-Ki*x3)*x1)/(x2) == 0, i_ref-
       x1==0);
13 f1=double(eq_point1.x1); %i-equilibrium
14 g1=double(eq_point1.x2); %v-equilibrium
15 h1=double(eq_point1.x3); %zeta-equilibrium
16
17 center1=-(Rs+Kp)/L;
18 radius1=Ki/L;
19 center2=0;
20 radius2=1;
21 center3=((f1)/(C*(g1)^2))*(Ki*h1-Vs);
22 radius3=0;%abs((Vs+Kp*i_ref-Ki*h1)/(C*g1)) + abs((-f1*Ki)/(
       C*g1));
23
24 %Plotting the centers
25 plot(center1,0,'k*')
26 hold on
27 plot(center2,0,'b*')
28 hold on
29 plot(center3,0,'r*')
30
31 %Plotting the circles
32 hold on
33 th = 0:pi/50:2*pi;
34 xunit1 = radius1 * cos(th) + center1;
35 yunit1 = radius1 * sin(th) + 0;
36 h11 = plot(xunit1, yunit1, 'k');
37
38 hold on
39 xunit2 = radius2 * cos(th) + center2;
```

```
yunit2 = radius2 * sin(th) + 0;
h22 = plot(xunit2, yunit2, 'b');

hold on
xunit3 = radius3 * cos(th) + center3;
yunit3 = radius3 * sin(th) + 0;
h33 = plot(xunit3, yunit3, 'r');

hold off
```

A.3 Jacobian Matrix Calculation

The created script is using the built-in MATLAB-function *jacobian()* to calculate the Jacobian matrix of the system.

```
syms i v z1 z2
jacobian([('r'*(-i)+'Kp'*('Kpo'*(('e')*(1/(v^2)-1/(v*'Vref'
    ))+'Kio'*z2-i))+'Ki'*z1)/('L'), ...
     1/('C'*v)*('Vs'-'Kp'*('Kpo'*(('e'/(v^2))-('e'/(v*'Vref'
         ))) + 'Kio'*z2-i)-'Ki'*z1)*('Kpo'*('e'/(v^2)-'e'/('
         Vref'*v)) + 'Kio'*z2), ...
     'Kpo'*('e'/(v^2) - 'e'/('Vref'*v))+'Kio'*z2-i, ...
        ('e')*(1/(v^2) - 1/('V_ref'*v))],...
     [i, v, z1, z2])

% Removed: -'Is'/'C' from the voltage equation, since this
    constant either way would disappear when doing the
    derivatives
```

A.4 SIMULINK Model of the PI-PBC of the Outer Voltage-Loop

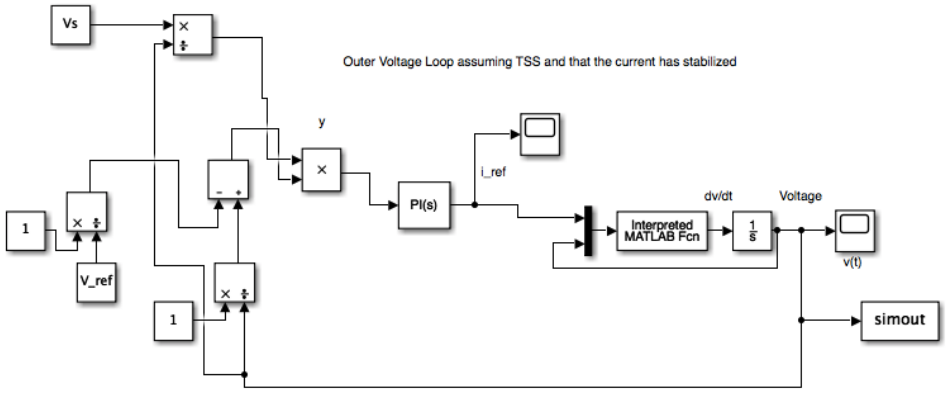

Figure A.1: SIMULINK model of the PI-PBC of the outer voltage-loop.

Figure A.1 shows the created SIMULINK model. It is a PI-outer loop control of in voltage-mode based on passivity, designed to obtain the reference value of the voltage. The converter system is described through the *Interpreted MATLAB Fcn* block. The code which is the input to this block can be seen in Appendix A.4 below. TSS is assumed in addition to that the current has already reached its steady-state value. Hence, the only descriptive equation is the voltage-dynamics equation. The *PI(s)*-block is used to control the y signal, and the tuning parameters are sat locally in this block. The part to the left for this block is creating the passive output signal, y. The sign of y has been changed, in order to let the tuning gains have positive values.

The *solver* in the SIMULINK-model is the variable step-length solver, called *ode45 (Dormand-Prince)*, with the default settings. This solver was chosen because the states in the model are continuous and the system itself not too complex, and in general because of the nonlinearities a variable step-length solver is advisable. The Dorman-Prince solver is a Runge-Kutta (4, 5) numerical ODE solver. More information about the math within the solver can be found in [69].

Corresponding Interpreted MATLAB Function for the SIMULINK Model of PI-PBC of the Outer Loop

```
function dvdt = f_o_simple(x)
u=x(1);
v=x(2);

V_ref=800;
Vs=700;
Is=20;
```

```
C=500*10^(-6);
z1ss=2.6;
Ki=10;
Kp=15;

dvdt = (-Is/C) + ((Vs-Ki*z1ss)*u)/(C*v);
end
```

A.5 SIMULINK Model of the PI-PBC of the Full Model

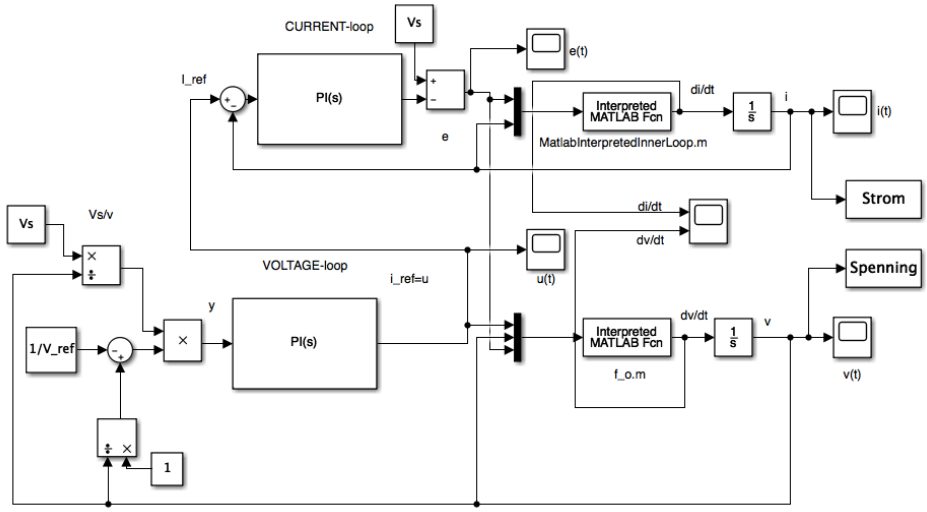

Figure A.2: SIMULINK model of the PI-PBC of the full converter-model.

The created SIMULINK model consists of two loops. At the bottom, the voltage outer-loop can be seen. It is pretty similar to the model describing only the outer-loop, but the *Interpreted MATLAB Fcn* is changed, to include the inner-current-loop as well. The interpreted MATLAB function cooperating with the outer-loop can be seen below, named "f_o". It can be observed that the reference-signal coming from the outer-loop, is now the reference for the inner-loop. Hence, the current-reference is a function of v. The upper loop in Figure A.2 is the inner-loop of the current dynamics. This loop is also cooperating with a MATLAB function called "MatlabInterpretedInnerLoop" found below. The compensated inner-loop control signal, e, is an input to the voltage-loop. The *PI(s)*-blocks is used to control the y signal for the voltage-loop and the current in the current loop. The tuning parameters are sat locally in this block. The sign of y has been changed, in order to let the tuning gains have positive values.

The *solver* in the SIMULINK-model is the variable step-length solver, called *ode45 (Dormand-Prince)*, with the default settings. This was chosen for the same reasons mentioned previously, in Appendix A.4.

Corresponding Interpreted MATLAB Functions for SIMULINK Model of PI-PBC of the Converter

```
1 function dvdt = f_o(x)
2 u=x(1);
3 v=x(2);
```

```
4 e=x(3);
5
6 C=500*10^-6;
7 Is=20;
8
9 dvdt = (-Is/C) + (e*u)/(C*v);
10 end
```

```
1 function didt = MatlabInterpretedInnerLoop(x)
2 e=x(1);
3 i=x(2);
4 Rs=1.1;
5 C=500*10^-6;
6 L=10*C;
7 Vs=700;
8
9 didt = -(Rs*i)/L+Vs/L - e/L;
10 end
```

A.6 Gershgorin Circles for the Complete Converter Model

The created script is using the built-in MATLAB-function *solve()* to solve the set of non-linear equations and finding the equilibrium point.

```
Vs=700;
Rs=1.1;
C=500*10^-6;
Is=20;
Kp=15;
Ki=5;
L=10*C;
V_ref=800;
Kpo=10;
Kio=0.2;

%calculate the equilibrium:
syms x1 x2 x3 x4
eq_point1 = solve(Rs*(-x1)+Kp*(Kpo*(Vs*((1/(x2^2))-(1/(x2*
    V_ref)))) +Kio*x4-x1)+Ki*x3 ==0, ...
    -Is + 1/(x2)*(Vs-Kp*(Kpo*Vs*(1/(x2^2)-1/(x2*V_ref)) +
        Kio*x4-x1)-Ki*x3)*(Kpo*Vs*(1/(x2^2)-1/(V_ref*x2)) +
        Kio*x4) ==0, ...
    Kpo*(Vs/(x2^2) - Vs/(V_ref*x2))+Kio*x4-x1 ==0, ...
        Vs*(1/(x2^2) - 1/(V_ref*x2)) ==0);
f1=double(eq_point1.x1); %i-equilibrium
g1=double(eq_point1.x2); %v-equilibrium
h1=double(eq_point1.x3); %zeta1-equilibrium
i1=double(eq_point1.x4); %zeta2-equilibrium
f11=min(f1);

center1=-(Rs+Kp)/L; %Current
radius1=Ki/L + (Kio*Kp)/L + (Kp*Kpo*Vs)/(L*(V_ref^3));
center2=0; %Zeta-1
radius2=1+Kio + ((Kpo*Vs)/(V_ref^3));
center3=(Kpo*Kp*Vs*f11)/(C*V_ref^4) - (Vs/(C*V_ref^2))*(f11
    + (Kpo*Vs/(V_ref^2))); %Voltage
radius3= (Kp*f11+Ki*f11)/(C*V_ref) + abs(-(Kio*Kp*f11 - Kio
    *Vs)/(C*V_ref));
center4=0; %Zeta-2
radius4=Vs/(V_ref^3);

%Plotting the centers
plot(center1,0, 'k*')
hold on
plot(center2,0, 'b*')
hold on
```

```
38 plot(center4,0, 'g*')
39 hold on
40 plot(center3,0, 'r*')
41 xlabel('Re')
42 ylabel('Im')
43 set(gca,'FontSize',18, 'LineWidth', 1.5)
44
45 %Plotting the circles
46 hold on
47 th = 0:pi/50:2*pi;
48 xunit1 = radius1 * cos(th) + center1;
49 yunit1 = radius1 * sin(th) + 0;
50 h11 = plot(xunit1, yunit1, 'k');
51
52 hold on
53 xunit2 = radius2 * cos(th) + center2;
54 yunit2 = radius2 * sin(th) + 0;
55 h22 = plot(xunit2, yunit2, 'b');
56
57 hold on
58 xunit3 = radius3 * cos(th) + center3;
59 yunit3 = radius3 * sin(th) + 0;
60 h33 = plot(xunit3, yunit3, 'r');
61
62 hold on
63 xunit4 = radius4 * cos(th) + center4;
64 yunit4 = radius4 * sin(th) + 0;
65 h44 = plot(xunit4, yunit4, 'g');
66
67 hold off
```

A.7 Eigenvalues and Participation-Matrix for the Full Converter Model

The created script is using the built-in MATLAB-functions *solve()* to solve the set of non-linear equations and finding the equilibrium point, and *eig()* to calculate the eigenvalues of the linearized matrix.

```
%Script that calculates the eigenvalues, eigenvectors and
    participation factors
Vs=700;
Rs=1.1;
C=500*10^-6;
Is=20;
Kp=15;
Ki=5;
L=10*C;
V_ref=800;
Kpo=10;
Kio=0.2;

%calculate the equilibrium:
syms x1 x2 x3 x4
eq_point1 = solve(Rs*(-x1)+Kp*(Kpo*(Vs*((1/(x2^2))-(1/(x2*
    V_ref))))+Kio*x4-x1)+Ki*x3 ==0, ...
    -Is + 1/(x2)*(Vs-Kp*(Kpo*Vs*(1/(x2^2)-1/(x2*V_ref))) +
        Kio*x4-x1)-Ki*x3)*(Kpo*Vs*(1/(x2^2)-1/(V_ref*x2))) +
        Kio*x4) ==0, ...
    Kpo*(Vs/(x2^2) - Vs/(V_ref*x2))+Kio*x4-x1 ==0, ...
        Vs*(1/(x2^2) - 1/(V_ref*x2)) ==0);
f1=double(eq_point1.x1); %i-equilibrium
g1=double(eq_point1.x2); %v-equilibrium
h1=double(eq_point1.x3); %zeta1-equilibrium
i1=double(eq_point1.x4); %zeta2-equilibrium
f11=min(f1);

%calculate the eigenvectors and eigenvalues:
A=[(-Rs-Kp)/L, -Kp*Kpo*Vs/(L*V_ref^3), Ki/L, Kio*Kp/L;...
    (Kp*f11)/(C*V_ref), (Kpo*Kp*Vs*f11)/(C*V_ref^4) - (Vs)
        /(C*V_ref^2)*(f11+Kpo*Vs/(V_ref^2)), -Ki*f11/(C*
        V_ref),-(Kio*f11*Kp-Kio*Vs)/(C*V_ref);...
    -1, -Kpo*Vs/(V_ref^3), 0, Kio;...
    0,-Vs/(V_ref^3),0,0];
[V,D,W]=eig(A); %D is only including the eigenvalues
V; %Right eigenvectors
W=transpose(W); %Left eigenvectors
Eigenvalues=eig(A); %Eigenvalues

%Participation factor
```

```
36 for  i=1:4
37      for  k=1:4
38      P(k,i)=abs(V(k,i)*W(i,k));
39      k=k+1;
40      end
41      i=i+1;
42 end
43
44 %Normalized P-matrix
45 for  j=1:4
46      for  g=1:4
47           G(g,j)=P(g,j)/sum(P(:,j));
48           g=g+1;
49      end
50      j=j+1;
51 end
52 P;
53 G;
```

B Derivations

B.1 Lyapunov Function for Inner-Loop Dynamics

Nonlinear stability theory is complex and might be hard to understand. Lyapunov stability is maybe the most understandable way of analyzing this. Say that V(x(t)) is non-increasing, in such a way that

$$\dot{V} = \nabla^T V(x) f(x) \leq 0$$

Then $V(x)$ is a dissipated quantity. $x(t)$ is a trajectory of $f(x)$. One intuitive example of a dissipated quantity is the energy of a closed LRC-circuit. The energy will never increase but might decrease because of losses, and change direction within the system.

Then V is a Lyapunov function given some conditions. Firstly V must be continuously differentiable. Secondly $V(x^*)$ and $\dot{V}(x^*)$ must be equal to zero. x^* is the point of interest and is often the equilibrium value of the function. The third condition is that $V(x)$ must be greater than zero and $\dot{V}(x)$ is less than zero, for a given domain except for the point of interest [70].

This means that x^* is the lowest point of the function and that every trajectory is going towards this point. So no matter where you start, within the defined domain, the conditions will "fall down" along the trajectory and towards the equilibrium point. If the conditions go all the way down, reaching this point, then it is said to be a strict Lyapunov function. If the mentioned domain is limited, it is regional stable within the domain. On the other hand, if the domain is all the real values, it is globally stable.

The difficulty is to find a Lyapunov function for the original function. Many possibilities have been suggested. In [71] the Hamiltonian function is mentioned, among with methods by Pai (1981), Michel, Milland, and Nam (1982), and Michel, Milland, and Vittal (1984).

Mathematical derivation of the Lyapunov function.

The equations describing the relevant system are seen below.

$$L\frac{di}{dt} = -R_s \cdot i + V_s - (V_s - K_p \cdot (i_{ref} - i))$$

$$C\frac{dv}{dt} = -I_s + i \cdot \frac{(V_s - K_p \cdot (i_{ref} - i))}{v}$$

In the case of time-scale separation, assume that the current, i, has reached its reference value, i_{ref}. Hence the current-equation is zero. The second equation gets equal to

$$C\frac{dv}{dt} = -I_s + i_{ref}\frac{V_s}{v}$$

When v has reached its steady-state value, V_*, the expression gets as following

$$0 = -I_s + i_{ref}\frac{V_s}{V_*}$$

By shifting the voltage-equation with

$$\tilde{v} = v - V_*$$

The new equation of interest is given as

$$C\frac{d\tilde{v}}{dt} = V_s i_{ref}\left(\frac{1}{v} - \frac{1}{V_*}\right)$$

Then the following equation can be used to describe the system

$$\frac{d\tilde{v}}{dt} = -K \cdot \nabla V(v)$$

where

$$K = \frac{V_S \cdot I_{ref}}{C}$$

and V(v) is the created Lyapunov function. Furthermore, the Lyapunov function can through integration and multiplication by (-1) be shown to be

$$V(v) = -\left(ln(|v|) - \frac{v}{V_*}\right) + K1$$

Where K1 just is a constant equal to

$$K1 = ln(V_*) - 1$$

in order for V(V_*) to be equal to 0 and V(V_*) greater than 0, as demanded. Further on it can be shown that the function fulfills all of the requirements for a proper Lyapunov function as earlier mentioned.
Firstly, the value of the function can be shown to be

$$\nabla V(v) = -\frac{1}{v} + \frac{1}{V_*} = 0 \implies v = V_*$$

at the point of interest, just as wanted. The function has to be convex, which is proven by showing that the second derivative is greater than zero.

$$\nabla^2 V(v) = \frac{1}{v^2}$$

which never is negative. The last step is to show that the time derivative is strictly negative.

$$\dot{V} = \nabla^\top V(v)\dot{v}$$

Where $\dot{v}$ is equal to the time derivative of $\tilde{v}$ seen above. Hence the time derivative of the Lyapunov function V(v) gets

$$\dot{V} = -\nabla^{\top} V(v) \cdot K \cdot \nabla V(v)$$

and the minus sign comes from the negative sign before the K in the expression of the derivative of the $\tilde{v}$ above.

Hence the function V(v) is a Lyapunov function for the system.

B.2 Solution to Equation (4.6)

The created script is using the built-in MATLAB-functions *solve()* to solve the third order equation with respect to x, and *roots()* to calculate the roots, i.e. eigenvalues, of the third order system.

```
1 syms a b c d x
2 eqn = a*x^3 + b*x^2 + c*x + d == 0;
3 solx = solve(eqn, x)
4
5 C = [a b c d];
6 roots(C)
```

λ_1 = (((d/(2*a) + b^3/(27*a^3) - (b*c)/(6*a^2))^2 + (-b^2/(9*a^2) + c/(3*a))^3)^(1/2) - b^3/(27*a^3) - d/(2*a) + (b*c)/(6*a^2))^(1/3) - b/(3*a) - (-b^2/(9*a^2) + c/(3*a))/(((d/(2*a) + b^3/(27*a^3) - (b*c)/(6*a^2))^2 + (c/(3*a) - b^2/(9*a^2))^3)^(1/2) - b^3/(27*a^3) - d/(2*a) + (b*c)/(6*a^2))^(1/3)

λ_2 = (- b^2/(9*a^2) + c/(3*a))/(2*(((d/(2*a) + b^3/(27*a^3) - (b*c)/(6*a^2))^2 + (c/(3*a) - b^2/(9*a^2))^3)^(1/2) - b^3/(27*a^3) - d/(2*a) + (b*c)/(6*a^2))^(1/3)) - (3^(1/2)*((-b^2/(9*a^2) + c/(3*a))/(((d/(2*a) + b^3/(27*a^3) - (b*c)/(6*a^2))^2 + (c/(3*a) - b^2/(9*a^2))^3)^(1/2) - b^3/(27*a^3) - d/(2*a) + (b*c)/(6*a^2))^(1/3) + (((d/(2*a) + b^3/(27*a^3) - (b*c)/(6*a^2))^2 + (-b^2/(9*a^2) + c/(3*a))^3)^(1/2) - b^3/(27*a^3) - d/(2*a) + (b*c)/(6*a^2))^(1/3))*1i)/2 - b/(3*a) - (((d/(2*a) + b^3/(27*a^3) - (b*c)/(6*a^2))^2 + (-b^2/(9*a^2) + c/(3*a))^3)^(1/2) - b^3/(27*a^3) - d/(2*a) + (b*c)/(6*a^2))^(1/3)/2

λ_3 = (- b^2/(9*a^2) + c/(3*a))/(2*(((d/(2*a) + b^3/(27*a^3) - (b*c)/(6*a^2))^2 + (c/(3*a) - b^2/(9*a^2))^3)^(1/2) - b^3/(27*a^3) - d/(2*a) + (b*c)/(6*a^2))^(1/3)) + (3^(1/2)*((-b^2/(9*a^2) + c/(3*a))/(((d/(2*a) + b^3/(27*a^3) - (b*c)/(6*a^2))^2 + (c/(3*a) - b^2/(9*a^2))^3)^(1/2) - b^3/(27*a^3) - d/(2*a) + (b*c)/(6*a^2))^(1/3) + (((d/(2*a) + b^3/(27*a^3) - (b*c)/(6*a^2))^2 + (-b^2/(9*a^2) + c/(3*a))^3)^(1/2) - b^3/(27*a^3) - d/(2*a) + (b*c)/(6*a^2))^(1/3))*1i)/2 - b/(3*a) - (((d/(2*a) + b^3/(27*a^3) - (b*c)/(6*a^2))^2 + (-b^2/(9*a^2) + c/(3*a))^3)^(1/2) - b^3/(27*a^3) - d/(2*a) + (b*c)/(6*a^2))^(1/3)/2

where

$$a = -1$$

$$b = \left(\frac{i_{ref}}{C \cdot v^{*2}}\right) \cdot (K_i \cdot \zeta^* - V_s) - \frac{R_s + K_p}{L}$$

$$c = \left(\frac{R_s + K_p}{L}\right) \cdot \left(\frac{i_{ref}}{C \cdot v^{*2}}\right) \cdot (K_i \cdot \zeta^* - V_s) - \frac{K_i}{L}$$

$$d = \left(\frac{K_i \cdot i_{ref}}{L \cdot C \cdot v^{*2}}\right) \cdot (K_i \cdot \zeta^* - V_s)$$

Eirik H. Lillefosse

Towards DC-microgrids with Stability-Preserving Plug-and-Play Features

NTNU
Norwegian University of
Science and Technology